AFCRL-62-253

THE INFRARED SPECTRUM OF HYDROGEN FLUORIDE: LINE POSITIONS AND LINE SHAPES

W. F. Herget, N. M. Gailar, and A. H. Nielsen

University of Tennessee
Physics Department
Knoxville, Tennessee

Contract No. AF19(604) - 7981
Project No. 7670
Task No. 767002

Scientific Report No. 1

March 1962

Prepared For

GEOPHYSICS RESEARCH DIRECTORATE
AIR FORCE CAMBRIDGE RESEARCH LABORATORIES
OFFICE OF AEROSPACE RESEARCH
UNITED STATES AIR FORCE
BEDFORD? MASSACHUSETTS

Alvin H. Nielsen, Project Director

Requests for additional copies by agencies of the Department of Defense, their contractors, and other Government agencies should be directed to the :

ARMED SERVICES TECHNICAL INFORMATION AGENCY
ARLINGTON HALL STATION
ARLINGTON 12, VIRGINIA

Department of Defense contractors must be established for ASTIA services or have their "need-to-know" certified by the cognisant agency of their project or contract.

All other persons and orginazitions should apply to the:

U. S. DEPARTMENT OF COMMERCE
OFFICE OF TECHNICAL SERVICES
WASHINGTON 25, D. C.

ABSTRACT

The goal of this investigation was to determine experimentally the true shape of the rotational absorption lines of the hydrogen fluoride fundamental band. The line shapes were to be measured at pressures where pressure broadening made the only significant contribution to the true line shape. The centers of the rotational lines of the fundamental and first overtone bands were to be measured. Chapter I of this manuscript is an introduction to the problems and goals of this investigation.

Chapter II of this manuscript discusses in detail the experimental aspects of this investigation. All data were taken with the vacuum-grating spectrograph recently completed at the University of Tennessee. Several instrumental changes, pertaining to calibration, glower stabilization, and filtering, are discussed. Several experimental difficulties, such as stray light, glower operation in vacuum, and motion of optical parts, are discussed along with their solutions. A description is given of the gas handling system that was constructed to permit safe and convenient handling of HF. A method for correcting measured spectral line shapes for the distortions caused by instrumental broadening is also explained.

Chapter III is devoted to the results of the line center and line shape measurements. Twenty-one fundamental

and seventeen first overtone line centers were measured at low pressure with an estimated accuracy of ±0.02 cm^{-1}. The fundamental and first overtone band centers were calculated to be 3961.43 cm^{-1} and 7750.83 cm^{-1}, respectively. Several other HF molecular constants were calculated. Pressure induced shifts in the centers of the rotational lines were measured.

The Lorentz expression for the shape of a pressure broadened line was found to fit the true line shape quite well if the power n of the distance from the line center was allowed to vary. For lines whose width at one-half their maximum per cent absorption was less than 2.2 cm^{-1}, n was found to be equal to 2. The value of n decreased for lines wider than the above to as low as 1.79 and had an average value of 1.85. In the range of pressures studied (1 cm to 5 atm pressure) n had no measurable dependence on pressure. Within experimental error, n was constant from the line center to at least 10 cm^{-1} from the line center for a particular line.

Chapter IV summarizes the results of this investigation and makes several suggestions for future experiments in this field. The Appendices include information on instrumental broadening corrections and line shape data.

ACKNOWLEDGEMENT

The following text was accepted by the Graduate School of the University of Tennessee as dissertation for the degree of Doctor of Philosophy in Physics. Since the major portion of this work was done under a contract with the Office of Aerospace Research, United States Air Force, the complete dissertation is being submitted as a technical report.

The author wishes to express his sincere thanks to Dr. Norman M. Gailar, who directed this dissertation, and to Dr. Alvin H. Nielsen, for his assistance and encouragement throughout the course of graduate study. The author also wishes to thank Dr. R. J. Lovell, Dr. W. E. Deeds, and Mr. H. R. Mink, of the University of Tennessee Physics Department, and Dr. D. F. Smith of the Union Carbide Nuclear Company, Oak Ridge, Tennessee, for their valuable assistance in various phases of this investigation.

The financial help of the University of Tennessee Physics Department through a teaching assistantship and a research assistantship, the latter through Contract No. AF19(604) - 7981 with the Office of Aerospace Research, United States Air Force, was most appreciated by the author.

Most thanks of all, though, must be reserved for the author's wife and parents for their moral and financial support through the years of graduate study.

TABLE OF CONTENTS

LIST OF TABLES

LIST OF FIGURES

FIGURE PAGE

CHAPTER I

INTRODUCTION

The energy levels of a system of molecules are not sharp. As a result, spectral lines that arise because of a transition from one energy level to another are not monochromatic. They have a frequency spread around an average or center frequency. The spectral lines are said to be broadened.

Energy levels are widened by four mechanisms:

1. Natural broadening is a direct consequence of the Heisenberg Uncertainty Principle. The width of an energy level is inversely proportional to the mean lifetime of the level.

2. Doppler broadening arises from the Doppler shift in frequency that is observed when a source of radiation (or absorption) has a velocity component in the direction of observation. The molecules of the gas under observation will have a Maxwellian distribution of velocities along the direction of observation.

3. Pressure broadening is due to collisions among molecules. It is assumed that the collision time is short

compared to the time between collisions, and only binary collisions are considered.

4. Statistical broadening is the name given to broadening that arises when pressures are so high that the collision time is long compared to the time between collisions.

Natural broadening is extremely small. In the infrared region of the spectrum, Doppler broadening is completely masked by pressure broadening even at pressures as low as 1 cm of Mercury. Statistical broadening becomes important at pressures well above 5 atm. Thus the shape of spectral lines in the infrared at moderate pressures (1 cm to 5 atm) is due to molecular collisions of short duration. One studies line shapes with the hope of finding out how molecules behave during collisions. Such information should lead to a better understanding of intermolecular forces.

To facilitate the study of shapes of spectral lines, one should have a spectrum in which the lines are far enough apart that their absorption will not overlap over a wide range of pressures and lengths of absorption paths. To make the theoretical calculations as simple as possible, one should choose a diatomic molecule for the study.

The molecule hydrogen fluoride probably fits these requirements better than any other molecule. Earlier work in this laboratory by Kuipers (12) demonstrated that HF could be handled properly and was quite suitable for a study of line shapes.

A type of broadening that has nothing to do with molecular interactions is called instrumental broadening. If a spectral line could be scanned with an infinitely narrow slit and if there were no imperfections in the optics of the spectrometer, then the true line shape would be obtained directly. Of course, a finite slit must be used, and the optics are not perfect. In actual practice one obtains a line shape that is more intense in the wings and less intense at the line center than the true line shape. Correction for this type of broadening can be made, but the higher the resolving power of the spectrometer and the better the optics, the less this correction need be.

The vacuum-grating spectrometer at the University of Tennessee is well suited to the study of spectral line shapes. The resolving power of this instrument with an appropriate grating is high, and the optics are good. This means that a wide range of line widths can be examined without corrections for instrumental broadening becoming too large. Since the spectrometer is used under vacuum, spectra

arising from atmospheric absorption can be eliminated. This present work is the first actual research that has been carried out on the spectrometer. As a result, several instrumental problems were encountered, but they have been largely overcome.

The aim of this investigation was to determine the true shape of as many spectral lines of the HF fundamental band as possible, and to compare the experimental results with theoretical calculations. Towards this aim, line shapes were obtained at a number of different pressures and appropriate cell lengths. It has generally been assumed that spectral lines have a Lorentz shape close to their line center. Recent measurements on HF by Smith (18) and on HCl by Benedict (2) indicate that a modified form of the Lorentz formula gave a good representation of the line shape at distances several wave numbers away from the line center. It is hoped that this present work will confirm and extend these earlier results.

This present work will be presented in the following manner: first there will be a discussion of the experimental details of the spectrometer itself, of handling HF, and of taking and handling data; second, the results of the measurements on line frequencies, shapes, and widths will be presented and analysed; and finally, some conclusions

will be drawn and recommendations for future work will be given.

CHAPTER II

EXPERIMENTAL DETAILS

I. THE SPECTROMETER AND SOME MODIFICATIONS

Optical Layout

The high resolution, vacuum-grating spectrometer at University of Tennessee has been described completely by Herndon and Nielsen (9). For convenience, ray diagrams of the optical system are shown in Figs. 1 and 2. M_1, M_2, and M_3 are spherical mirrors. M_4 is a flat mirror. Mirrors M_5, M_6, and M_7 and prism P comprise a basic Perkin-Elmer Interchange Unit.* Mirrors M_8 and M_9 are off-axis paraboloids. Mirror M_{10} is an off-axis paraboloid with a 48-inch focal length. M_{11} is a flat mirror with a 2-inch square hole cut in its center. M_{12} is a flat mirror, and M_{13} is an ellipsoidal mirror.

Preliminary measurements on the HF spectrum indicated that the prism monochromator arrangement was not entirely satisfactory. Also, use of a Fabry-Perot interferometer proved to be a rather inconvenient method of

---

*Drawing No. 021-0701, Perkin-Elmer Corporation, Norwalk, Connecticut.

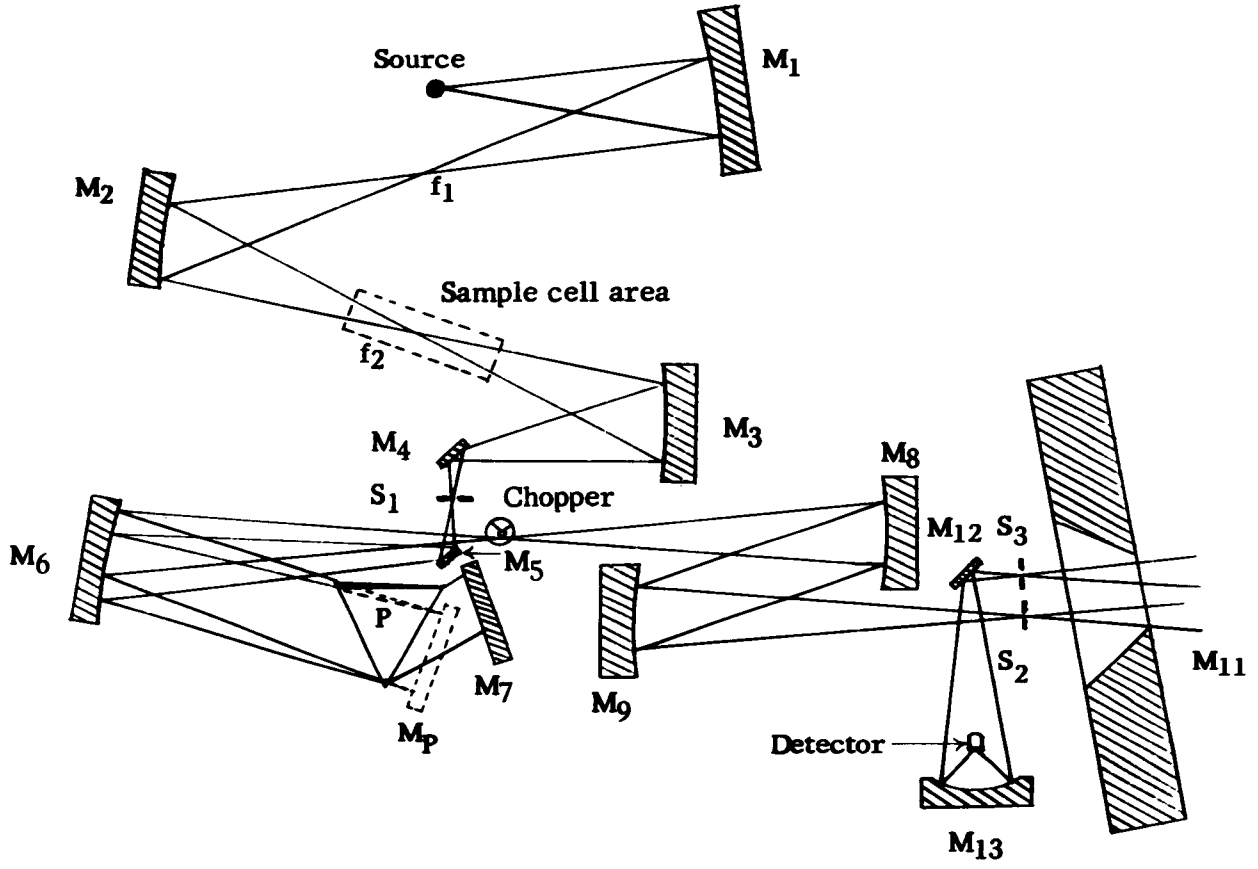

Fig. 1. Optical scheme for getting radiation to the grating monochromator.

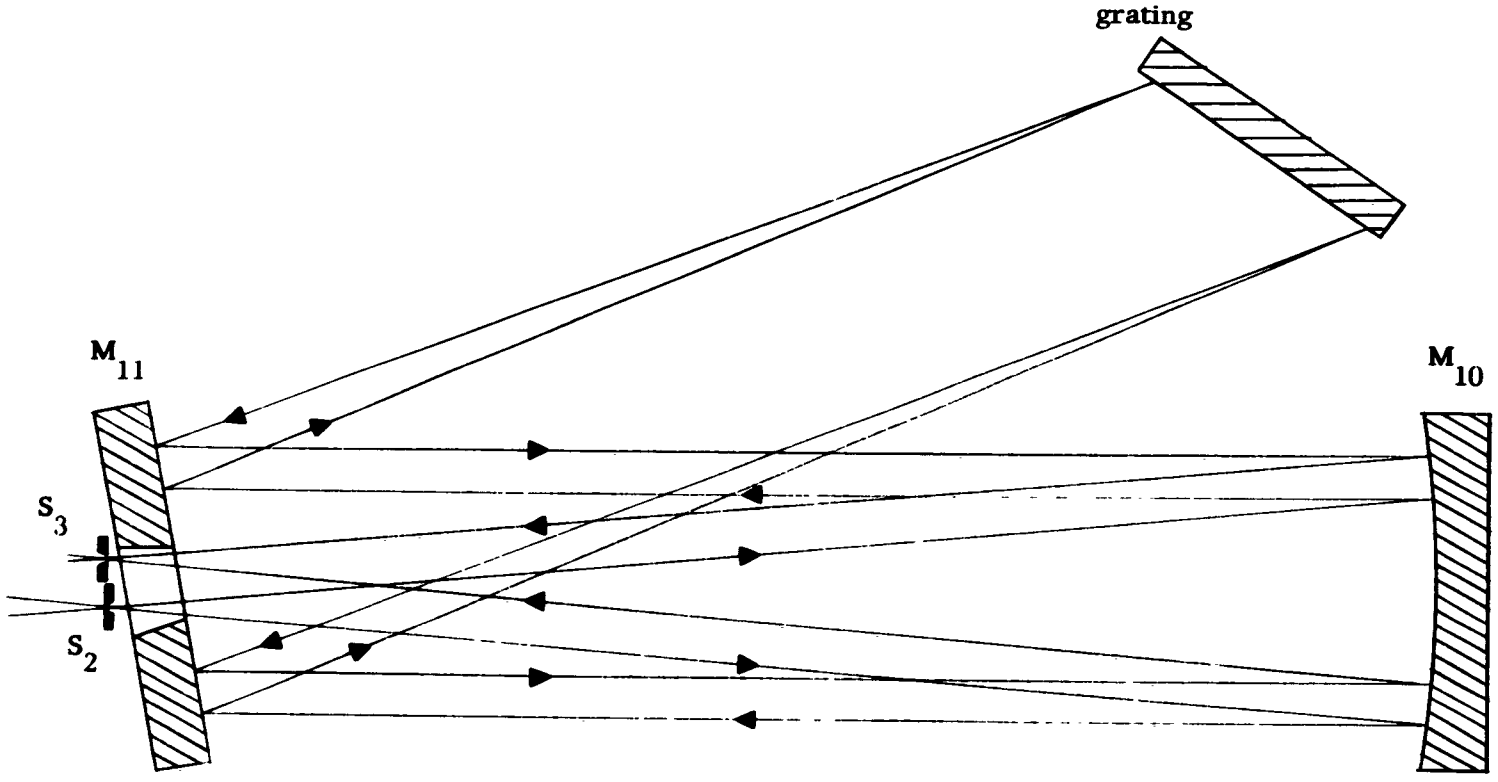

Fig. 2. Ray diagram of the grating monochromator.

calibration. Changes to these parts of the spectrometer and several additions to the spectrometer will now be discussed.

The Monochromator

The first step in making intensity measurements is to calculate per cent absorption. To do this with accuracy it is necessary to be sure that only one order of wavelength reaches the detector. That is, in the grating equation $\nu = mk/\sin\theta$, it is important that m be allowed only one value. Originally, a foreprism of NaCl was used to sort out orders. Although the filtering of the prism was adequate, several disadvantages resulted from its use:

1. The surfaces of the prism gradually deteriorated because of condensation of atmospheric water vapor when air was allowed to enter the evacuated spectrometer unless the air was passed through a drying tower.

2. The prism position continually had to be maximized. That is, for every short spectral range the position of the prism required adjustment to permit maximum energy to fall on the grating, because the prism drive was not tied in with the grating drive. Only by doing this could reproducible results be obtained.

3. In order to use a greater range of wavelengths, the foreprism section was designed to use interchangeable

prisms. This design used a prism calibration system which did not have an absolute wavelength scale. This feature often proved time consuming and annoying, especially when the spectrometer was being aligned.

The simplest solution to the difficulties was to eliminate the prism and use an appropriate band-pass filter. The prism was removed, and the Littrow mirror mount was adjusted so as to hold a plane mirror in position M_p. This change can be seen in Fig. 1. A germanium-on-glass composite filter was obtained from the Bausch and Lomb Optical Company. This filter passes about 80 per cent of the radiation between 2 and 3 microns, has rather sharp cutoffs, and passes only about 1 per cent of the radiation outside the cutoffs. The filter is mounted just in front of slit S_1.

Calibration Equipment

The spectrometer was originally equipped with optics for a Fabry-Perot interferometer for calibration purposes. The source, a zirconium arc, was mounted inside the spectrometer and proved to have a very short life in vacuum. Another drawback in the use of the interferometer was caused by temperature fluctuations. Changes greater than $1^{\circ}C$ caused errors in calibration. Rather than redesign the

interferometer, it was decided to use a different method of calibration. The use of a hollow cathode neon emission source for calibration lines has been discussed by Rao and his co-workers (16), (17). The hollow cathode source used the optics of the interferometer, and was mounted in place of the zirconium source.

Since the hollow cathode source used here is used in vacuum, its construction differs somewhat from Rao's. A diagram is shown in Fig. 3. When a proper amount of neon gas (about 2 or 3 cm pressure) has been admitted to the hollow cathode source, a 500 volt DC potential difference usually causes the source to light automatically. The voltage is then reduced so that the current will be between 50 and 100 ma DC.

Light from the hollow cathode source is focused at the top of slit S_2. It then travels the same path through the grating section as infrared light, though slightly off-axis. It emerges from the grating section at the bottom of slit S_3 and is reflected by a plane mirror to a 1P28 RCA photomultiplier tube.

Glower Stabilizer

To aid in making accurate intensity measurements the glower output should remain quite constant for extended

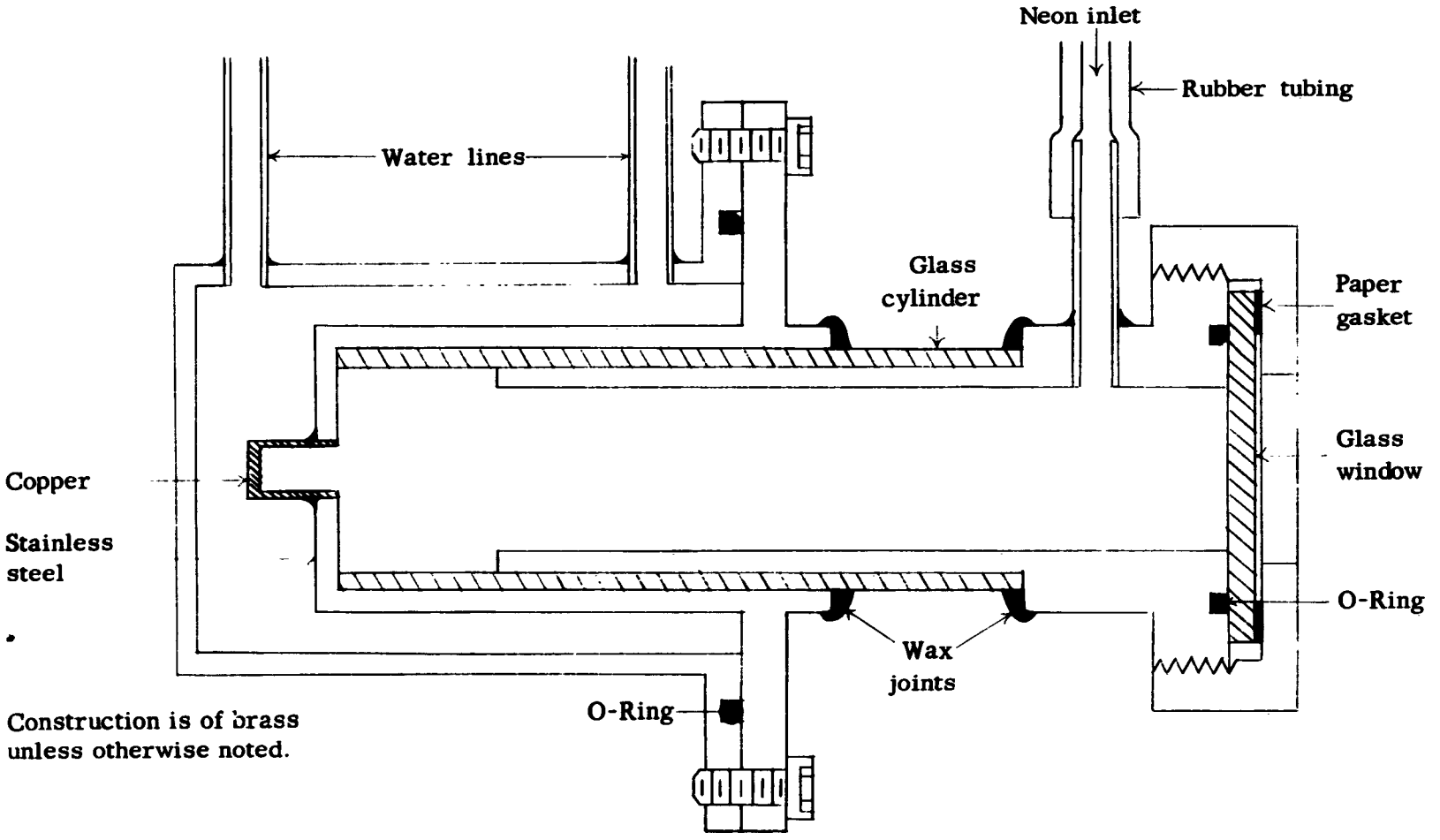

Fig. 3. The hollow cathode neon source.

periods of time. A system in which a photocell monitors the near infrared output of the glower was developed by Dr. W. E. Deeds (5). The stabilizer keeps the glower output constant to better than 1 per cent.

Coarse and fine controls permit the glower current to be set between 0.4 and 0.9 amps. In order to light a glower one sets the controls at usual operating conditions and heats the glower with a propane torch or some other suitable heat source. As the glower begins to glow it is placed under observation of the photocell and soon reaches a stable output.

A ballast resistance is kept in series with the glower at all times. The ballast prevents very fast current surges (which the stabilizer is not designed to handle) from causing the glower to go out.

Miscellaneous

Various gratings that were available were illuminated by equal intensities of light from the glower and were compared at equal spectral slit widths in the region of the HF spectrum. It was found that the 15,240 lines per inch grating, when used in first order, diffracted more 2.5 micron energy than other available gratings.

Infrared light was detected by an uncooled Kodak Ektron lead sulphide detector.

The neon and infrared signals were chopped by thirteen cycle per second choppers. Each signal was amplified by Model 107 Perkin-Elmer amplifiers and then sent to separate pens of a Leeds and Northrup two-pen Speedomax Recorder.

II. INSTRUMENTAL DIFFICULTIES

Drift

An instrumental problem that has not been completely solved is that of "drift." Drift shows up in two ways. First, the grating drive may be stopped at the peak of some absorption line, but instead of the recorder pen tracing a straight line on the chart paper, it slowly drifts towards lower energy. The grating can be turned to bring the pen back to the peak of the line. Second, a spectral line can be scanned, the grating drive reversed, and the line then rerun. The lines do not always exactly overlap on the chart paper.

It was finally discovered that the cork gaskets in the mirror holders had shrunk (probably from continued exposure to vacuum conditions), thus permitting the mirrors to move slightly. The cork gaskets were replaced with

fairly hard rubber gaskets, and all evidences of drift disappeared for several months. However, a slight drift can now be detected over a period of several hours, but in the time required to calibrate a spectral line this small drift has a negligible effect.

The Nernst Glower

Glowers obtained prior to 1954 from the Stupakoff Division of the Carborundum Company performed very well in vacuum. A batch of glowers obtained from the same company in 1958 gave off a fine white powder when used in vacuum. This powder is believed to be due to a boiling off of the binder that is used to hold the glower oxides together. To prevent the powder from being deposited on mirrors, a glower housing was constructed. The glower light passed through a window (KBr, LiF, etc.) that was sealed onto the housing. The window was much easier to clean than the mirrors.

The window serves another useful purpose. Occasionally gases are admitted to the spectrometer chamber so that they can be observed under low pressure and long path length. Some of these gases (CO and CH_3Cl, for example) cause the glower current to fluctuate at a rate too rapid for the glower stabilizer to handle. The window and housing prevents these gases from reaching the glower.

The method of Ebers and Nielsen (7) is used to attach leads to the glowers. In this method several inches of platinum wire are wrapped around each end and heated until a bead is formed. Leads are then spot-welded to the beads. The ends of the glower become quite hot during this procedure, and the areas between the hot and cool parts of the glower become quite fragile. However, it was found that leads simply could be wrapped around the ends of the glower without attaching the bead, and the glower could still be lit. If the glower was allowed to burn for an hour or so in this manner and then allowed to cool, it would become quite strong. Beads could then be attached in the usual manner and no difficulty resulted.

Stray Light

When the spectrometer is at atmospheric pressure, many of the spectral lines of the 2.7 micron water vapor band are 100 per cent absorbing. It was discovered that although the grating was set for the peak of one of these lines, the light intensity indicated by pen position would drop when the slits (S_2 and S_3) were closed. The intensity would drop still further when a shutter was placed in front of the source.

The difference in intensity between "slits closed-shutter out" and "slits closed-shutter in" is caused by

light that reaches the detector by being reflected off the back of slit S_3, then off other surrounding surfaces, and then towards the detector. Since the light traveling to the grating section and the light leaving slit S_3 cross in this area, the stray light can never be completely eliminated. However, this light is constant in intensity and can be reduced to a few per cent of the desired light by baffles that are shown in a top view of the detector section in Fig. 4(a). Their positions are determined by moving them while watching the recorder and taking care not to cut out any of the desired light.

The intensity difference between a spectral line that absorbs 100 per cent and "slits closed-shutter out" is caused by stray light that is developed in the grating section. Two sources of stray light showed up as pen deflections within a few degrees of central image, and on each side of it. The presence of the filter assured one that the light was not of the wavelength indicated by angular position. Various parts of the grating and of mirrors M_{10} and M_{11} masked with strips of paper until eventually the sources of trouble were found. Both sources of stray light were finally eliminated by masking mirror M_{11} as shown in Fig. 4(b).

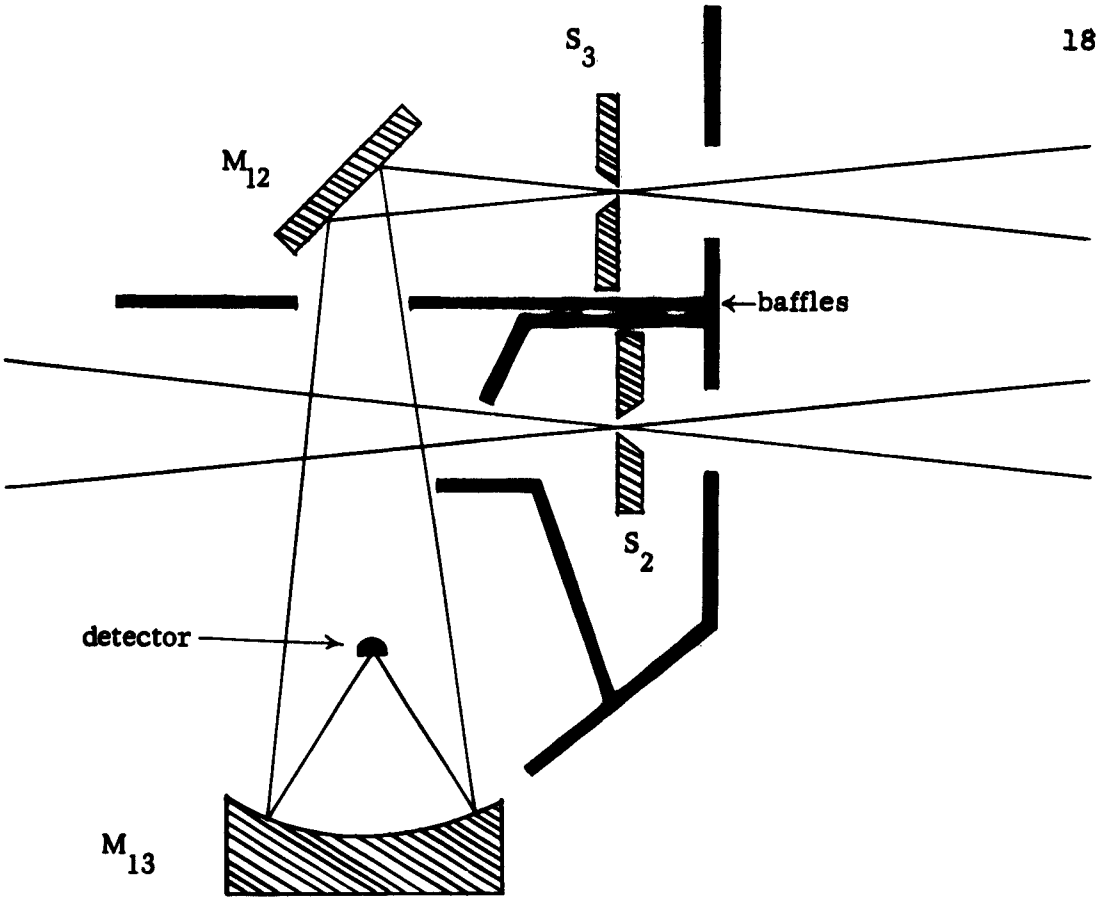

a.

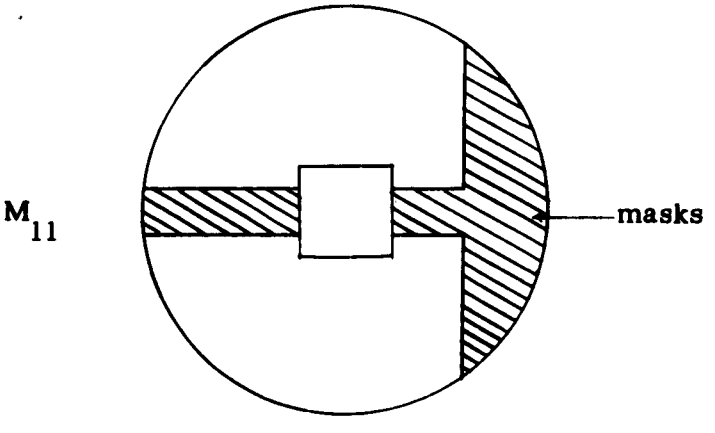

b.

Fig. 4. Stray light baffles in the detector section (a), and stray light masks on mirror M_{11}(b).

The frequency range of light that the detector sees at any one instant is that light falling of S_3. However, the frequencies of light on either side of this frequency range fall across the face of M_{11}, waiting their turn to be driven across S_3 by the grating. This light falls in a band about 1 inch high across the middle of M_{11}. Some of the light from this band is reflected back towards M_{10} and then towards S_3. This source of stray light is eliminated by the horizontal mask on mirror M_{11}.

The optics of the grating section are such that at about 5 degrees on the low angle side of the main central image a smaller central image appears. This smaller central is caused by light from the grating that reflects off the edge of M_{11} towards M_{10}, and then twoards S_3. This smaller central image and its associated spectra are eliminated by the vertical mask on mirror M_{11}.

One other source of stray light in the grating section was eliminated by placing a small mask at the center of mirror M_{10}. This mask eliminates light from S_2 that has been rendered parallel by M_{10} and falls directly on S_3.

The masks and baffles described above lower the intensity of stray light to about 5 per cent of the desired light. This small amount of stray light can be handled without much difficulty, and the method is described in the

section on determination of the zero-line and the base-line.

Water Vapor

If the spectrometer chamber is pumped on for several days, the pressure can be reduced to about 50 microns. However, enough moisture remains in the chamber to cause the strong lines of the 2.7 micron water vapor band to absorb as much as 10 per cent of the incident light. This absorption was troublesome, as the lines P(5 and 6) of HF have almost the same line centers as two of the water lines. Furthermore, the water absorption interfered with measurements that were made on H_2F_2. It was felt that the presence of water vapor was not as much a fault of the pump as of a leak either in the water cooling system or in the spectrometer chamber itself. Attempts to locate such a leak were partially successful, but not completely so.

The problem was solved by constructing a cold trap inside the spectrometer chamber. The trap consists of a coil of copper tubing suspended below the spectrometer table. The two ends of the coil lead through the spectrometer chamber bulkhead. One end was left open, and the other end was connected to a Dewar of liquid nitrogen. The liquid nitrogen was allowed to boil off through the coil,

and all traces of water vapor spectra were quickly frozen out.

III. GAS HANDLING SYSTEM AND ABSORPTION CELLS

The Peculiar Problem of HF

Because HF is extremely corrosive, the entire gas handling system is constructed of monel, nickel, and stainless steel. All permanent joints are silver soldered. HF reacts to some extent with these metals, but soon forms surface fluorides which prevent further reactions. HF also absorbs on the metal surfaces, but after approximately one-half hour the pressure ceases changing, and an equilibrium appears to be reached.

The absorption cell windows are of sapphire, which has resisted corrosion very well, except for one case. When HF was left in the cell for 6 or 7 hours at 5 atm pressure, an opaque crust formed on the windows. The crust could be easily wiped off if the cell were taken apart. The windows do become slightly fogged after repeated exposures to HF. At present, the windows transmit about 70 per cent of the radiation at 2.5 microns after having been used over two years. No "window bands" have been observed.

At room temperature HF is highly polymerized. To reduce the polymer absorption, all data were taken at a

temperature of 100°C except for the data at 5 atm pressure, which were taken at 120°C.

The Gas Handling System

Figure 5 shows a block diagram of the gas handling system. Three connections are available for admission of sample gases. The valves are types 411 and 413 Hoke packless diaphragm valves of monel construction. All removable connections use Hoke No. 410 gland, seat, and nut fittings. Hastings thermocouple gauges are used to measure vacuum. A chemical trap made of a 12-inch by 2-inch diameter brass cylinder filled with a mixture of 75 per cent alumina and 25 per cent soda lime is used in removing HF from the system to prevent oil pump contamination and fumes in the laboratory. The cold trap is a glass cylinder which has a ground joint connection to the system. The Bourdon gauge is equipped with a monel Bourdon tube and is used for rough pressure measurements. Accurate pressure measurements up to 128 cm pressure can be made with a Taylor Differential Pressure Transmitter (Model No. 399RF). The transmitter has a phosphor bronze bellows. Figure 6 shows a block diagram of the differential pressure measuring system.

Figures 7 and 8 show photographs of the gas handling system developed. The gas handling system proper

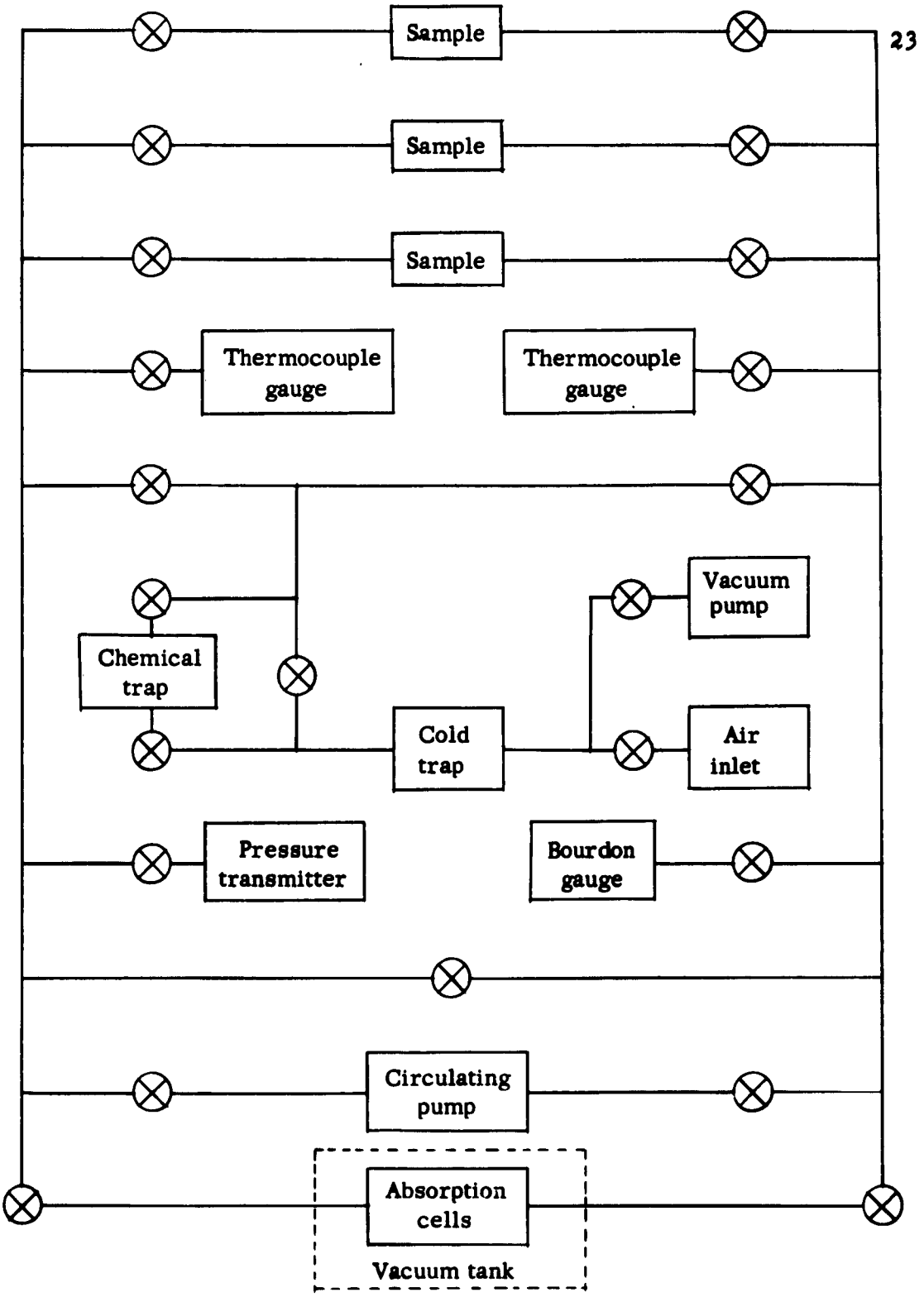

Fig. 5. Block diagram of the gas handling system.

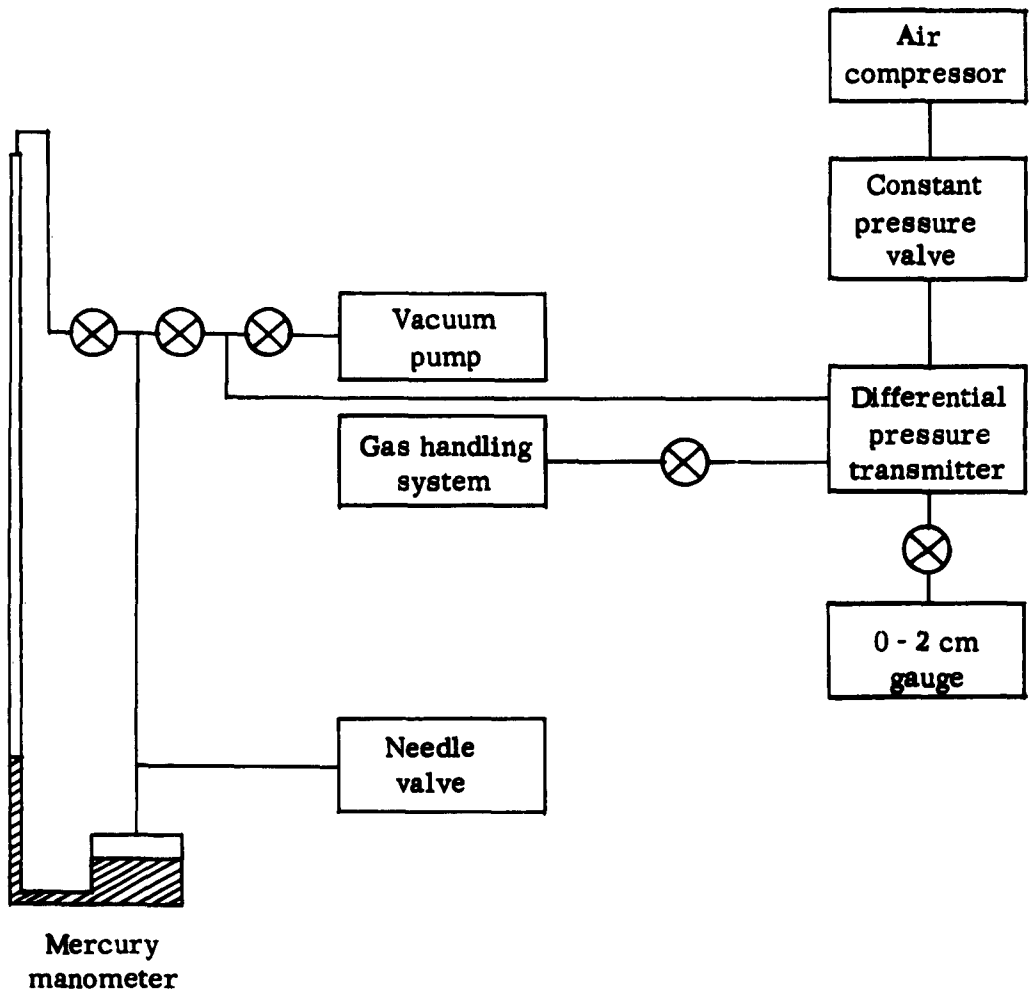

Fig. 6. Block diagram of the differential pressure measuring system.

Fig. 7. Front view of the gas handling system.

Fig. 8. Rear view of the gas handling system.

(Fig. 5) is enclosed in an aluminum box equipped with strip heaters. The entire gas handling system, including the Bourdon gauge, tubing, and absorption cells, are heated to 100°C. Temperatures of equipment inside the vacuum chamber are measured with a Leeds and Northrup thermocouple-potentiometer system. Thermocouple leads are attached to the outside of an absorption cell so that they would not come in contact with HF. It was found that this method gave accurate measurement of the temperature of a gas in the cell.

Absorption Cells

Two absorption cells were used in this work. The 1 and 5 atm pressure data were taken in the 0.047 cm cell shown in Fig. 9(a). The cell is constructed of monel. A cylinder 3 inches long is attached to each side of the cell, and the whole apparatus is wrapped with asbestos covered wire for heating purposes.

The 1, 5, and 50 cm pressure data were taken in a cell with a path length of 10 cm. The window holding section of this cell is shown in Fig. 9(b). Brass cylinders of various length can be used with the window holding sections. This cell was also wrapped for heating purposes.

Both cells are fitted with sapphire windows. Either cell can be mounted on a selsyn-driven rack and pinion so

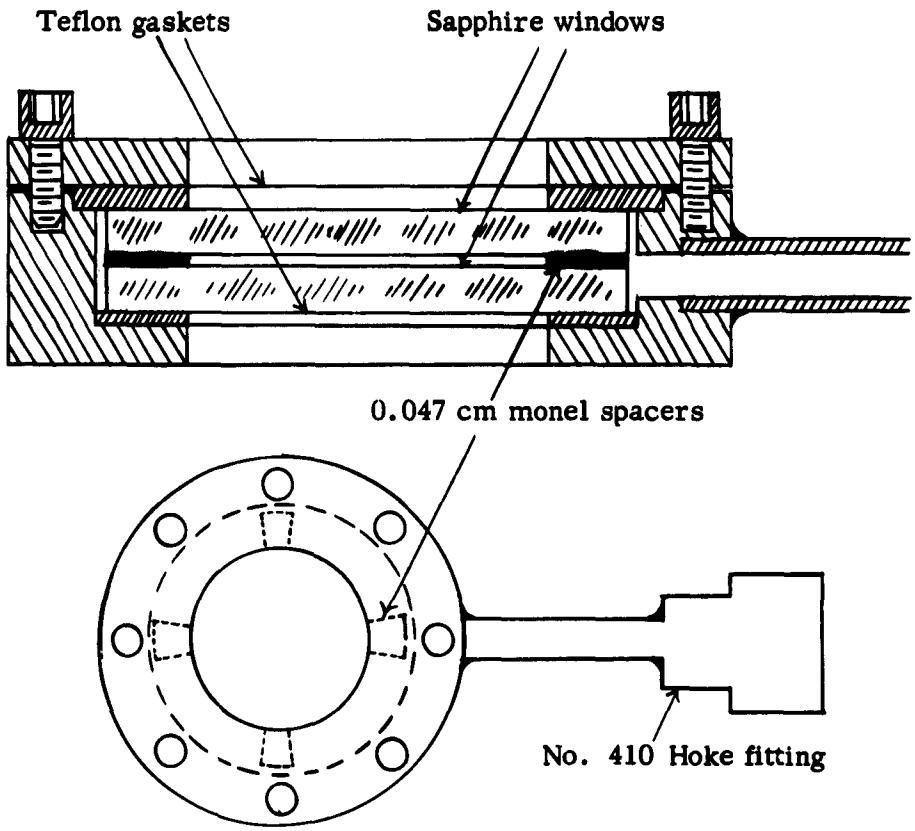

a.

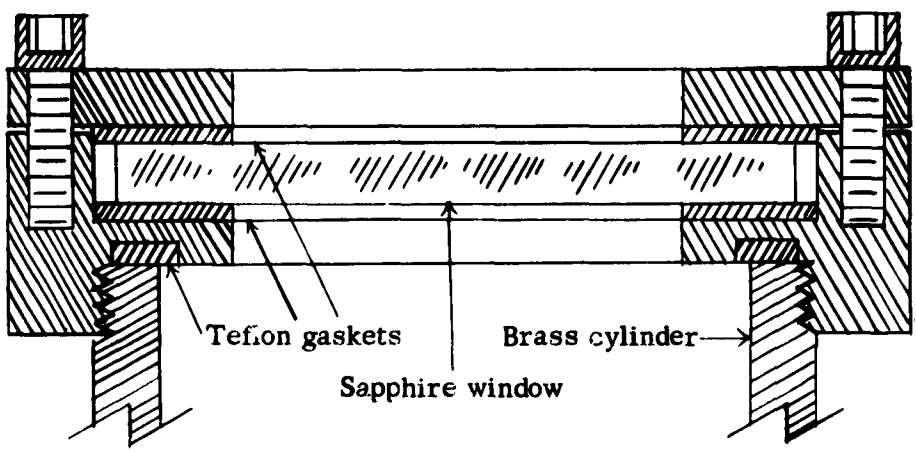

An identical holder screws to other end of cylinder.

b.

Fig. 9. The 0.047 cm cell (a), and the window holder for the 10 cm cell (b).

that it can be raised from or lowered into the infrared beam from outside the spectrometer tank.

IV. CALIBRATION TECHNIQUE

As stated in the section on experimental modifications, neon emission spectra and infrared absorption spectra can be recorded simultaneously on a two-pen recorder. Figure 10 shows a portion of the R branch of HF and the neon lines that lie in the same region. With proper technique, knowledge of the wave numbers of the neon lines permits calculation of the wave numbers of the HF lines.

In order to devise a calibration scheme the glower was removed and replaced by another neon emission source (later called the neon calibrating source), and the HF spectral region was scanned. Neon emission lines were recorded by both pens. Comparison of identical neon lines showed that the two pens recorded them at slightly different positions on the chart paper. This difference was appreciably greater than the amount by which the two pens were offset. This difference was not constant over the entire spectral range, but decreased slowly with increasing angle (decreasing wave number). When the central images of the two neon beams were recorded, the two pens recorded

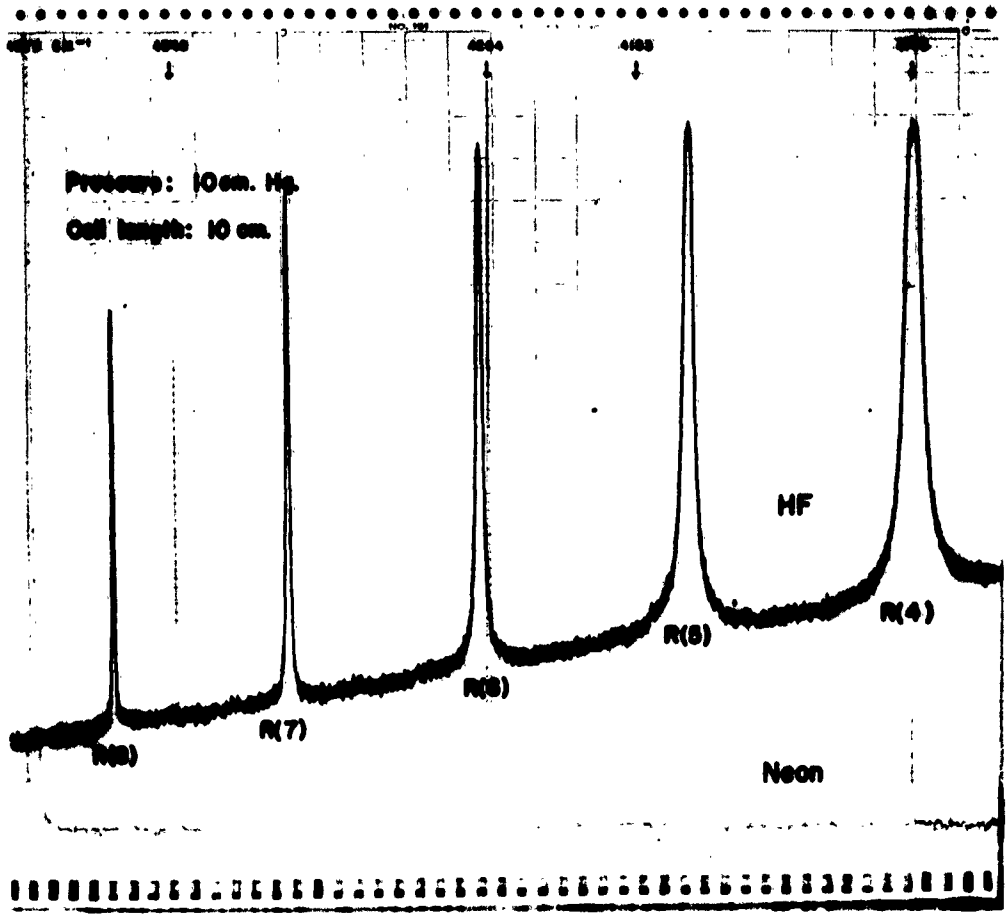

Fig. 10. A portion of the HF spectrum and neon calibration lines.

their respective beams at a separation greater than the offset of the pens. Indeed, when the central images, or emission lines, are obtained by rotating the grating in discrete amounts rather than by continuous rotation, the effect of pen offset is nullified. Yet the central images, or lines, are still recorded at appreciably different positions.

This difference is ascribable to the fact that light from the hollow cathode neon source falls on the entrance slit above the light from the glower, traverses the spectrometer always off axis, and leaves the exit slit below the light from the glower. This off-axis condition is necessary in order to introduce the neon light into the spectrometer and to collect it later without interfering with the glower radiation. Since the neon light is off-axis, the angle of incidence and the angle of diffraction for it is different from the similar angles for the axial rays; thus the difference in position shown by the two pens is to be expected.

The calibration problem can be stated as follows: one pen records neon emission lines, the wave numbers of which are well known. The other pen records HF absorption lines, the wave numbers of which are to be determined. At a given position of the grating the wave numbers of the

energies being recorded by the two pens differ from each other, and this difference is a function of wave number. The calibration problem was to devise a method by which the known neon wave numbers on one pen would give wave numbers on the other pen.

At first a simple correction curve was found from a spectral chart with neon lines recorded by both pens. The difference in wave number between the positions as shown by two pens of any emission line was plotted against the wave number of that line. In principle then, the wave number of the energy from the glower falling on the PbS detector while a neon line was falling on the photomultiplier could be found by applying a correction from the curve. The correction curve, however, was not linear. In addition, it was found that if a mirror was repositioned, or if either neon source was repositioned, the curve would be changed. The curve was, therefore, not usable because when the neon calibrating source was replaced by the glower, the curve was no longer applicable.

These difficulties were avoided by taking into account the difference between the central images as recorded by the two pens. When the region of the central image is scanned by rotating the grating, the angular separation of the position of the central images as recorded

by the two pens is found. Then various neon lines are recorded by both pens in the HF spectral region. The positions of the lines recorded by light falling on the photomultiplier are adjusted in accordance with the central image separation. Specifically, the central image recorded by the photomultiplier always occurs at a smaller angle than does the central image recorded by the PbS detector. This angular difference is added to the recorded angular positions of the various neon emission lines from the photomultiplier. These adjusted angular positions still are less than the angular positions of the same lines from the PbS. If these new differences are plotted against the wave numbers of the neon lines, a linear correction curve results. Also, any change in position of mirrors or sources results, at most, in shifting this curve up or down; the slope stays the same.

Therefore, when any adjusting of the instrument is done, it suffices to find one correction, and the whole correction curve is determined. Also, when the neon calibrating source is replaced by the glower, only one correction need be found.

The glower correction curve is obtained by comparing the neon lines with the well-known absorption lines of CO. CO is chosen because its first overtone lies in the same

spectral region as HF, and its lines have been measured very accurately by Rank (15). The wave numbers of the neon lines were calculated from the values listed by Rao (17).

By the use of these calibration procedures one accurately known wave number for glower light is found for each neon line. However, it was found that the neon lines are not close enough together to permit linear interpolation between them. In the HF region it is estimated that if linear interpolation is used over a range of 10 cm^{-1}, an error of about 0.02 cm^{-1} will result. As can be seen in Fig. 10, the neon lines are generally further apart than 10 cm^{-1}. Higher orders of neon light do not overlap in the HF region, so that only the fourth order of red and yellow lines were available for calibration purposes.

The frequency of a spectral line, $\nu(cm^{-1})$, is related to the grating constant, $K(cm^{-1})$, and the angular distance from central image, θ(degrees), by the expression

$$\nu = \frac{K}{\sin\theta} \quad . \tag{1}$$

The wave numbers of the neon lines will be assumed to have been divided by their order (4) so all wave numbers are first order. Ordinarily, one might calculate K by

knowing ν and θ accurately. Then, knowing K and the angular position of some spectral line, θ', its frequency ν' could be calculated. This procedure cannot be used with this spectrometer since two grating drives are used. A positioning drive is used to turn the grating to the spectral region of interest, and it is not precise enough to make accurate determinations of the angle θ.

The scanning drive is very accurate on this spectrometer, and thus precise angular differences can be measured. Two neon lines are chosen, and the first is called ν_1. The grating equation $\nu_1 = K/\sin\theta$ is written. The second neon line is called ν_2 and is said to be at an angle $\theta + \varphi$. The angle φ can be measured with high precision. The grating equation for this line can be written $\nu_2 = K/\sin(\theta+\varphi)$. These two equations can be solved simultaneously for the unknowns K and θ. The wave number of any point lying between ν_1 and ν_2 can then be found since the angular distance of the point from θ is accurately known.

As a check of the accuracy which results when using the grating equation in this manner, several sets of three neon lines were measured. Two of the lines were used in the above way to calculate the third. The measured value and the known value always agreed to within ± 0.02 cm^{-1}.

The factor limiting the precision of measurements seems to be the reproducibility of measurements of line positions (the effect of "drift", as discussed earlier). It is felt that wave numbers can be measured with an overall precision of ±0.02 cm^{-1}. As a check of the accuracy of measurements, and to see if any gross systematic errors existed, twelve first overtone CO lines were measured. The positions of these lines were all measured to within ±0.02 cm^{-1} of the values measured by Rank. This CO band lies on the high wave number side of HF. To check the accuracy further, several lines of the $2\nu_2 + \nu_3$ band of CO_2, which lies on the low wave number side of HF, were measured. The values measured agreed to within ±0.02 cm^{-1} of the values reported by Courtoy (4).

V. DATA TAKING AND HANDLING

Determination of Line Centers

The line centers of central images and spectral lines were determined in the following manner. Measurements of angular positions are made directly on the chart paper. A number of points are measured off midway between the sides of the spectral line. Points near the top half of the spectral line are weighted the most. A straight line is then drawn through these points perpendicular to

the edge of the chart paper. This line determines the angular position of the center of the spectral line, or central image, in question. Calibration can then be carried out as discussed in the preceding section.

Determination of the Base-Line and the Zero-Line

After a spectral line has been recorded by the spectrometer, the base-line and the zero-line have to be determined before per cent absorption measurements can be made. The base-line is the position on the chart paper corresponding to zero per cent absorption. The zero-line is the position on the chart paper corresponding to 100 per cent absorption. The first step in determining the base-line and zero-line was to scan the entire HF region with the absorption cell evacuated. This scan determined the background line. (All data were recorded with the spectrometer tank evacuated.) The background line proved to be a smooth curve, small portions of which (10 to 15 cm^{-1}) could be taken as a straight line.

For absorption lines that were not overlapped by adjacent lines one determined the base-line by simply drawing a straight line from one wing to the other of the line in question.

Many of the high pressure lines were overlapped by adjacent lines. In these cases the background for a

particular region, say the whole R branch, was scanned. Then, with the same instrument settings, the same region would be scanned again with the desired pressure of gas in the absorption cell. Although these spectra were recorded at rather fast scanning speeds, comparison of the two would give fairly satisfactory per cent absorption data in the regions between adjacent lines where absorption did not vary rapidly with wave number. The regions where absorption varied rapidly with wave number could then be scanned at slow speeds and the background could be fixed from the high speed scans.

As discussed in the section on stray light, the zero-line could not be determined simply by closing the slits. For lines that did absorb 100 per cent even without corrections for instrumental broadening the zero-line was easy to determine. Absorption of 100 per cent is indicated by a flat portion of the spectral line that extends through the line center. An example can be seen in Fig. 11(a).

Most data taken in the 10 cm cell did absorb 100 per cent at the line center. However, all 1 cm pressure data and some high J 5 and 50 cm pressure data did not absorb 100 per cent (before corrections for instrumental broadening). In some instances these weak lines could be scanned at the desired pressure, and then scanned again

at a pressure high enough to make the line absorb 100 per cent; this latter scan would determine the zero-line for the former scan. In other instances it was more convenient to scan a desired line and then, at the same instrument settings, scan another line that did absorb 100 per cent; again, this latter scan would determine the zero-line for the former scan.

A different method of determining the zero-line had to be used for the data taken in the 0.047 cm cell. Since the absorption coefficient at the line center remains essentially constant, even the strongest HF lines would absorb no more than 60 or 70 per cent at any pressure in this short cell. As long as the instrument settings (glower current, amplifier controls, etc.) were kept fixed, the zero-line was a straight line on the chart paper for the whole HF region. One could therefore use the zero-line of some other spectral lines to determine the zero-line for the HF lines. In actual practice enough CO_2 was admitted to the whole spectrometer chamber to make several lines of the $2\nu_2 + \nu_3$ band absorb 100 per cent. The zero-line of these CO_2 lines could be used as the zero-line of the HF lines. This CO_2 band lies at the low wave number side of the HF band.

Tests of the reproducibility of the data indicate that absorption can be measured to about ±1 per cent absorption. The error results mainly from measurements in the wings, where one invariably measures less absorption than is actually present.

Continuous Scanning Versus Point-by-Point Measurements

An examination was made of two techniques for taking data on spectral lines. One technique is that of automatically scanning slowly across a line. The other technique is that of manually setting the grating at specific wavelengths and letting the chart run for a minute at each setting in order to determine the deflection accurately. Both methods should give the same result as long as the response of the pen is fast enough for the energy change being recorded.

Figure 11(a) is a photograph of a portion of an automatic scan of the R(2) line of HF at a pressure of 5 cm in the 10 cm cell. Figure 11(b) is a photograph of the same portion of a manual scan of R(2) under the same conditions. Readings were taken at equal intervals of arc (0.0028°). Figure 12 compares the two techniques by showing a plot of per cent absorption as a function of relative grating angle for each set of data. Smooth curves drawn

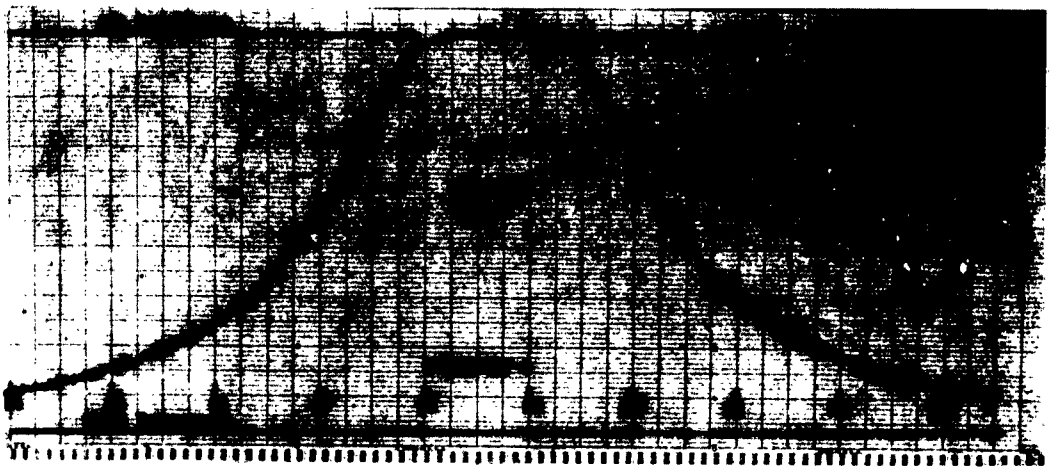

a.

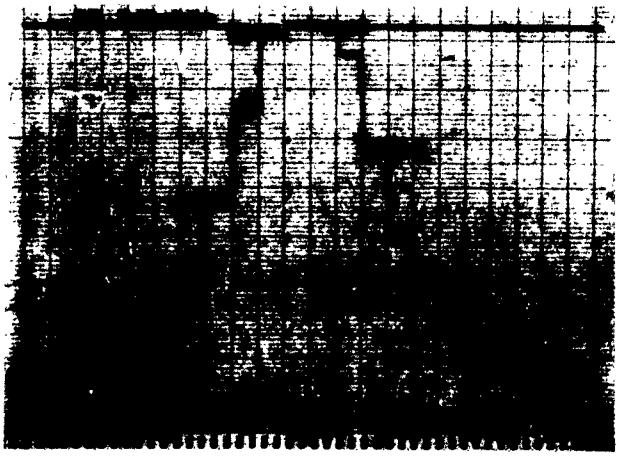

b.

Fig. 11. Automatic (a) and manual (b) scans of R(2) at 5 cm pressure.

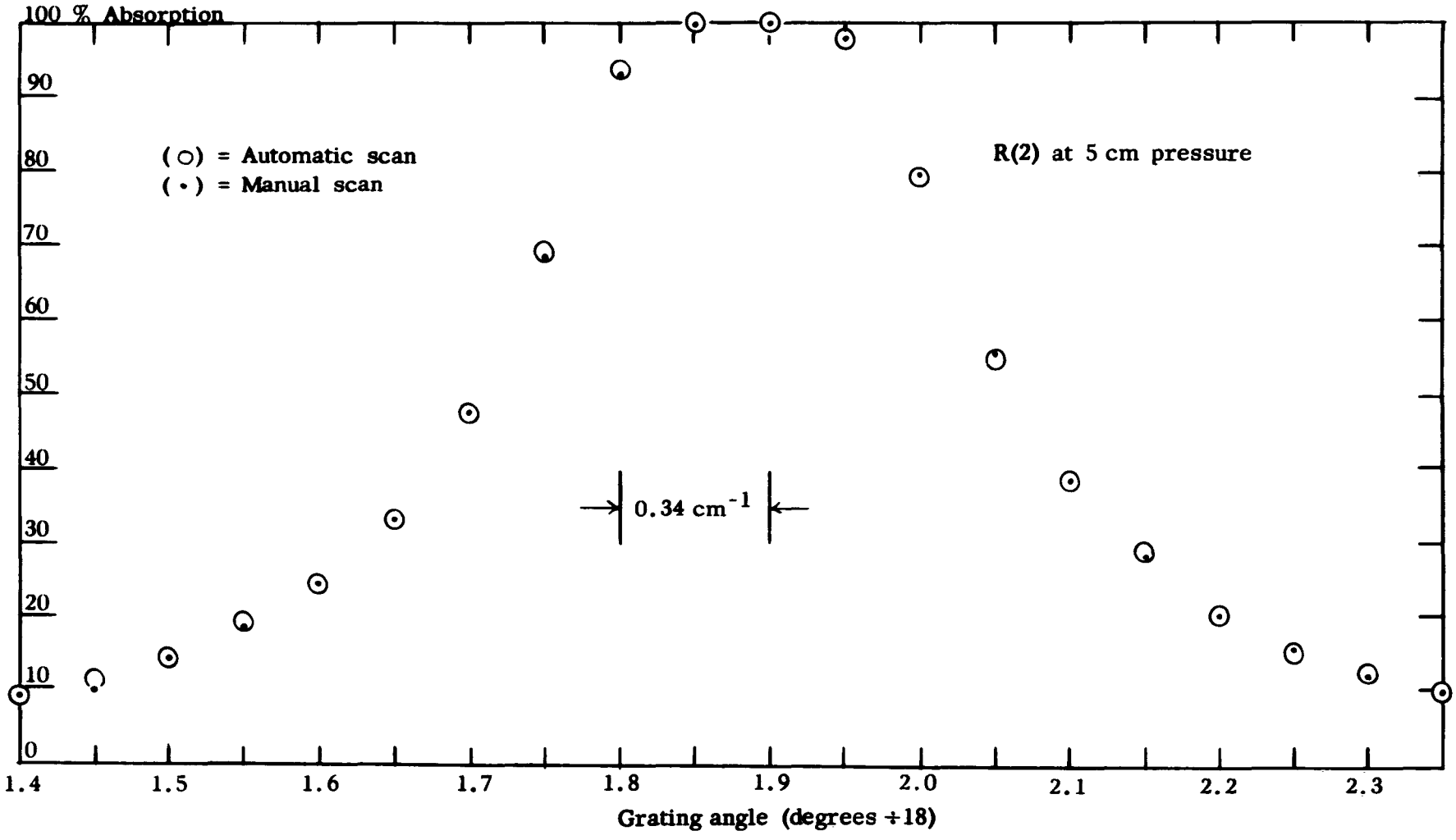

Fig. 12. Per cent absorption versus relative grating angle for automatic and manual scans of R(2) at 5 cm pressure.

through the two sets of data would agree to within about 1 per cent absorption. The reproducibility of the scanning drive is demonstrated by the agreement of the two methods. For the automatic scan the grating was turned at a speed of one-twelfth of a degree per hour, which is the slowest scanning speed available.

Figure 12 shows that if a spectral line is wide enough, automatic and manual scans give the same results. Automatic scanning is the most convenient method, and was used whenever possible. In actual practice the manual scan technique was used to take all 10 cm cell data that absorbed less than 100 per cent of the incident light. These data included the most narrow of the spectral lines. The automatic scan method was used to take all other 10 cm cell data and also to take all 0.047 cm cell data.

Calibration procedures can be carried out using either technique, but the techniques should not be intermixed. That is, if the central images are recorded by automatic scan, then any neon, CO, or HF lines should also be recorded by automatic scan. Different pen positions with respect to grating positions will be obtained from the two techniques because the overall response of the two recording systems are not the same. The two techniques will

predict the same wave number for any point in question to within ±0.02 cm^{-1}.

Corrections for Instrumental Broadening

Instrumental broadening of spectral lines is caused mainly by the use of spectrometer slits with finite width. Imperfect alignment and imperfect optics also contribute to instrumental broadening. The total effect on the line shape traced by the recording pen is an increase in absorption in the wings and a decrease in absorption at the line center, as compared with the true line shape. The effects of instrumental broadening are shown in Fig. 13. Far out in the wings of a line, where the absorption changes slowly with frequency, the measured shape and the true shape are essentially the same. The quantities A(v) and a(v) that appear in Fig. 13 will be defined later.

The first step in the process of correcting for instrumental broadening is to determine the "slit function." This function describes the line shape (normalized to unit area) that is obtained when a monochromatic absorption (or emission) line is scanned by the spectrometer. A monochromatic absorption line is impossible to obtain, but a very narrow absorption line is a good substitute. CO was found to be a convenient source of very narrow absorption lines.

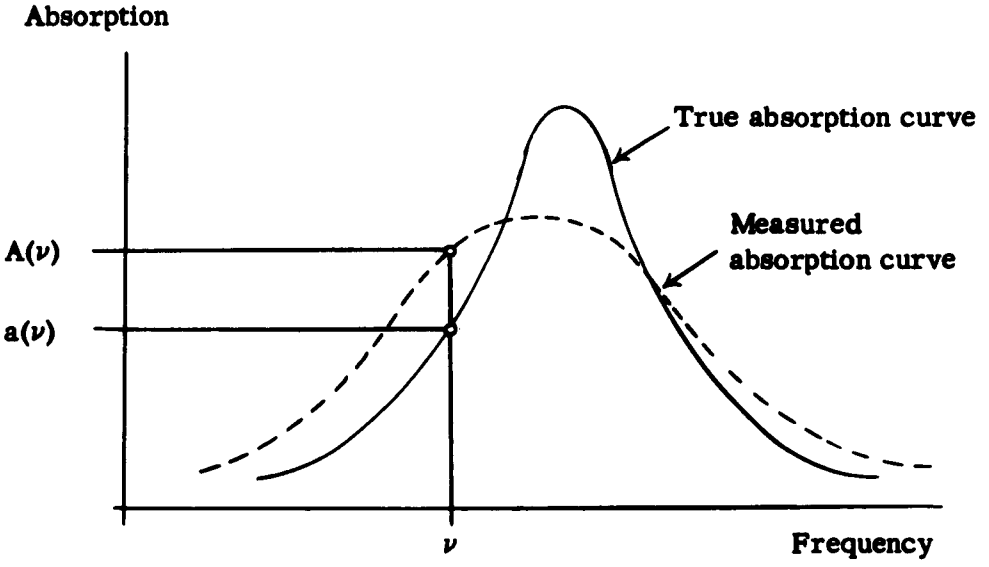

Fig. 13. True and measured absorption curves.

The natural width of a CO line is on the order of 10^{-5} cm^{-1}. This width is negligible compared to Doppler width of a CO line, which is about 10^{-3} cm^{-1} at room temperature. The spectrometer chamber was evacuated, and CO was admitted to a pressure of 0.5 cm. The R(6) line of the first overtone of CO was recorded with a 75 micron physical slit width and found to have a measured half-width at half-maximum of 0.06 cm^{-1}. This line was recorded again at a pressure of 1.0 cm and found to have essentially the same half-width. Since the half-width did not increase with pressure, pressure broadening did not contribute to the line shape, and the Doppler half-width could be taken as the true half-width. Since the true half-width was appreciably smaller than the measured half-width, this CO line could serve as a satisfactory approximation to a monochromatic absorption line. The shape obtained when the CO line was scanned by the spectrometer could be normalized to unit area and then be used as the slit function.

Figure 14(a) is a plot of absorption as a function of frequency for the R(6) line of CO. The line was measured at 0.5 cm pressure with a path length of 8.5 m and with a 75 micron physical slit width. The curve has been normalized to unit area, and is called the slit function, $S(\nu, \nu_o)$. $S(\nu, \nu_o)$ gives the absorption at frequency

$\nu(cm^{-1})$ produced by a monochromatic source of frequency $\nu_0(cm^{-1})$ and of unit intensity, when the predominant contribution to broadening is instrumental.

The width of the slit function will be a function of ν_0, since the spectral slit width depends on the frequency of light that is being scanned by the spectrometer. In fact, over the range of the HF spectrum the spectral slit width resulting from a physical slit width of 75 microns would change from 0.135 cm^{-1} at 4285 cm^{-1} to 0.082 cm^{-1} at 3700 cm^{-1}. However, as long as spectral lines several times the width of the slit function are to be corrected, it is felt that the changing physical slit width will not have too great an effect on line widths. Therefore, the slit function will be assumed not to vary with ν_0.

It is convenient to plot the slit function in terms of the distance (in cm^{-1}) from its center frequency $\nu - \nu'$, where ν' is the center frequency. Note that ν' is also the frequency at which the spectrometer is set. Figure 14(b) is a plot of the slit function, $S(\nu - \nu')$, as a function of $\nu - \nu'$. The shape of the slit function does not depend on ν'.

With reference to Fig. 13, assume that the true absorption curve is known. Let $a(\nu)$ be the true absorption in the frequency range ν to $\nu + d\nu$ if measured with

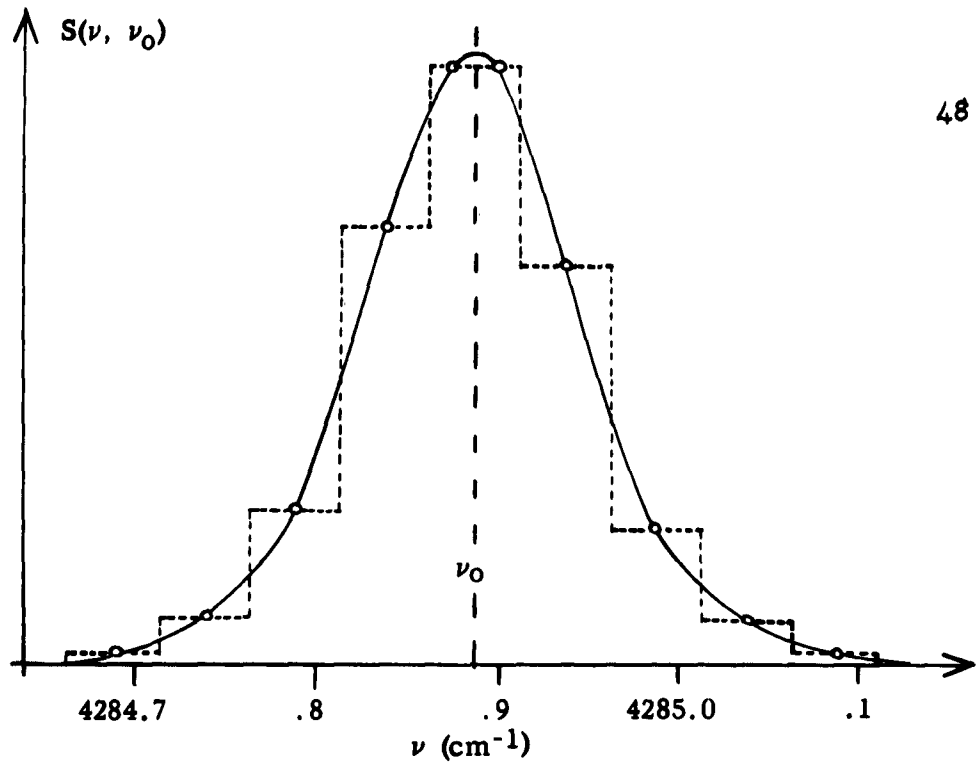

a.

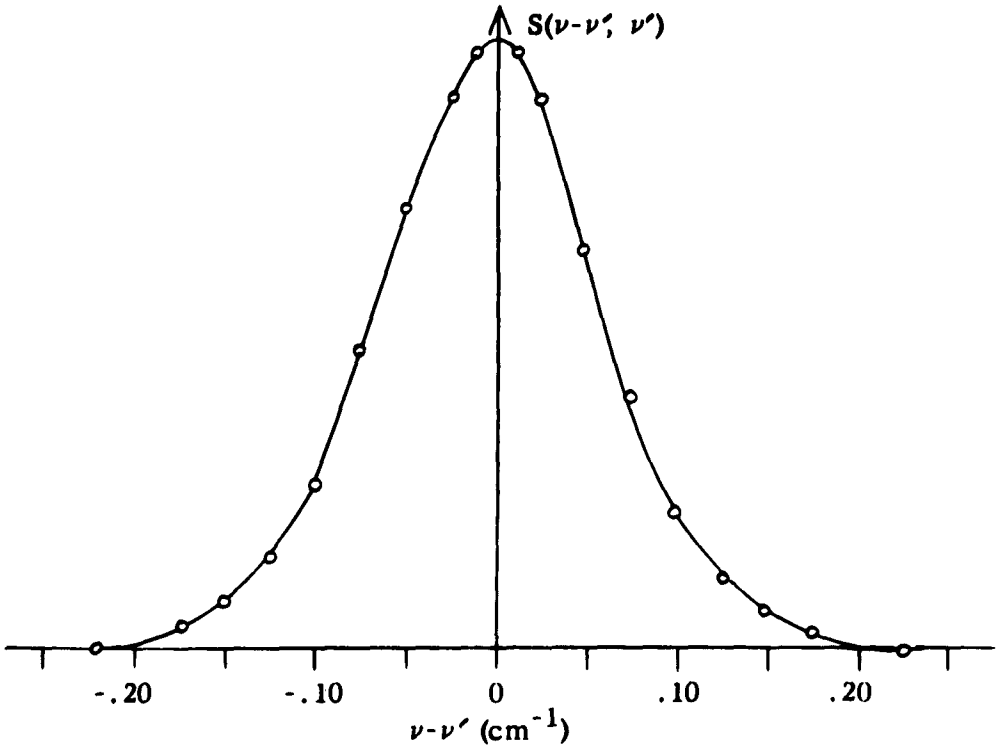

b.

Fig. 14. Slit function versus frequency, ν (a), and slit function versus frequency difference, $\nu - \nu_0$ (b).

monochromatic light. Then the measured absorption $A(\nu)$, in this frequency range will be composed of contributions not only from the range ν to $\nu + d\nu$, but also from the range of frequencies transmitted by the spectrometer when it is set on frequency ν.

One can therefore write

$$A(\nu) = \int_{-\infty}^{\infty} S(\nu - \nu')\, a(\nu')\, d\nu' \,, \qquad (2)$$

where $S(\nu - \nu')$ is the value of the slit function at ν when its center is at ν', and $a(\nu')$ is the true average absorption in the range ν' to $\nu' + d\nu'$. Note that in actual practice $A(\nu)$ and $S(\nu - \nu')$ are known and $a(\nu')$ is unknown. The limits of integration have been written as $-\infty$ to $+\infty$. However, since the measured and true absorption curves agree in the wings of a spectral line, where absorption changes slowly with ν, the correction procedure never had to be carried out to further than about 3 cm^{-1} from the line center. On very wide spectral lines absorption changed so slowly with frequency that the measured and true absorption curves agreed over the whole line shape, and no correction for instrumental broadening was needed.

The solving of Equation (2) requires an electronic computer. The computers available at the University of Tennessee cannot handle numerical integration, so it was necessary to replace the continuous frequency variable by

a number of discrete frequency steps μ (for narrow spectral lines one took $\mu = 0.02$ cm^{-1}, and for wide spectral lines one took $\mu = 0.05$ cm^{-1}). Equation (2) goes over to the sum

$$A(\nu_m) = \sum_{-\infty}^{\infty} S(\nu_m - \nu_n)\, a(\nu_n), \tag{3}$$

or, in a more concise notation

$$A_m = \sum_{-\infty}^{\infty} S_{mn}\, a_n \quad . \tag{4}$$

This last equation can be written in matrix form as

$$(A_m) = (S_{mn})(a_n). \tag{5}$$

The matricies (A_m) and (a_n) are column matrices whose elements are the average per cent absorptions in successive intervals of μ along the measured and true spectral lines, respectively. (S_{mn}) is a matrix constructed from the slit function elements. The method of constructing the slit function matrix is shown in Appendix A.

The first attempt at the calculation of (a_n) used a method developed by Deeds (5). This method was an exact method and involved the calculation of the inverse of the slit function matrix, $(S_{mn})^{-1}$, since solution of Equation (5) gives

$$(a_n) = (S_{mn})^{-1}\, (A_m) \quad . \tag{6}$$

Line shapes calculated in this manner oscillated wildly about a line shape that may have been close to the true line shape. It is felt that these oscillations were caused by errors made in measuring the wings of the slit function. One may be able to measure absorption to within ±0.5 per cent with very careful measurements. However, in the wings of the slit function where at some point the CO would be absorbing as little as 0.5 per cent, it would be fairly easy to have 100 per cent error. Wing errors are caused by uncertainty in the location of the base-line. These errors become quite significant in the calculation of the elements of the inverse of the slit function matrix.

It was therefore decided to try an approximation method similar to that developed by D. E. Smith, V. Anderson, and G. Kuipers and used in the work of Kuipers (12). First the measured line shape, (A_n), was multiplied by the slit function, (S_{mn}) to give the curve

$$(A^{(1)}_m) = (S_{mn})(A_n). \tag{7}$$

This curve was subtracted from the measured curve, and the difference was added to the measured curve. This operation gave the curve

$$(a^{(1)}_m) = (A_m) + [(A_m) - (A^{(1)}_m)], \tag{8}$$

which is a first approximation to the true curve, (a_m). This first approximation is then multiplied by the slit function to give the curve

$$(A^{(2)}_m) = (S_{mn})(a^{(1)}_n). \tag{9}$$

The difference and sum operation is performed again to give

$$(a^{(2)}_m) = (a^{(1)}_m) + [(A_m) - (A^{(2)}_m)]. \tag{10}$$

This curve, $(a^{(2)}_m)$, is a second approximation to (a_m). The whole operation is performed once more to give

$$(A^{(3)}_m) = (S_{mn})(a^{(2)}_n) \tag{11}$$

and

$$(a^{(3)}_m) = (a^{(2)}_m) + [(A_m) - (A^{(3)}_m)]. \tag{12}$$

The curve $(a^{(3)}_m)$ is a third approximation to the true curve, (a_m).

These calculations were carried out for each measured line shape by an IBM 1620 computer. After each approximation was obtained, the computer multiplied it by the slit function and compared the result with the measured curve. For instance, $(S_{mn})(a^{(3)}_n)$ is compared with (A_m). The closer an approximation is to the true curve, the closer the approximation multiplied by the slit function will be to the measured curve. In all cases the third approximation proved to be the best. When the slit function

was multiplied into higher approximations, the results grew further away from the measured curve. Very wide lines were found to need no correction for instrumental broadening. The correction method did not give acceptable results when applied to spectral lines that were narrower than lines about five times as wide as the slit function.

The relative shapes of some of the curves used in the approximation method are shown in Fig. 15. The true curve, the experimental curve, and the experimental curve multiplied by the slit function are shown.

The measured data were "smoothed" before being multiplied by the slit function, and each approximation was also smoothed. In the smoothing process five consecutive points on a line were fitted to a parabola. The center point, $A(\nu_i)$ in Fig. 16, was then moved so that it would lie on the parabola. This process was carried out for each point on the line.

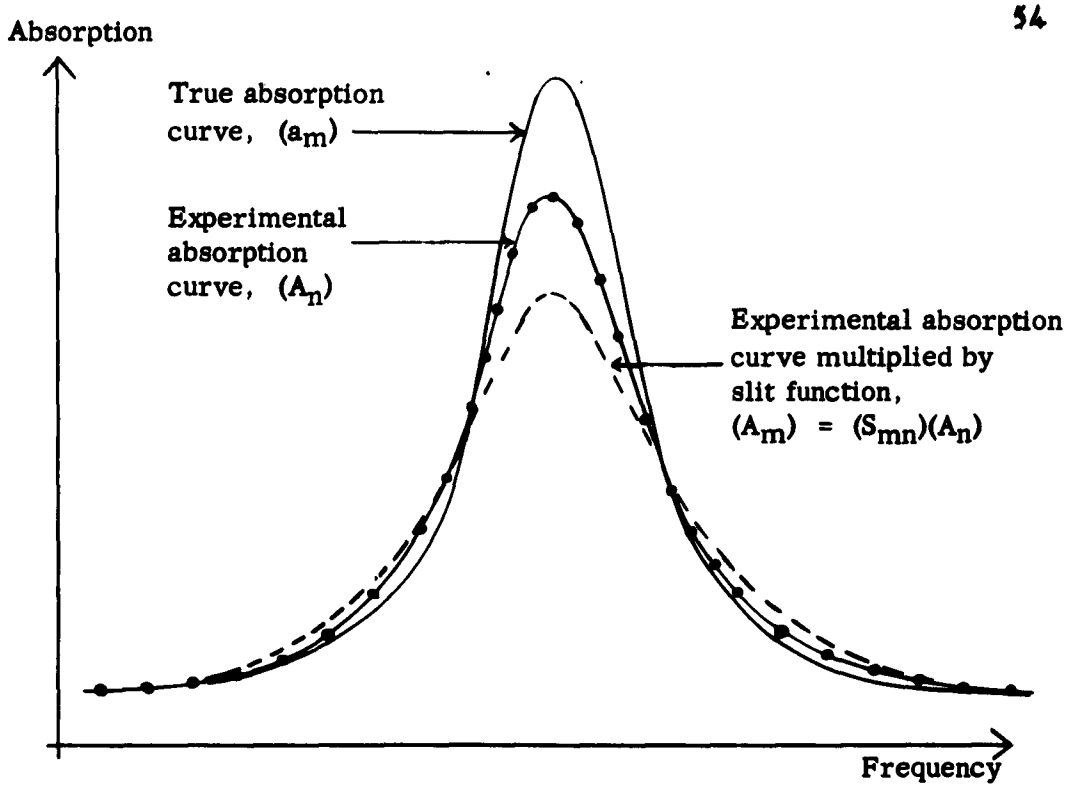

Fig. 15. Some curves used in the slit correction procedure.

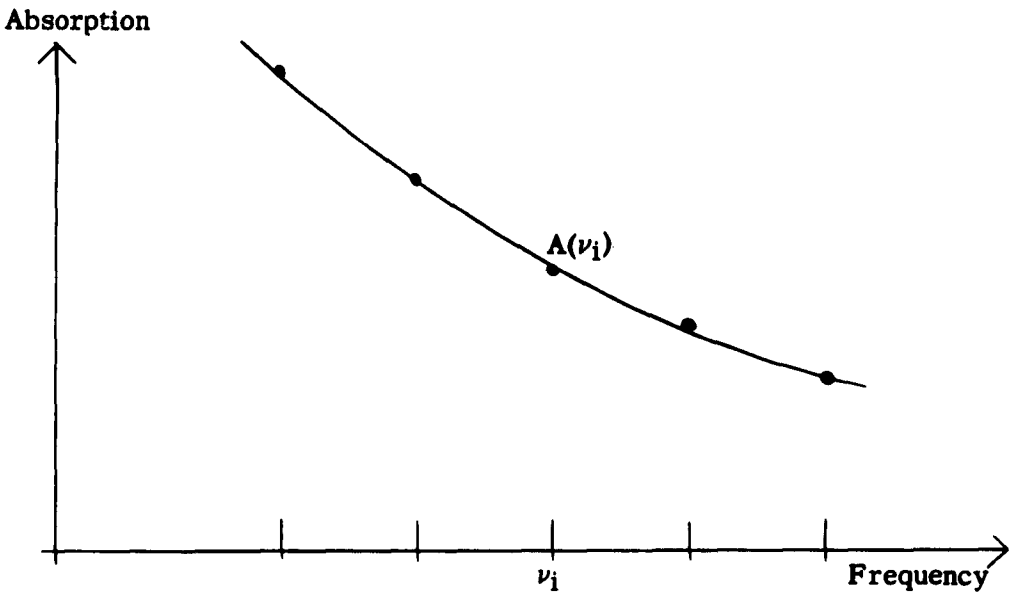

Fig. 16. Method of smoothing spectral lines.

CHAPTER III

RESULTS AND TREATMENT OF DATA

I. LINE POSITIONS

Frequencies of the Fundamental and First Overtone Lines

The center frequencies of eleven HF absorption lines of the fundamental were measured in the R branch and six were measured in the P branch at 1 cm pressure in the 10 cm cell. Because of the decrease in signal to noise ratio towards low wave numbers, P(7, 8, and 9) were measured at 5 cm pressure and P(10) was measured at 50 cm pressure. Each line center was measured three times, and agreement on separate measurements was within about ±0.02 cm^{-1}.

A rotational analysis of the line centers was carried out using the method of Herzberg (10) and following the same notation as used by Mann and his coworkers (14). The wave numbers of the individual rotational lines may be expressed as

$$\nu_m = \sum_{k=0}^{N} c_k m^k \ , \qquad (13)$$

where m = J+1 for the R branch, and m = -J for the P branch. The coefficients, c_k, will be discussed in the following section. A least squares fit of the observed wave numbers to Equation (13) was carried out on an IBM

1620 computer. Several values of N were tried, and it was found that a polynomial of degree N = 7 gave the best fit. Table I lists the observed and calculated line centers for the HF fundamental.

The line centers for the first overtone were measured at 10 cm pressure in the 10 cm cell. Gratings with 15,240 and 7,620 lines per inch were each used in second order, and the two determinations agreed to within ±0.02 cm^{-1}. The rotational analysis showed that a polynomial of degree N = 5 gave the best fit. The results are given in Table II.

Spectroscopic Constants

The c_k of Equation (13) are defined in terms of the usual spectroscopic constants (up to order 7) in the following way (the order of magnitude of each constant is given in cm^{-1}):

$c_o = \nu_o$	3960
$c_1 = (B'+B'')$	40
$c_2 = (B'-B'') - (D'-D'')$	1
$c_3 = -2(D'+D'') + (H'+H'')$	10^{-3}
$c_4 = -(D'-D'') + 3(H'-H'')$	10^{-5}
$c_5 = 3(H'+H'') + 8Y_{04}$	10^{-7}
$c_6 = (H'-H'')$	10^{-8}
$c_7 = 8Y_{04}$	10^{-11}

TABLE I

OBSERVED AND CALCULATED LINE CENTERS
FOR THE HF FUNDAMENTAL

Spectral Line	Observed (cm^{-1})	Calculated (cm^{-1})	Obs.-Calc. (cm^{-1})
R(10)	4301.45	4301.45	0.00
R(9)	4279.94	4279.94	0.00
R(8)	4256.33	4256.34	-0.01
R(7)	4230.78	4230.77	+0.01
R(6)	4203.31	4203.30	+0.01
R(5)	4173.99	4173.98	+0.01
R(4)	4142.85	4142.85	0.00
R(3)	4109.95	4109.95	0.00
R(2)	4075.29	4075.31	-0.02
R(1)	4038.96	4038.98	-0.02
R(0)	4001.02	4001.00	+0.02
P(1)	3920.33	3920.32	+0.01
P(2)	3877.72	3877.71	+0.01
P(3)	3833.68	3833.67	+0.01
P(4)	3788.21	3788.24	-0.03
P(5)	3741.48	3741.47	+0.01
P(6)	3693.42	3693.41	+0.01
P(7)	3644.09	3644.11	-0.02
P(8)	3593.67	3593.65	+0.02
P(9)	3542.13	3542.14	-0.01
P(10)	3489.76	3489.75	+0.01

TABLE II

OBSERVED AND CALCULATED LINE CENTERS
FOR THE HF FIRST OVERTONE

Spectral Line	Observed (cm^{-1})	Calculated (cm^{-1})	Obs.-Calc. (cm^{-1})
R(8)	7978.37	7978.37	0.00
R(7)	7966.23	7966.21	+0.02
R(6)	7950.70	7950.69	+0.01
R(5)	7931.82	7971.84	-0.02
R(4)	7909.67	7909.69	-0.02
R(3)	7884.28	7884.28	0.00
R(2)	7855.65	7855.65	0.00
R(1)	7823.84	7823.84	0.00
R(0)	7788.90	7788.88	+0.02
P(1)	7709.73	7709.73	0.00
P(2)	7665.64	7665.62	+0.02
P(3)	7618.55	7618.57	-0.02
P(4)	7568.62	7568.62	0.00
P(5)	7515.85	7515.85	0.00
P(6)	7460.30	7460.30	0.00
P(7)	7402.05	7402.06	-0.01
P(8)	7341.22	7341.20	+0.02

The constant Y_{04} is one of the Dunham (6) constants. Since only twenty-three spectral lines could be measured for line centers in the fundamental in the 10 cm cell, only the constants up to c_3 could be meaningfully determined. Even though observed and calculated line centers agreed quite well, the smaller constants were as much as several orders of magnitude in error, and some had the wrong sign.

In the work of Mann (14) twenty-three rotational bands were analysed in emission, and many more lines in each band could be measured than in the present work. Mann was able to obtain good values of c_5 and c_6 for many bands. His values of B_v, D_v, and H_v were then obtained from the averages of values calculated from individual bands. Table III lists the meaningful values of the c_k obtained for the fundamental and first overtone in this present work.

Since H_v is much less than D_v, the equations for c_3 and c_4 could be used to calculate D' and D". Then B' and B" could be obtained from the equations for c_1 and c_2. Table IV lists the values obtained for ν_0, B_v, and D_v in this present work along with Mann's values. The symbols (0-1) and (0-2) stand for the fundamental and first overtone transitions, respectively. The values of B_v measured in this present work agree quite well with Mann's values. Mann's values for D_v are probably more accurate than those of this work since more lines were measured in

TABLE III

COEFFICIENTS OF ROTATIONAL ANALYSIS
FOR THE FUNDAMENTAL AND
FIRST OVERTONE
OF HF

Constant	Fundamental (cm^{-1})	First Overtone (cm^{-1})
c_0	3961.43	7750.83
c_1	40.3512	39.5857
c_2	-0.7707	-1.5257
c_3	-8.873×10^{-3}	-8.001×10^{-3}
c_4	3.74×10^{-5}[a]	0.1270×10^{-5}

[a]Mann's value

TABLE IV

CALCULATED VALUES OF
ν_o, B_v, AND D_v
FOR HF

Constant	Transition	Present Work (cm^{-1})	Mann, et al (cm^{-1})
ν_o	(0-1)	3961.43	3961.60
ν_o	(0-2)	7750.83	7750.98
B_o	(0-1)	20.5609	20.5590[a]
B_o	(0-2)	20.5557	
B_1	(0-1)	19.7902	19.7883
B_2	(0-2)	19.0300	19.0355
D_o	(0-1)	.002243	.002120[a]
D_o	(0-2)	.002064	
D_1	(0-1)	.002193	.002064
D_2	(0-2)	0.001937	0.002010

[a]Averaged from (0-1) and (0-2) transitions.

each band. For the reasons discussed in the section on calibration procedures, it is felt that the band centers obtained in this present work are accurate to at least ± 0.02 cm^{-1}.

Calculated values of the band centers for the (0-1) and (0-2) transitions obtained in this present work are somewhat different from Mann's values. Among the many transitions reported by Mann is the set (5-0), (5-1), and (5-2). It was noted that when the (0-1) and (0-2) frequencies of this present work were added to Mann's (5-1) and (5-2) frequencies, respectively, the sums were exactly equal to Mann's (5-0) frequency. Such agreement did not exist if Mann's (1-0) and (2-0) frequencies were used. Similar results were observed for similar sets of transitions.

It appeared, therefore, that a more consistent set of vibrational term values might be obtained by using the (0-1) and (0-2) band centers of this present work rather than Mann's (1-0) and (2-0) band centers, along with Mann's band centers for the higher overtones. The vibrational term values, E_v, can be expressed in terms of the Dunham coefficients, Y_{k0}, and the vibrational quantum number, v, by the expression developed by Dunham (6):

$$E_v = \sum_k Y_{k0} \left(v + \tfrac{1}{2}\right)^k . \qquad (14)$$

Nine band centers were fit to this expression (k ranged from 0 to 6) by a least squares, double precision routine on an IBM 7090 computer.* The observed and calculated band centers are listed in Table V. The various transitions which were used to calculate each overtone band center are also listed. The (0-1) and (0-2) band centers are those of this present work. The (3-0) and (4-0) band centers are the averages of Mann's and Kirkpatrick's (13) values. Mann's values are used for all other band centers. Each band center was weighted according to an estimation of its accuracy. The molecular constants that could be obtained are listed in Table VI.

Line Center Shifts

Within experimental error, the line centers measured at 5 and 50 cm pressure were the same as those measured at 1 cm pressure. Line centers measured at 1 atm pressure showed slight shifts from the 1 cm pressure line centers, but the shifts were the same order of magnitude as experimental error. Line centers measured at 5 atm pressure differed from those measured at 1 cm by as much as tenths of wave numbers. Table VII lists the line centers measured

*Private communication from N. M. Gailar. A more complete analysis is to be carried out, and the results will be published at a later date.

TABLE V

OBSERVED AND CALCULATED
BAND CENTERS
FOR HF

v	ν_o(Obs.) (cm^{-1})	Transitions used in calculation of ν_o	Weight Factor	ν_o(Calc.) (cm^{-1})
1	3961.43[a]	(0-1)	6	3961.43
2	7750.83[a]	(0-2)	5	7750.83
3	11372.92[b]	(3-0)	4	11372.91
4	14831.75[b]	(4-0), (4-1)+(0-1)	3	14831.78
5	18131.10[c]	(5-0), (5-1)+(0-1), (5-2)+(0-2)	4	18131.08
6	21273.86[c]	(6-1)+(0-1), (6-2)+(0-2)	4	21273.86
7	24262.43[c]	(7-2)+(0-2), (7-3)+(3-0)	4	24262.43
8	27098.23[c]	(8-3)+(3-0), (8-4)+(4-0)	3	27098.23
9	29781.69[c]	(9-4)+(4-0)	1.5	29781.69

[a]Values measured in this present work.

[b]Average of Mann's and Kirkpatrick's values.

[c]Values measured by Mann.

TABLE VI

SOME MOLECULAR CONSTANTS OF HF

Constant	Present Values (cm^{-1})	Mann's Values (cm^{-1})
Zero point energy	2046.24	2046.97
ω_e	4137.89	4139.04
B_e	20.9562	20.9560
Y_{10} (Dunham Const.)	4137.46	4138.73
Y_{20} (Dunham Const.)	-89.42	-90.05
Y_{30} (Dunham Const.)	0.796	0.932

TABLE VII

LINE CENTERS AND LINE SHIFTS MEASURED AT 1 AND 5 ATM PRESSURE

Spectral Line	ν_o 1 atm (cm^{-1})	ν_o 5 atm (cm^{-1})	Shift: 5 atm wrt 1 cm (cm^{-1})	Shift: 5 atm wrt 1 atm (cm^{-1})
R(12)				-0.03[a]
R(11)				-0.03[a]
R(10)				-0.05[a]
R(9)				-0.06[a]
R(8)	4256.30	4256.23	-0.10	-0.07
R(7)	4230.74	4230.68	-0.10	-0.06
R(6)	4203.29	4203.14	-0.14	-0.12
R(5)	4173.97	4173.88	-0.10	-0.08
R(4)	4142.83	4142.70	-0.14	-0.12
R(3)	4109.91	4109.82	-0.13	-0.09
R(2)	4075.28	4075.29	+0.01	+0.01
R(1)	4039.00	4039.01	+0.04	+0.01
R(0)	4001.05	4001.17	+0.13	+0.12
P(1)	3920.30	3920.22	-0.11	-0.08
P(2)	3877.76	3877.78	+0.06	+0.02
P(3)	3833.72	3833.73	+0.05	+0.01
P(4)	3788.22	3788.21	-0.01	-0.01
P(5)	3741.48	3741.49	+0.01	+0.01
P(6)	3693.37	3693.44	+0.01	+0.07
P(7)	3644.13	3644.19	+0.06	+0.02
P(8)	3593.69	3593.74	+0.07	+0.05

[a]These values were measured in the 10 cm cell; all others were measured in the 0.047 cm cell.

at 1 and 5 atm pressure. Each value is the average of at least two measurements. The shifts of the 5 atm pressure line centers with respect to the 1 cm and 1 atm pressure line centers are also listed.

Lines R(2) and R(6) were measured for line centers at 4, 3, and 2 atm pressure, in addition to 5 and 1 atm pressure. Line center shifts are plotted as functions of pressure for these lines in Fig. 17. It is seen that the shifts are proportional to pressure to within ± 0.02 cm^{-1}.

Spectral line shifts similar to those observed in HF have been observed in HCl by Jaffe and his coworkers (11). Their data, plotted in terms of line shift per unit pressure, are shown in Fig. 18. The line shifts observed in HF in this present work were divided by the pressure changes involved (5 and 4 atm) and the results averaged for each line. The results are plotted in terms of line shift per unit pressure in Fig. 19. The curve joining the points allows for an error of ± 0.02 cm^{-1} in any measurement. The curve connecting Jaffe's data is as drawn by him.

The shifts discussed above are self-induced, both for HF and HCl. Recently Jaffe and his coworkers (3) have reported on HCl shifts caused by the presence of the noble gases. Argon and neon caused shifts in HCl that exhibit somewhat the same J dependence as the self-induced HF shifts. Krypton and xenon caused shifts in HCl that

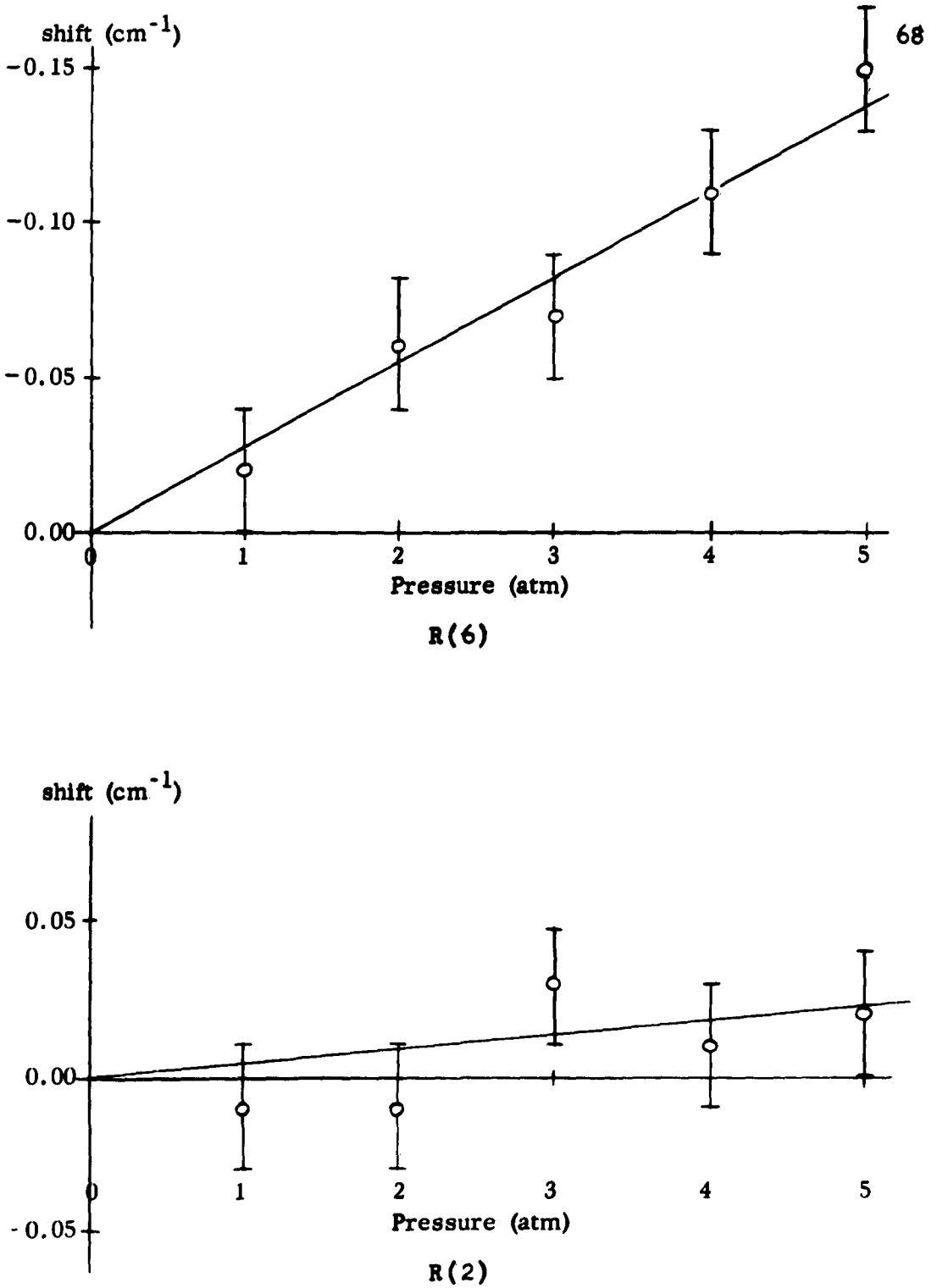

Fig. 17. Measured line shifts for R(6) and R(2).

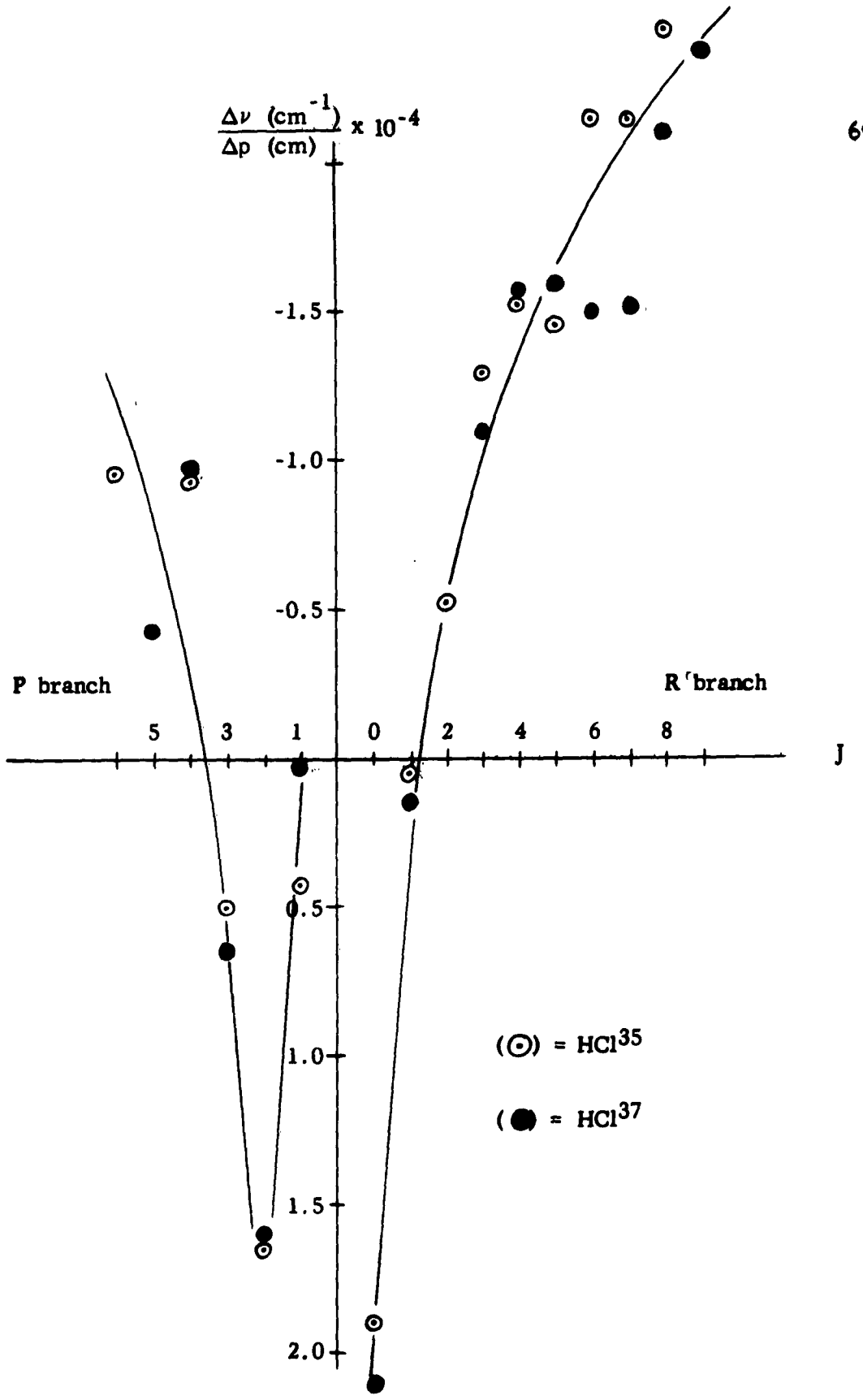

Fig. 18. Line center shift per unit pressure in HCl.

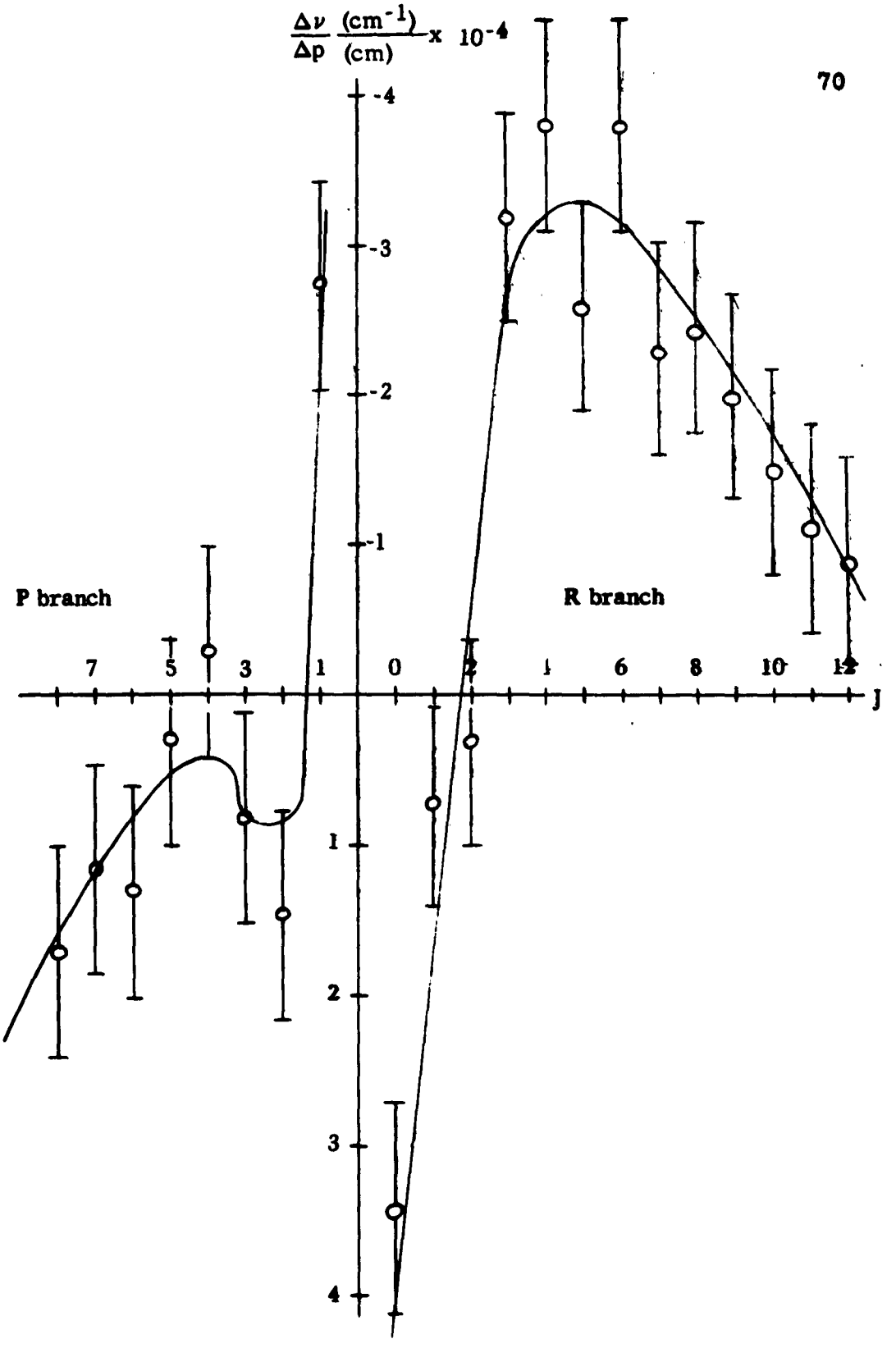

Fig. 19. Line center shift per unit pressure in HF.

increased with J number in both the R and P branches. At present there is no theory that accounts for the J dependence of line shifts.* However, Jaffe points out that the foreign gas induced shifts have some dependence on the polarizability of the foreign gas. The polarizability of HF is quite close to that of argon and neon. Thus the reaction between the permanent dipole moment of one molecule and the induced dipole moment of another molecule may well have some effect on line shifts.

II. LINE SHAPES

General Treatment

In his treatment of the high pressure (about 5 atm pressure) HF absorption lines measured by Kuipers (12), D. F. Smith (18) found that the data could be fitted by a modified form of the Lorentz expression. The well-known Lorentz expression for the shape of a spectral line can be expressed as

$$\alpha = \frac{\alpha_o (\Delta\nu)^2}{(\nu - \nu_o)^n + (\Delta\nu)^2} , \qquad (15)$$

---

*Private communication from DeForest Smith, after his attendance at the Symposium on Line Shapes, Rehovoth, Israel, August, 1961.

with the exponent n = 2. The quantity α is the absorption coefficient (in cm^{-1}) at frequency ν (in cm^{-1}). The quantity α_o is the maximum value of the absorption coefficient and is measured at the line center, ν_o. The quantity $\Delta\nu$ is the "Lorentz half-width" of the line and is equal to $|\nu - \nu_o|$ measured where $\alpha = \frac{1}{2}\alpha_o$. The absorption coefficient at a particular frequency is related to the per cent transmission, T, at that frequency by the expression

$$T = e^{-\alpha L}, \qquad (16)$$

where L is the path length (in cm) in the absorbing gas. Smith found that n = 1.8 gave a satisfactory fit of the Kuipers data at distances greater than several wave numbers from the line center. The methods of Smith were used in the analysis of the data of this present work in order to determine $\Delta\nu$ and n.

In the following sections n will be referred to as the "Lorentz exponent." Another half-width measurement that will be used is called the "half-absorption half-width" and will be represented by the symbol $\delta\nu$. The half-absorption half-width is the value of $|\nu - \nu_o|$ measured at one-half the maximum per cent absorption of the line in question.

The original data, as measured by the author, are presented as per cent absorption versus wave number in an

earlier report by Nielsen, et al (5). The first step in the treatment of these data was to correct the absorption lines for the effects of instrumental broadening, as discussed in the section on data taking and handling. Then α was calculated from Equation (16), with the aid of an IBM 1620 computer, for convenient values of ν.

A correction then had to be made to the 50 cm and 5 atm pressure lines for the effects of overlapping by neighboring lines. For example, at the center of R(2) at 5 atm pressure the absorption would be mainly from R(2) itself, but there would also be measurable contributions from R(0, 1, 3, 4, and 5) and P(1, 2, and 3). Following Smith, the absorption due to neighboring lines at frequency ν was calculated from the expression

$$\sum_i \alpha_i = \sum_i \frac{\alpha_{o_i} (\Delta\nu_i)^2}{(\nu - \nu_{o_i})^{1.8} + (\Delta\nu_i)^2} \quad . \qquad (17)$$

The quantities α_{o_i} and $\Delta\nu_i$ were estimated for the i^{th} line from the 1 atm data. The sum was computed for all lines that had an appreciable α_i at ν except the one in question. Usually the sum was calculated at three points for a particular line: at $\nu = \nu_o$ and $\nu = \nu_o \pm 10$ cm^{-1}. A smooth curve drawn through the three points gave an α correction curve for all frequencies across the one line in question. A value of α obtained from the correction

curve at a particular frequency could be subtracted from the observed α at that frequency to obtain the true value of α for the line in question at that frequency.

After all lines were corrected for overlap from other lines, the data were ready to be submitted to Smith's treatment. Equation (15) can be rearranged to give

$$\frac{\alpha_o - \alpha}{\alpha} = \frac{(\nu - \nu_o)^n}{(\Delta\nu)^2} . \qquad (18)$$

From this equation two other useful equations can be obtained:

$$\left(\frac{\alpha_o - \alpha}{\alpha}\right)^{1/n} = (\Delta\nu)^{-2/n}\ \nu - (\Delta\nu)^{-2/n}\ \nu_o ; \qquad (19)$$

and

$$\text{Log}\ \frac{\alpha_o - \alpha}{\alpha} = n\ \text{Log}\ \left|\nu - \nu_o\right| - 2\ \text{Log}\ (\Delta\nu) . \qquad (20)$$

Both equations are of the form

$$y = mx + b , \qquad (21)$$

and therefore graphs of Equations (19) and (20) should yield straight lines. For Equation (19) one plots

$$\frac{\nu_o - \nu}{\left|\nu - \nu_o\right|}\ \left(\frac{\alpha_o - \alpha}{\alpha}\right)^{1/n}$$

as a function of ν. The term $\frac{\nu_o - \nu}{\left|\nu - \nu_o\right|}$ is introduced as a sign factor to make the curve continuous rather than "V"

shaped. If n is estimated properly, the graph of Equation (19) will be a straight line. Actually, n was assumed to be either 2 or 1.8 in order to graph Equation (19). This graph is used to determine the line center and not to determine n. Where the curve crosses the frequency axis, $\nu = \nu_o$. This intercept determines the line center. As an example, Fig. 20 shows the graph of Equation (19) for R(1) at 1 atm pressure.

On narrow spectral lines calibration was carried out at the same time that intensity measurements were made. In these cases the value of ν_o obtained from a graph of Equation (19) agreed with the value measured directly from the recorder chart. On wide lines calibration was carried out separately from intensity measurements, and in this case Equation (19) gave a value of ν_o relative to other values of ν for a line, but not an absolute value.

The value of ν_o obtained from the graph of Equation (19) was then used in Equation (20), where $\text{Log } \frac{\alpha_o - \alpha}{\alpha}$ is plotted as a function of $\text{Log } |\nu - \nu_o|$. This plot should give a straight line with slope n. The Lorentz half-width, $\Delta\nu$, can be calculated from the intercept where $\text{Log } |\nu - \nu_o| = 0$. This intercept is equal to $-2 \text{ Log } (\Delta\nu)$. Figure 21 shows the graph of Equation (20) for R(1) at 1 atm pressure. Graphs of Equations (19) and (20) were made for all spectral lines.

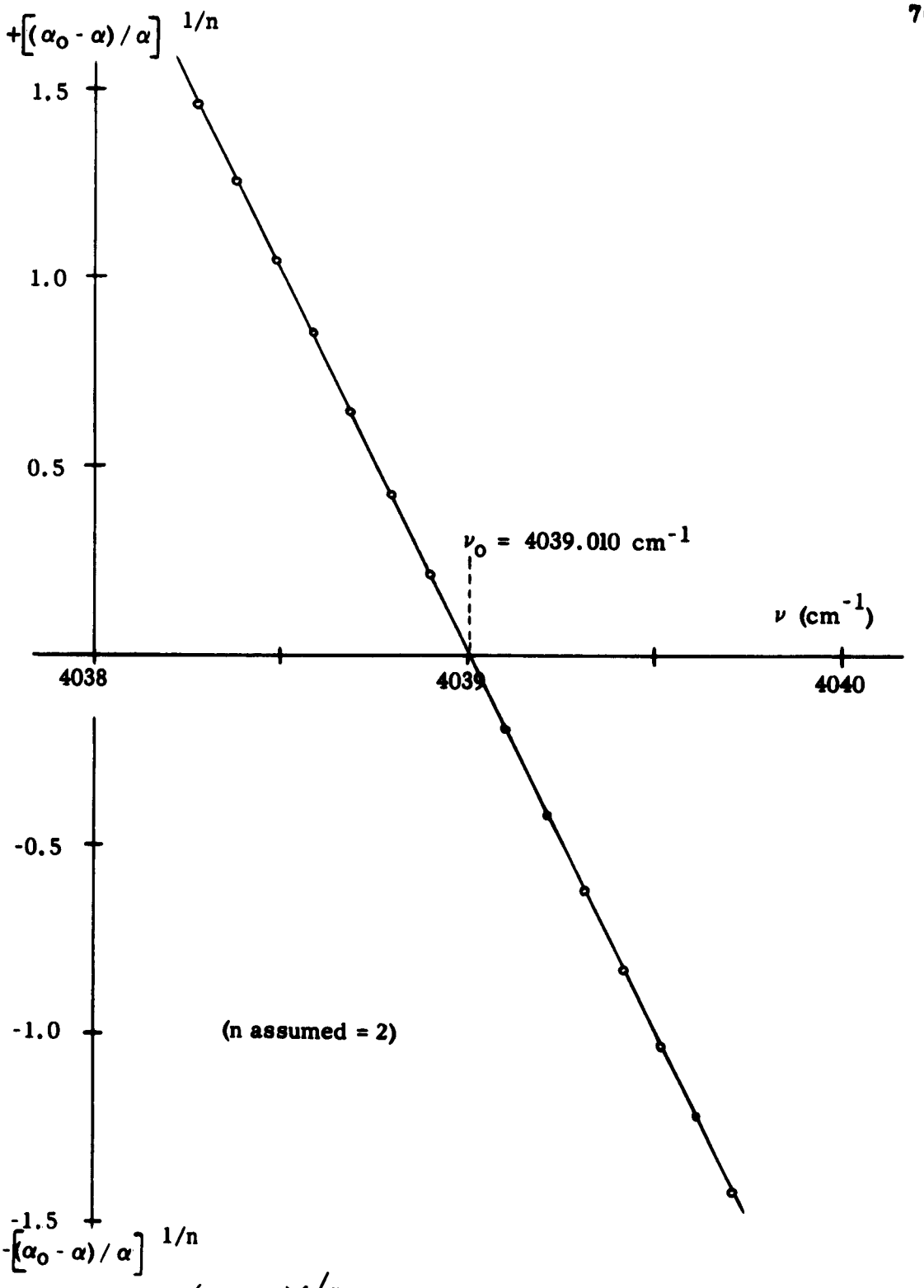

Fig. 20. $\left(\frac{\alpha_o - \alpha}{\alpha}\right)^{1/n}$ versus ν for R(1) at 1 atm pressure.

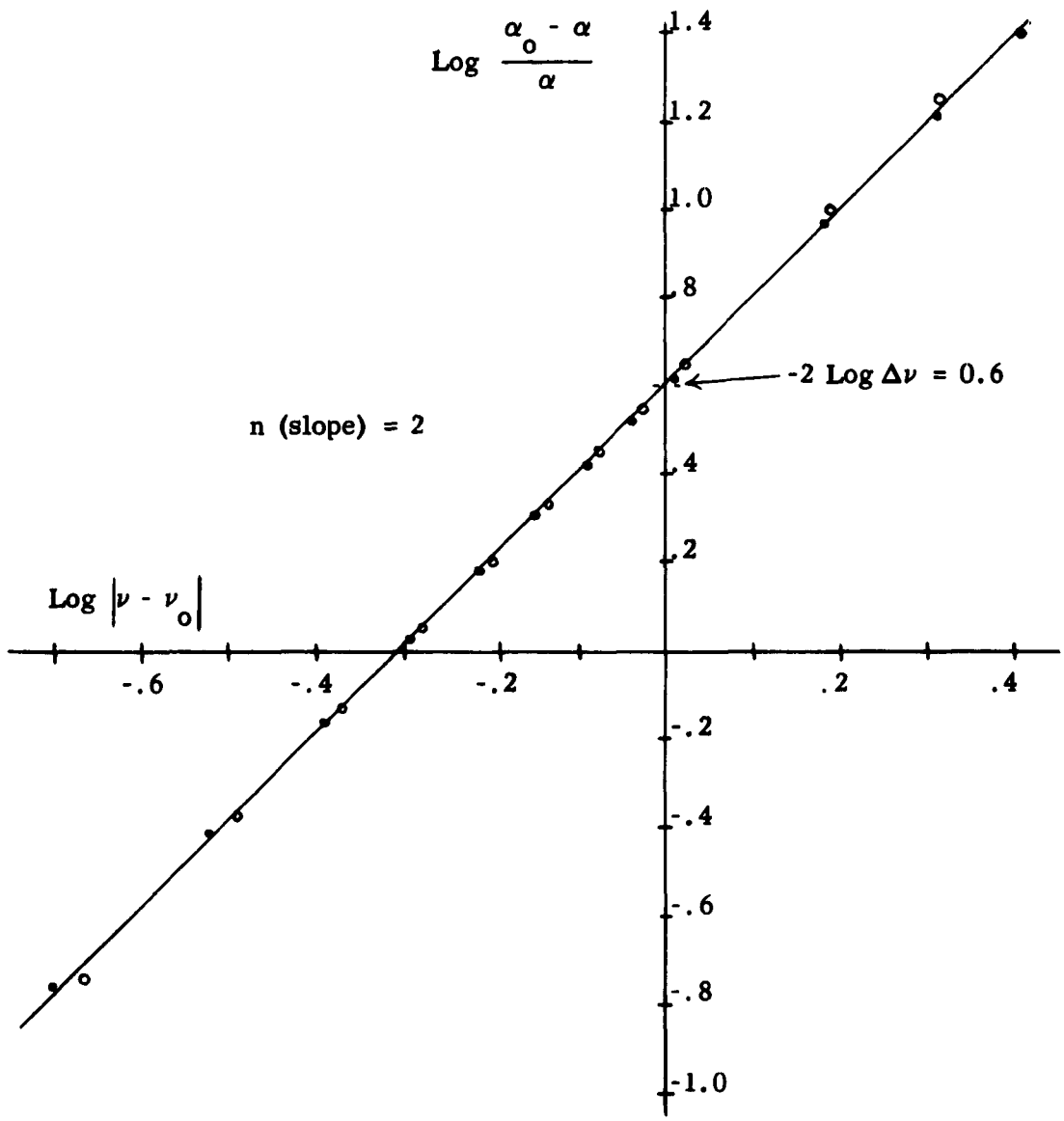

Fig. 21. Log $\frac{\alpha_o - \alpha}{\alpha}$ versus Log $|\nu - \nu_o|$ for R(1) at 1 atm pressure.

Since the 1, 5, and 50 cm pressure lines all absorb 100 per cent at their line centers (for the 10 cm cell), α_o could not be determined from their curves. However, α_o is constant for lines of the same J value (at constant temperature) as long as pressure broadening is the main cause of the line broadening. Thus the values of α_o measured at 1 atm pressure could be used for corresponding lines at lower pressures.

As more and more lines were subjected to analysis, a pattern began to emerge. Most of the data for each spectral line yielded straight lines when plotted with Equations (19) and (20). Data from portions of a spectral line where absorption was less than 10 per cent usually curved away from a straight line, and data from very close to the line center usually scattered, both for reasons discussed below. Absorption due to H_2F_2 was observed in the 50 cm and 5 atm pressure spectra, and the lines P(1, 2, 3, and 4) had to be treated separately at these pressures. The method used to correct for instrumental broadening appeared to break down when applied to the narrowest spectral lines.

The discussion of line shapes will now be divided into four parts: the central portion of lines, where absorption is greater than 10 per cent; the line wings; the dimer region; and the lines that were too narrow to be corrected for the effects of instrumental broadening.

Central Portions of Spectral Lines

As discussed in the section on data taking, it was felt that one could measure absorption with an accuracy of ±1 per cent absorption. This overall accuracy means that in the wings the per cent error in a measurement could become quite large. For example, the true absorption might be 2 per cent and one might measure 1 per cent. As a result, the quantity $\frac{\alpha_o - \alpha}{\alpha}$ can be rather inaccurate in the wings. In actual practice Equations (19) and (20) were not applied to data of less than 10 per cent absorption for the narrower lines, nor to data with $|\nu - \nu_o|$ greater than 10 cm^{-1} for the wider lines. The quantity $\frac{\alpha_o - \alpha}{\alpha}$ also becomes inaccurate as α approaches α_o, so that data close to the line center (within about 10 per cent of the maximum per cent absorption) could not be used with Equations (19) and (20).

The data which were used with Equations (19) and (20) are presented in Appendix B. In addition to drawing curves for Equations (19) and (20), the data were also fitted to Equation (20) by an IBM 1620 computer. The computer calculated the slope of the curve (the Lorentz exponent n) and the intercept where Log $|\nu - \nu_o| = 0$ ($-2 \log \Delta\nu$). The results of the calculations are listed in Table VIII. If no values are given for a spectral line at a particular pressure, it is because the lines were

TABLE VIII

VALUES OF LORENTZ EXPONENT AND HALF-WIDTH
CALCULATED BY IBM 1620 COMPUTER
FROM DATA IN APPENDIX B

Spectral line	5 atm, 120°C n	5 atm, 120°C Δν (cm^{-1})	1 atm, 100°C n	1 atm, 100°C Δν (cm^{-1})	50 cm, 100°C n	50 cm, 100°C Δν (cm^{-1})	5 cm, 100°C n	5 cm, 100°C Δν (cm^{-1})
R(8)					1.99	0.069		
R(7)					2.00	.089		
R(6)	2.01	0.76	1.98	0.158	(2.00)	.108		
R(5)	2.03	1.13	2.01	.238	2.01	.158	(2.00)	0.0180
R(4)	2.03	1.53	1.97	.354	1.85	.204	(2.00)	.0225
R(3)	1.93	1.92	1.99	.446	1.87	.268	1.98	.0308
R(2)	1.79	1.97	2.00	.537	1.85	.315	1.89	.0375
R(1)	1.82	2.07	1.98	.496	1.83	.325	2.03	.0348
R(0)	1.83	1.86	1.99	.453	1.79	.278	1.96	.0316
P(1)	a	a	2.05	.460	a	a	1.98	.0305
P(2)	a	a	2.00	.565	a	a	2.01	.0352
P(3)	a	a	2.04	.551	a	a	2.00	.0354
P(4)	1.95	1.80	2.00	.453	a	a	1.99	.0317
P(5)	(2.00)	1.48	1.97	.295	1.86	.214	(2.00)	0.0224
P(6)	(2.00)	1.22	2.00	0.174	(2.00)	.158		
P(7)					(2.00)	0.128		

[a]Dimer region

Note: Values in parenthesis are estimates. A full explanation is given in the text.

either too weak or too narrow to be handled. These cases are discussed later. Several exponent values are enclosed in parenthesis. The computer calculated exponents significantly different from 2.00 (2.05, for example) for these lines. These were rather narrow lines, and it is felt that experimental errors led to values of n significantly different from 2.00. Actually, an exponent of 2.00 fit the data for these lines within experimental error.

First consider the results of the Lorentz half-width measurements. Lines with the same value of $|m|$ ($m = J + 1$ for the R branch, and $m = -J$ for the P branch) should have their Lorentz half-widths proportional to pressure if they are truly Lorentzian. In this case $\frac{\Delta\nu}{p}$ would be constant for any one line at different pressures. Table IX lists the values of $\frac{\Delta\nu}{p}$ calculated from the half-widths listed in Table VIII. Also listed are values of $\frac{\Delta\nu}{p}$ calculated from the uncorrected (for instrumental broadening) data* using the equivalent width method of Benedict, et al (1). These latter calculations were made only for those lines that were not overlapped by other lines.

---

*Private communication from R. J. Lovell. Complete results on the equivalent width measurements will be published at a later date.

TABLE IX

HALF-WIDTH PER UNIT PRESSURE
FOR EACH SPECTRAL LINE

Spectral Line	5 atm $\Delta\nu/p$ (cm^{-1}/atm)	1 atm $\Delta\nu/p$ (cm^{-1}/atm)		50 cm $\Delta\nu/p$ (cm^{-1}/atm)	5 cm $\Delta\nu/p$ (cm^{-1}/atm)	
R(8)				0.105		
R(7)				0.135		0.165[b]
R(6)	0.153	0.158	0.160[b]	0.166		0.187
R(5)	0.226	0.238	0.254	0.240	0.274	0.265
R(4)	0.306	0.354	0.348	0.310	0.342	0.342
R(3)	0.384	0.446	0.433	0.408	0.468	0.476
R(2)	0.394	0.537	0.540	0.479	0.570	0.586
R(1)	0.414	0.496	0.508	0.494	0.529	0.495
R(0)	0.372	0.453	0.453	0.423	0.480	0.462
P(1)	a	0.460	0.464	a	0.464	0.482
P(2)	a	0.565	0.557	a	0.535	0.548
P(3)	a	0.551	0.572	a	0.538	0.522
P(4)	0.360	0.453	0.472	a	0.482	0.458
P(5)	0.296	0.295	0.313	0.326	0.341	0.361
P(6)	0.250	0.174	0.221	0.240		0.225
P(7)				0.195		0.200

[a]Dimer region

[b]Figures in this column were obtained using the equivalent width method.

Figure 22 shows the quantity $\frac{\Delta\nu}{p}$ plotted as a function of $|m|$ for the data treated by the D. F. Smith method. Values of $\frac{\Delta\nu}{p}$ are seen to be quite close together for lines of the same $|m|$ value for the 5 cm and 1 atm pressure data, and for the 50 cm and 5 atm pressure data that were fitted by a Lorentz exponent essentially equal to 2. Figure 23 shows $\frac{\Delta\nu}{p}$ plotted as a function of $|m|$ for data treated by the equivalent width method. The values of $\frac{\Delta\nu}{p}$ measured by the two methods agree quite well.

Now consider the Lorentz exponent, n, looking first at the 5 cm and 1 atm pressure results. Except for R(2) at 5 cm pressure, all lines have the exponent essentially equal to 2. The average value of n for the 5 cm pressure lines is 1.99; for the 1 atm pressure lines the average value of n is 2.01. In fact, one can take n = 2.00 for each line and calculate the Lorentz shape, and the calculated and observed line shapes will agree within the experimental error of ±1 per cent absorption. The agreement between observed and calculated line shapes is shown for two typical spectral lines in Figs. 24 and 25. The observed line shape has been corrected for instrumental broadening. The Lorentz line shape is calculated using Equations (15) and (16) with the measured values of α_o and $\Delta\nu$.

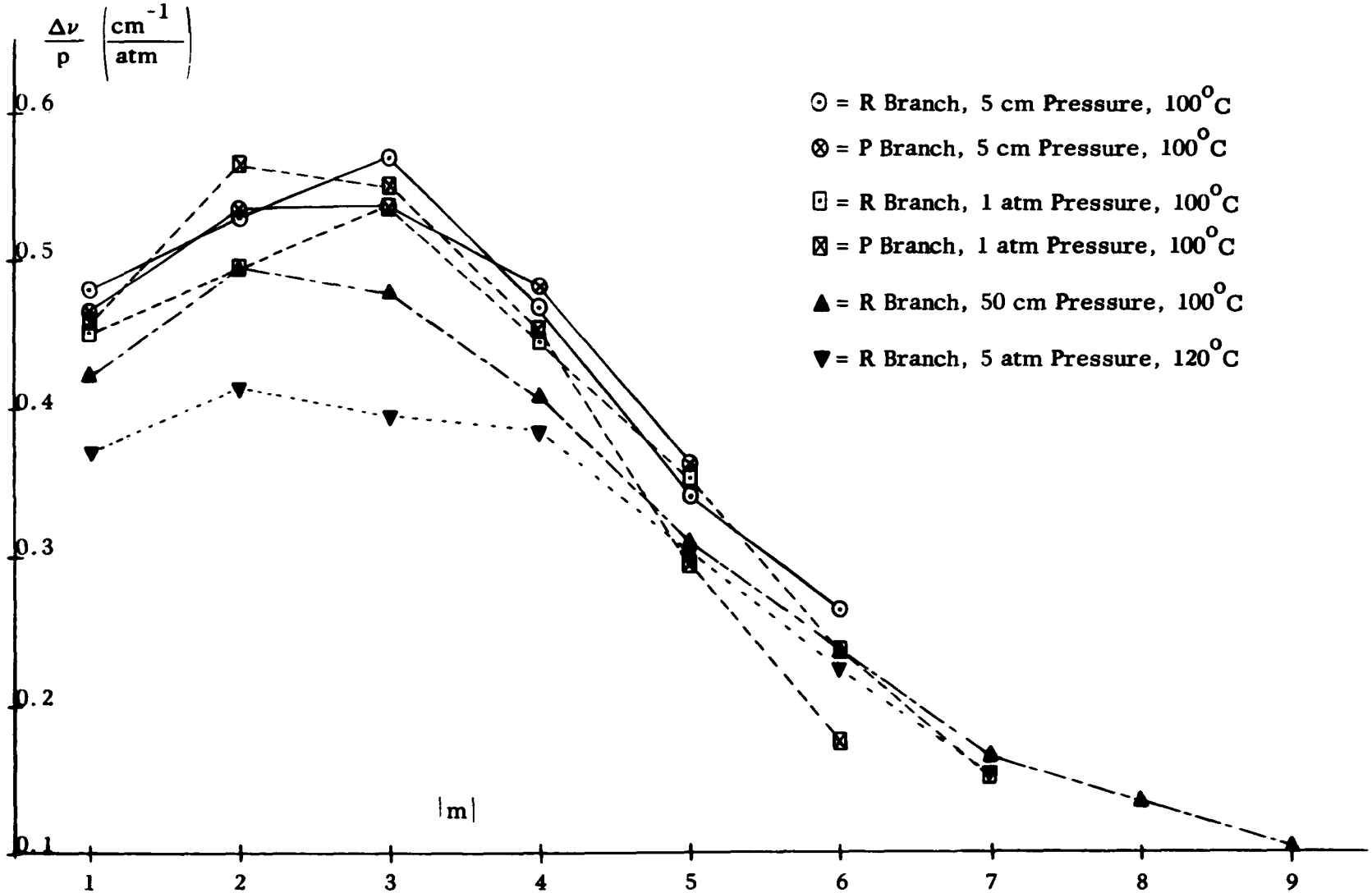

Fig. 22. $\frac{\Delta\nu}{p}$ versus $|m|$ based on D. F. Smith method.

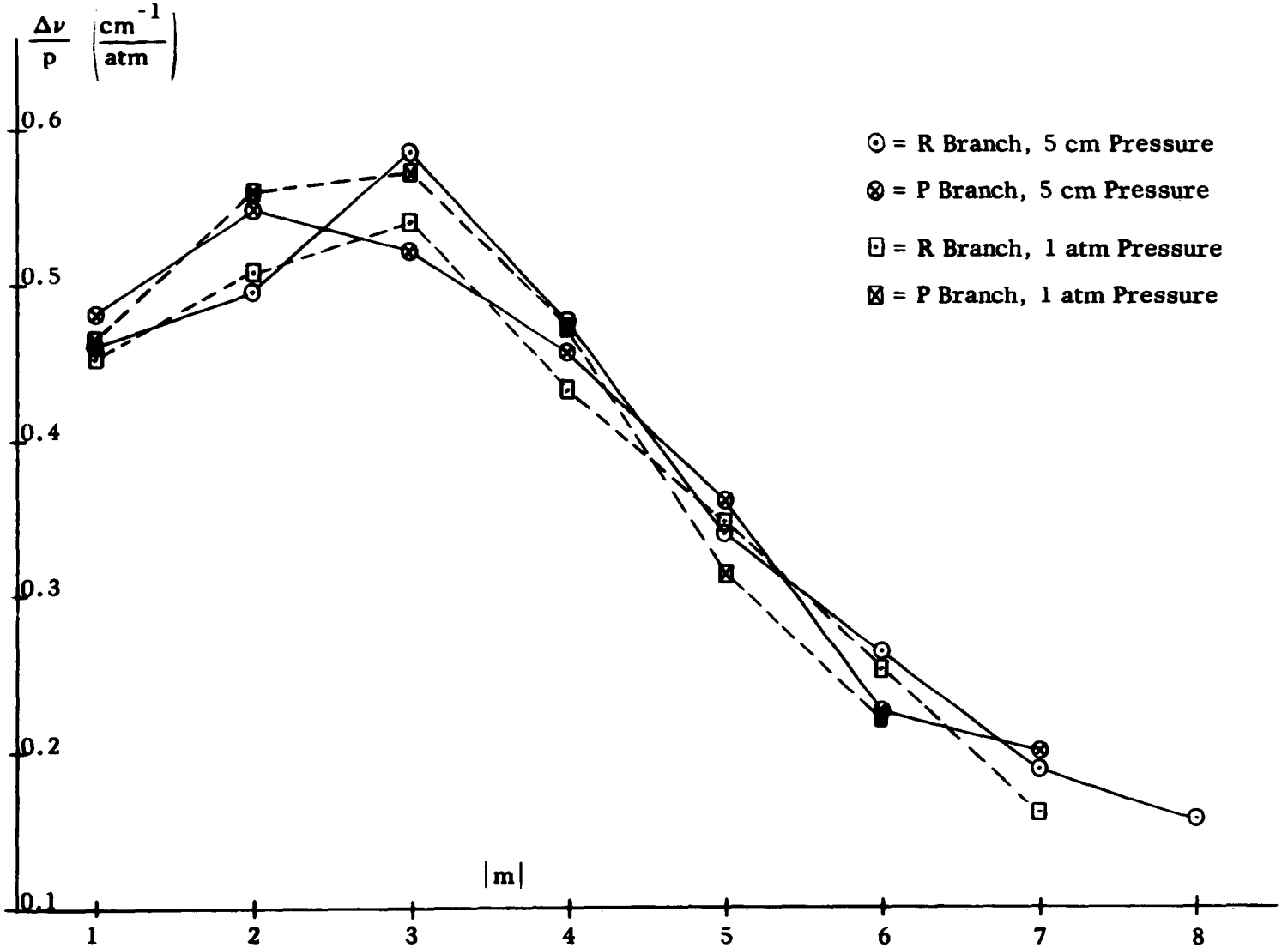

Fig. 23. $\frac{\Delta\nu}{p}$ versus $|m|$ based on equivalent width method.

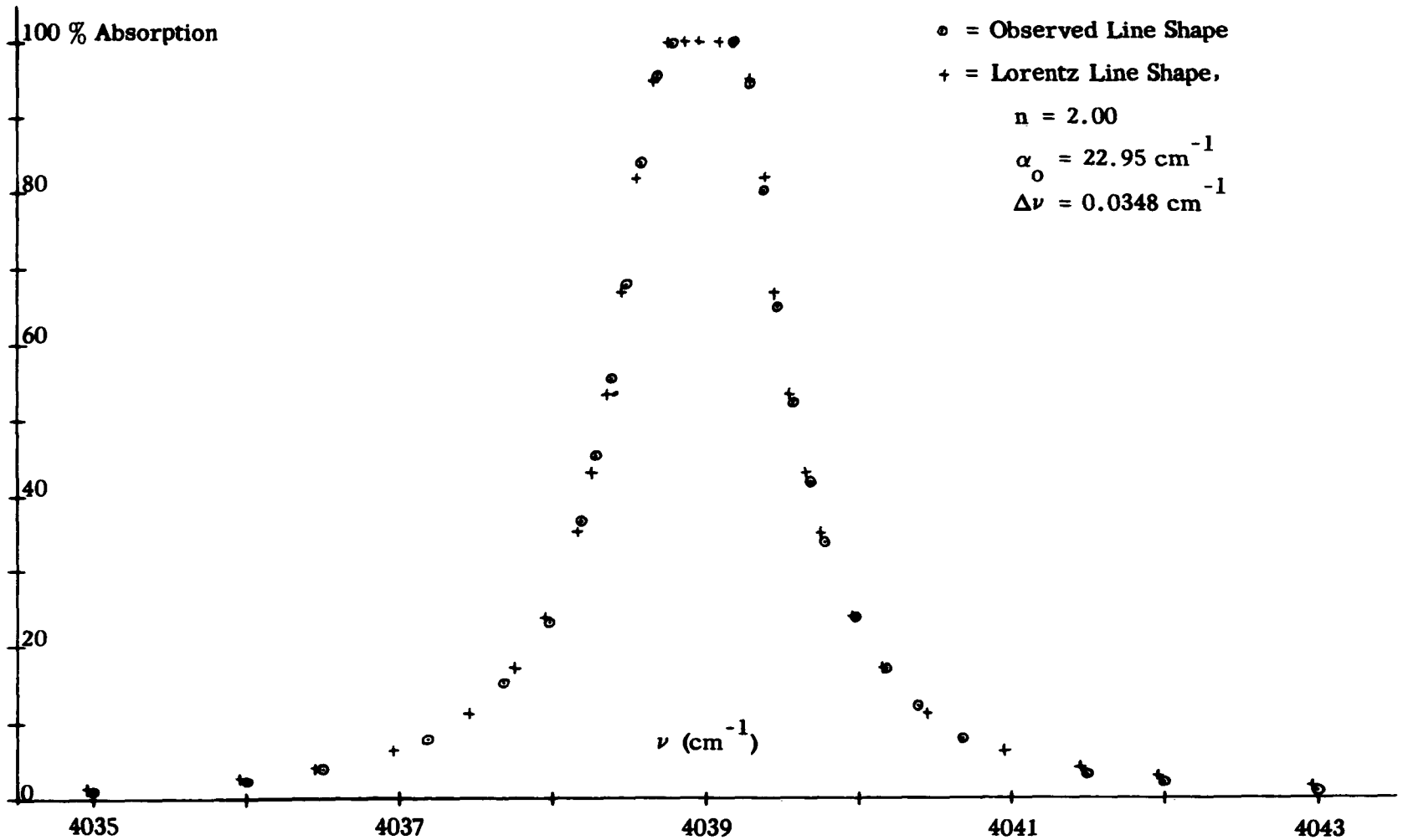

Fig. 24. Observed and calculated line shapes for R(1) at 5 cm pressure.

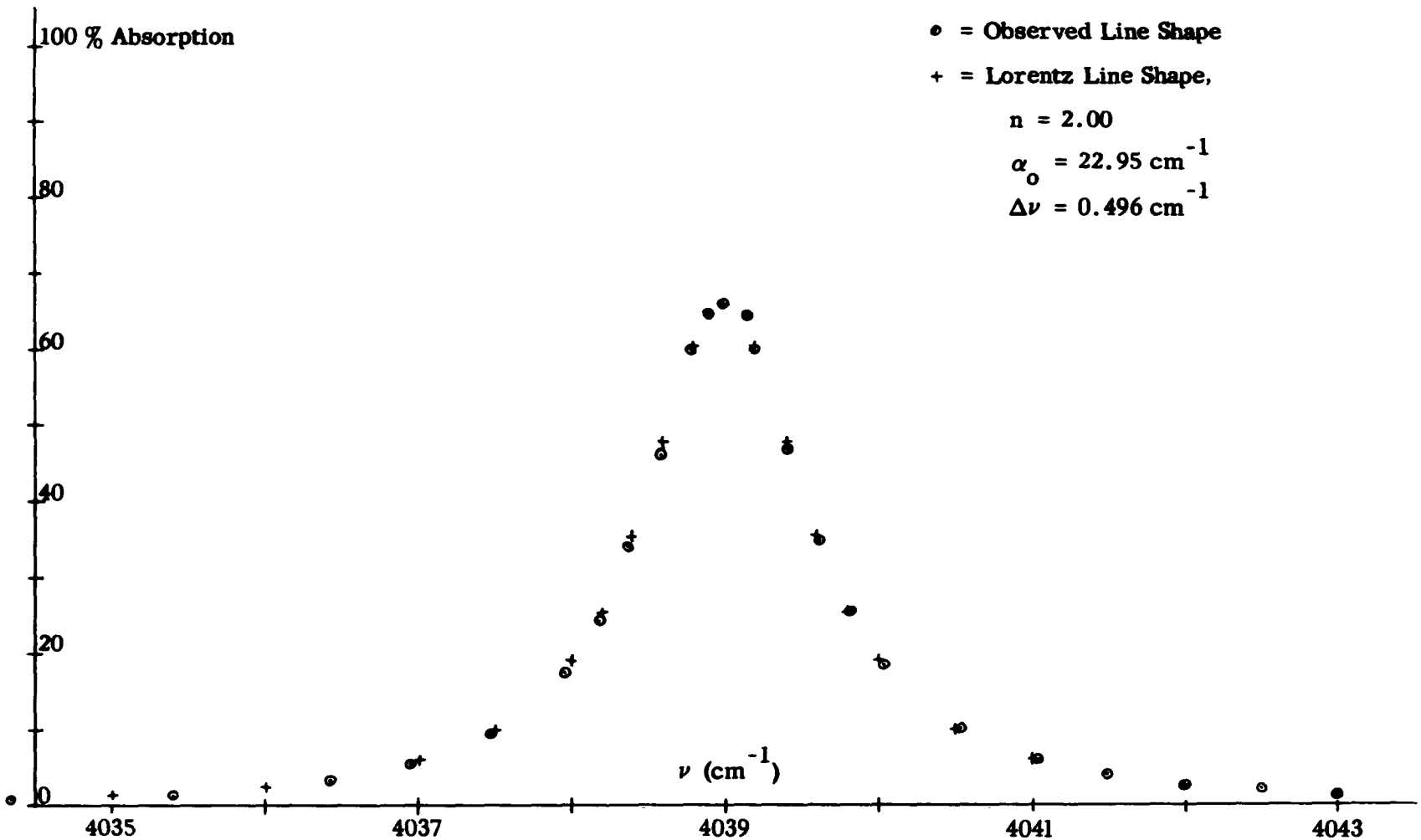

Fig. 25. Observed and calculated line shapes for R(1) at 1 atm pressure.

The slight variations of the measured values of the Lorentz exponent from 2 are felt to be caused by the large per cent error involved in measuring the wing data. As discussed above, the quantity $\frac{\alpha_o - \alpha}{\alpha}$ is not as accurate in the wings as it is over the central portion of a spectral line. The measured exponent 1.89 for R(2) at 5 cm pressure is probably caused by an undetected experimental error. The data for this line, when plotted with Equation (20), scatter much more than that of other lines. However, the Lorentz half-width listed for this line in Table VIII is probably correct, since a line slope n = 2, that was drawn to fit the data as well as possible, gave the same value of $\Delta\nu$ as did n = 1.89. The calculated and observed line shapes are within 1 per cent absorption of each other over the whole breadth of the line. In the wings the observed data indicated that there was zero per cent absorption much nearer the line center than the calculated line shape would indicate. This error seems to be a natural result of the method used to determine the base line, and is not felt to be of any significance.

It appears that one can safely say that HF spectral lines measured at 5 cm pressure in a 10 cm cell and at 1 atm pressure in an 0.047 cm cell are at least very close to the true Lorentz shape. In the wings, say at $|\nu - \nu_o| =$ 5 cm^{-1}, the difference in per cent absorption calculated

using an exponent of 2.0 or 1.8 is too small to be measured (about 0.3 per cent absorption). The exponent 2.0 actually fits the observed data better than the exponent 1.8 in the wings.

The 50 cm and 5 atm pressure data show a wide range of values of the exponent n. The more narrow lines at both pressures were found to have values of n quite close to 2.00. The wide lines were found to have values of n as low as 1.79. To compare the exponents of various spectral lines at different pressures, n was plotted as a function of the half-absorption half-width, $\delta\nu$. The value of $\delta\nu$ obtained for each line was close to the center of the range of values of $|\nu - \nu_o|$ which were used to determine n in the first place. It was estimated that an error in the value of n of ± 0.03 would not greatly effect the line shape. The plot of n versus $\delta\nu$ for the 50 cm and 5 atm pressure data are shown in Fig. 26. The range of exponents obtained for the 5 cm and 1 atm pressure data are indicated also.

The most important result of Fig. 26 is that the change in n occurs in the same range of $\delta\nu$ values for both the 50 cm and 5 atm pressure data. This result leads to the conclusion that n (at least for pressures of 5 atm or less) does not appreciably depend on pressure. The exponent n seems to be a function of $\delta\nu$, but n could also

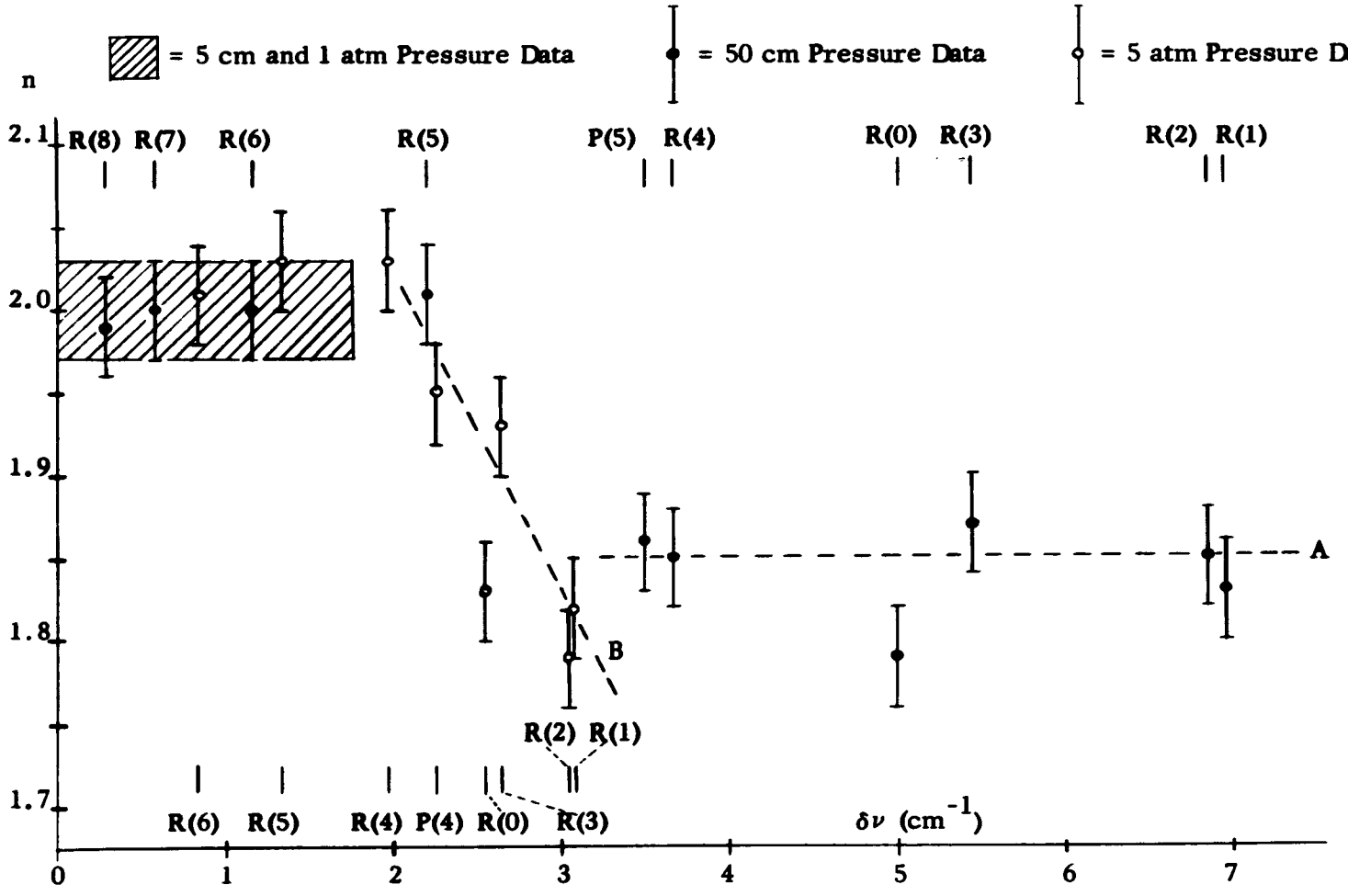

Fig. 26. Dependence of Lorentz exponent, n, on half-absorption half-width, δν.

be a function of $|\nu - \nu_o|$. It may well be that n is a constant that depends on $\delta\nu$ for the central portion of a line, and that n becomes a slightly decreasing function of $|\nu - \nu_o|$ far from the line center. The effect of the exponent of a particular line on the shapes of neighboring lines will be discussed later.

Another result of interest is the exponent for R(0). The dotted line "A" at n = 1.85 fits the 50 cm pressure exponents for P(5) and R(1, 2, 3, and 4) quite well. The measured exponent for R(0) is considerably lower. Similarly, the dotted line "B" fits the varying 5 atm pressure exponents for P(4) and R(1, 2, and 3) quite well, and again the R(0) exponent is considerably lower. This lower than average exponent for R(0) was also observed by Benedict and his coworkers (2) in their work with HCl.

A comparison of the observed and calculated line shapes at 5 atm pressure shows some differences. The lines R(4, 5, and 6) are fitted quite well with n = 2 except for the high wave number side. For $\nu - \nu_o$ greater than 2 cm^{-1}, the observed absorption is less than the calculated absorption. This same asymmetry is observed in R(3) using n = 1.9. The difference between observed and calculated absorption is greater than the estimated experimental error. Examples of the asymmetry are shown in Figs. 27 and 28. Similar asymmetry in line shapes was also observed by

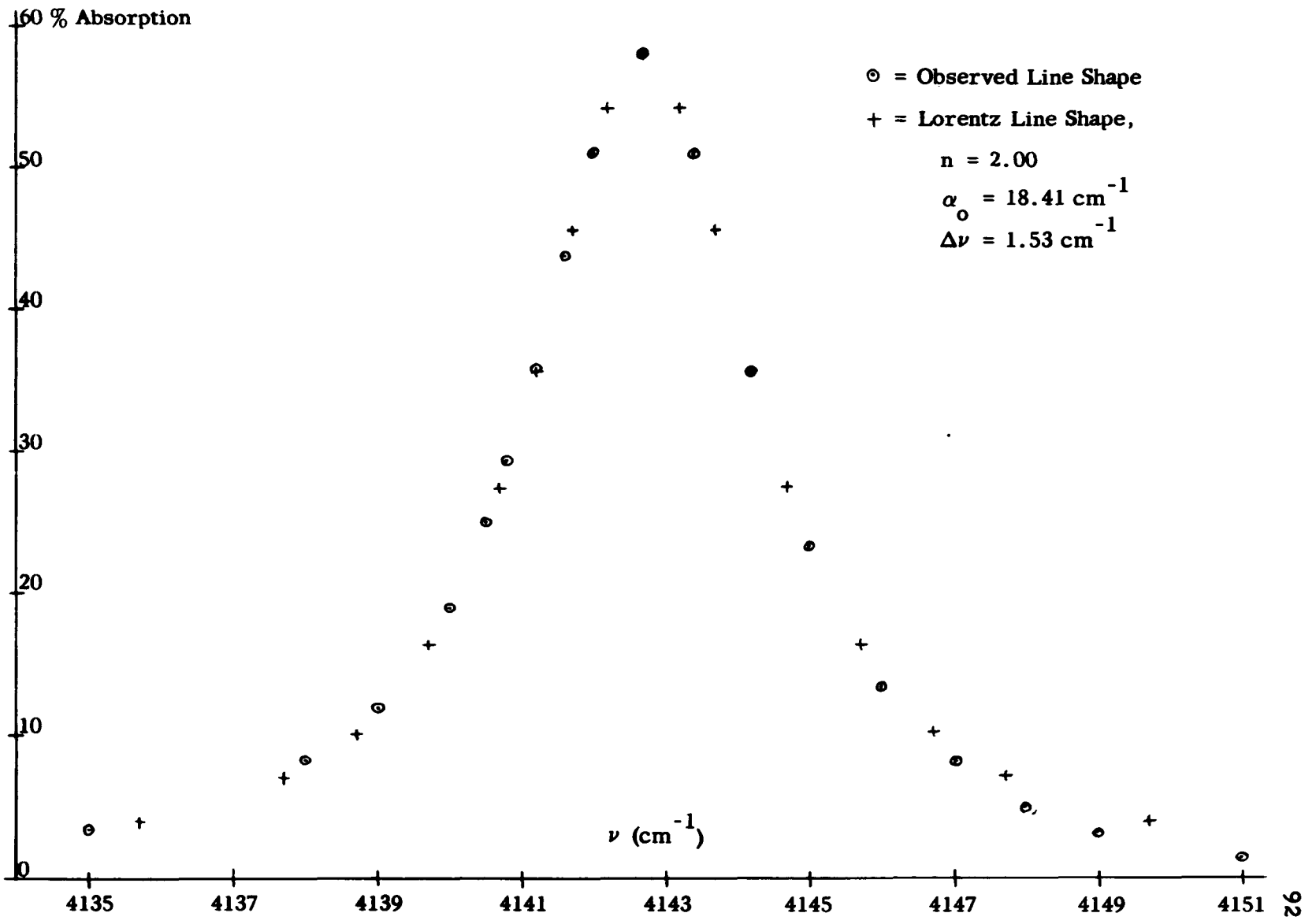

Fig. 27. Observed and calculated line shapes for R(4) at 5 atm pressure.

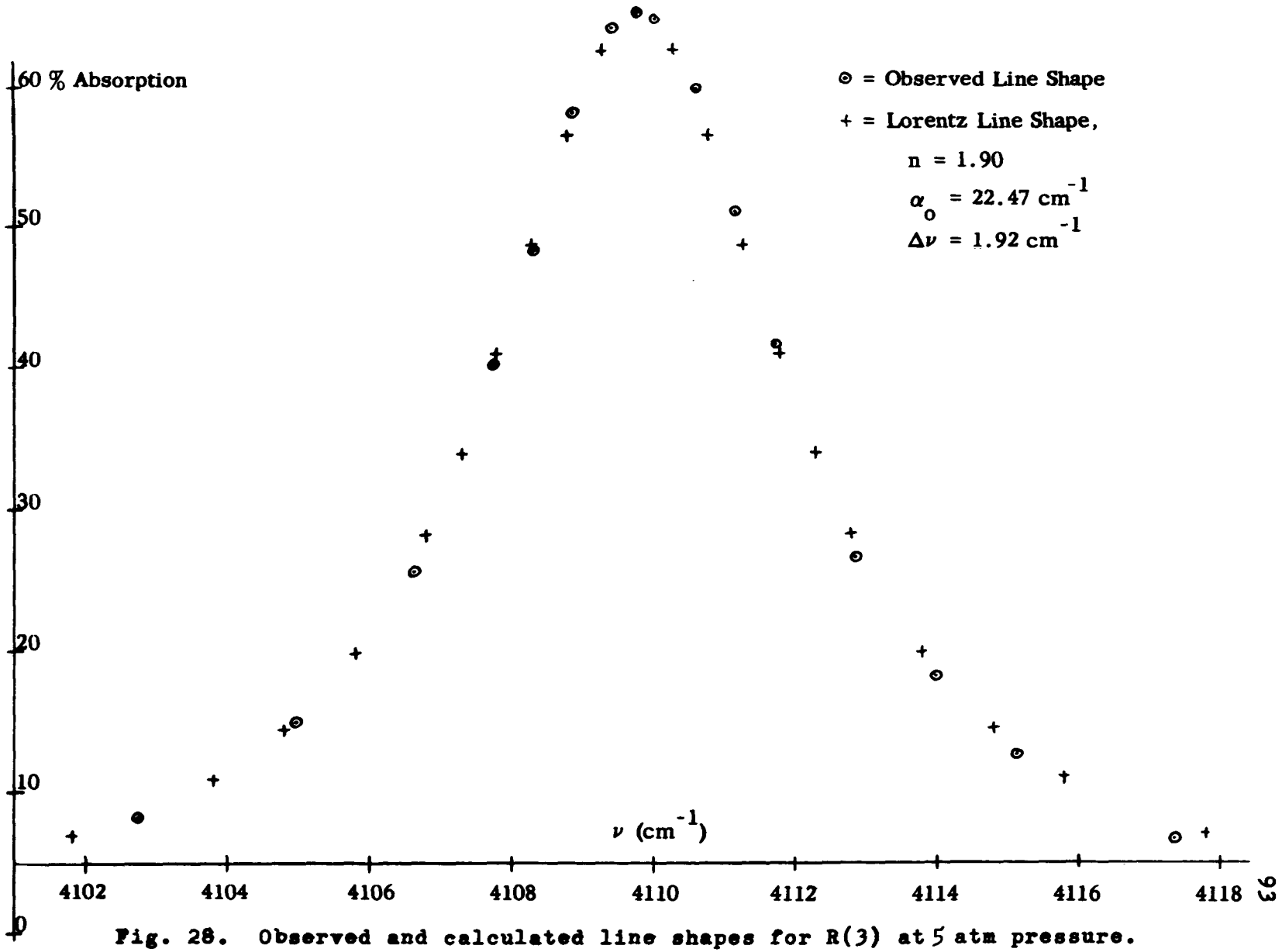

Fig. 28. Observed and calculated line shapes for R(3) at 5 atm pressure.

Benedict and his coworkers in their work with HCl. R(2) appears to be symmetric. R(0 and 1) appear to have slightly more observed than calculated absorption on the high wave number side of the line center. The calculated and observed line shape of R(0) is shown in Fig. 29. The small difference in observed and calculated absorption on the low wave number side of R(0) could well be due to the H_2F_2 band that is centered near the HF band center.

The strongest H_2F_2 absorption occurs in the region of P(1, 2, and 3), and these lines could not be treated. The data for the high J lines in the P branch are not as accurate as for other lines because of an unknown amount of H_6F_6 absorption and because of the drop in signal-to-noise ratio towards low wave numbers.

Figures 30, 31, and 32 show observed and calculated shapes for the lines R(7, 3, and 0), respectively, at 50 cm pressure. The lines R(7, 6, 5, 4, and 3) show the same asymmetry as the 5 atm pressure lines, but it is not as pronounced. R(0) is fitted quite well by the exponent 1.80. For comparison, several points have been calculated in Fig. 31 with n = 2. It is seen that the exponents 1.85 and 2.00 give quite different line shapes when one is close to the line center.

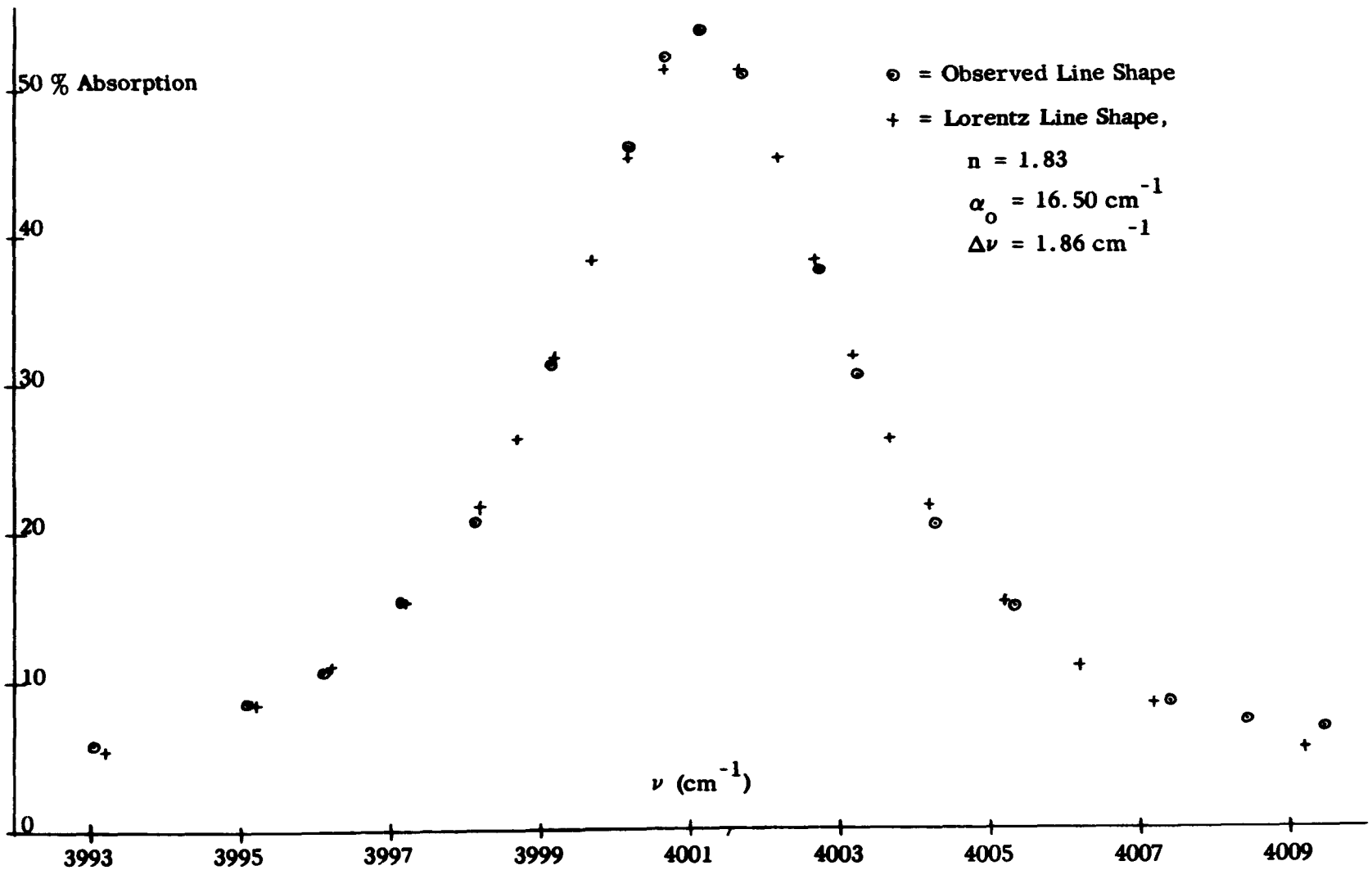

Fig. 29. Observed and calculated line shapes for R(0) at 5 atm pressure.

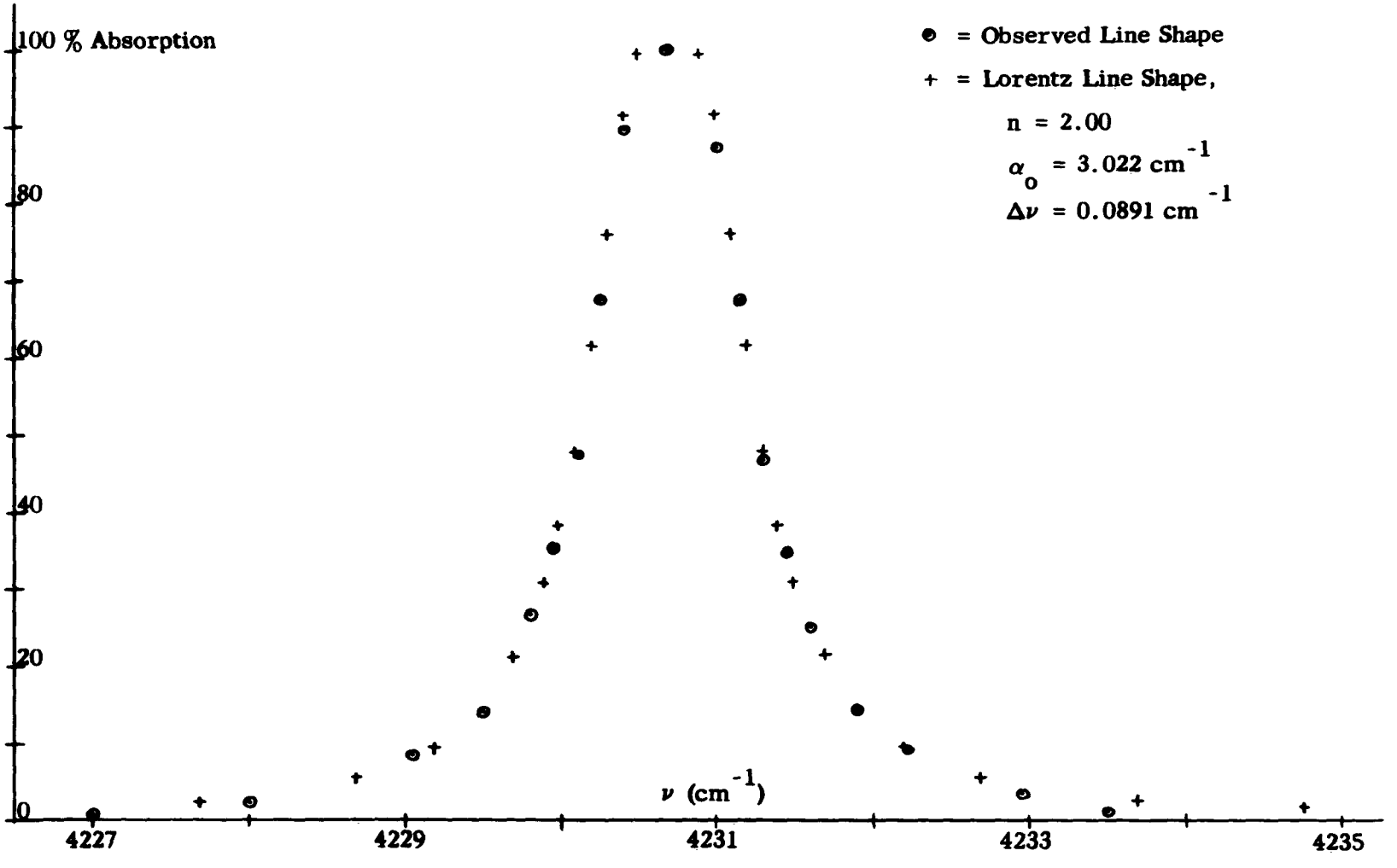

Fig. 30. Observed and calculated line shapes for R(7) at 50 cm pressure.

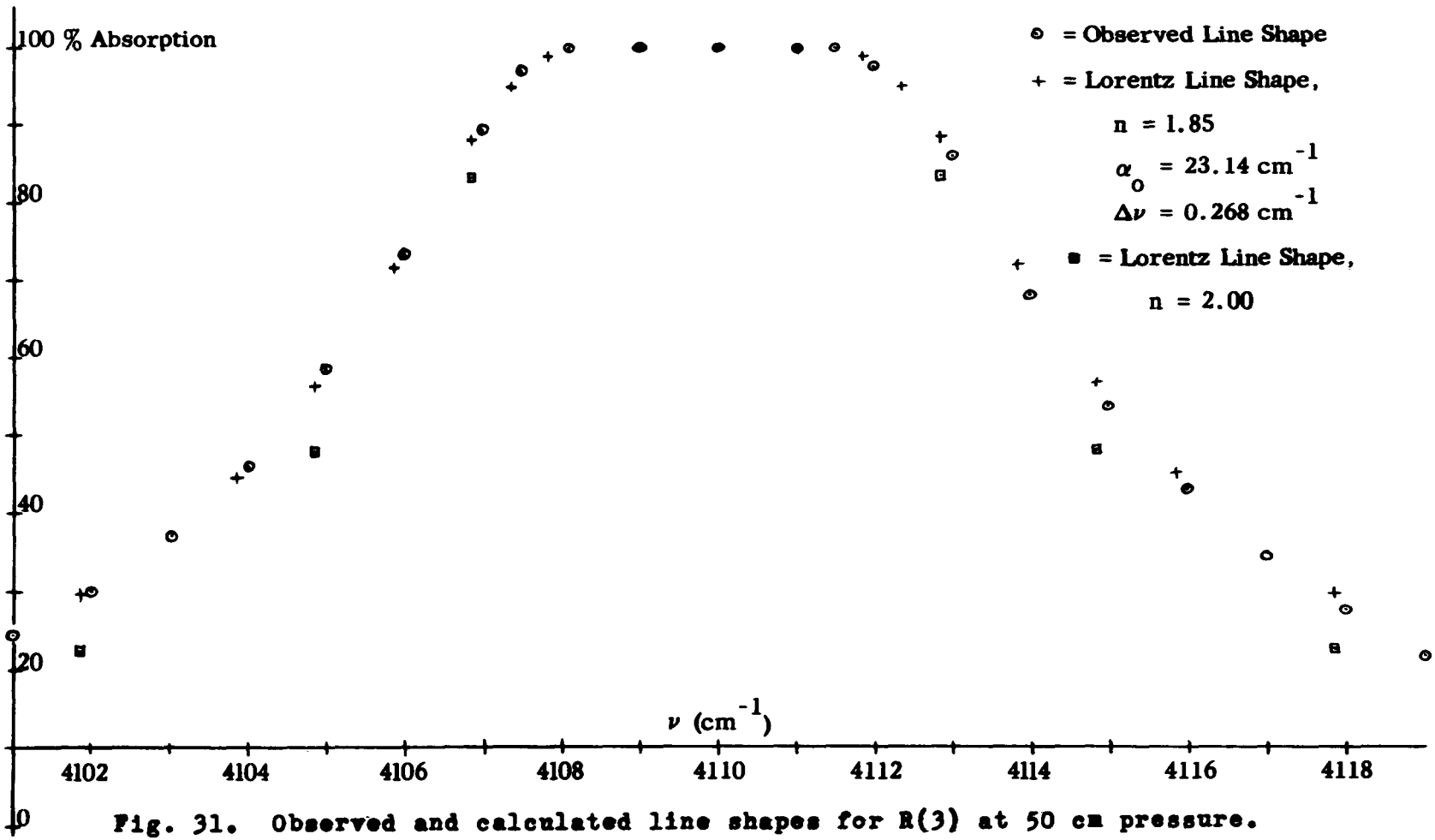

Fig. 31. Observed and calculated line shapes for R(3) at 50 cm pressure.

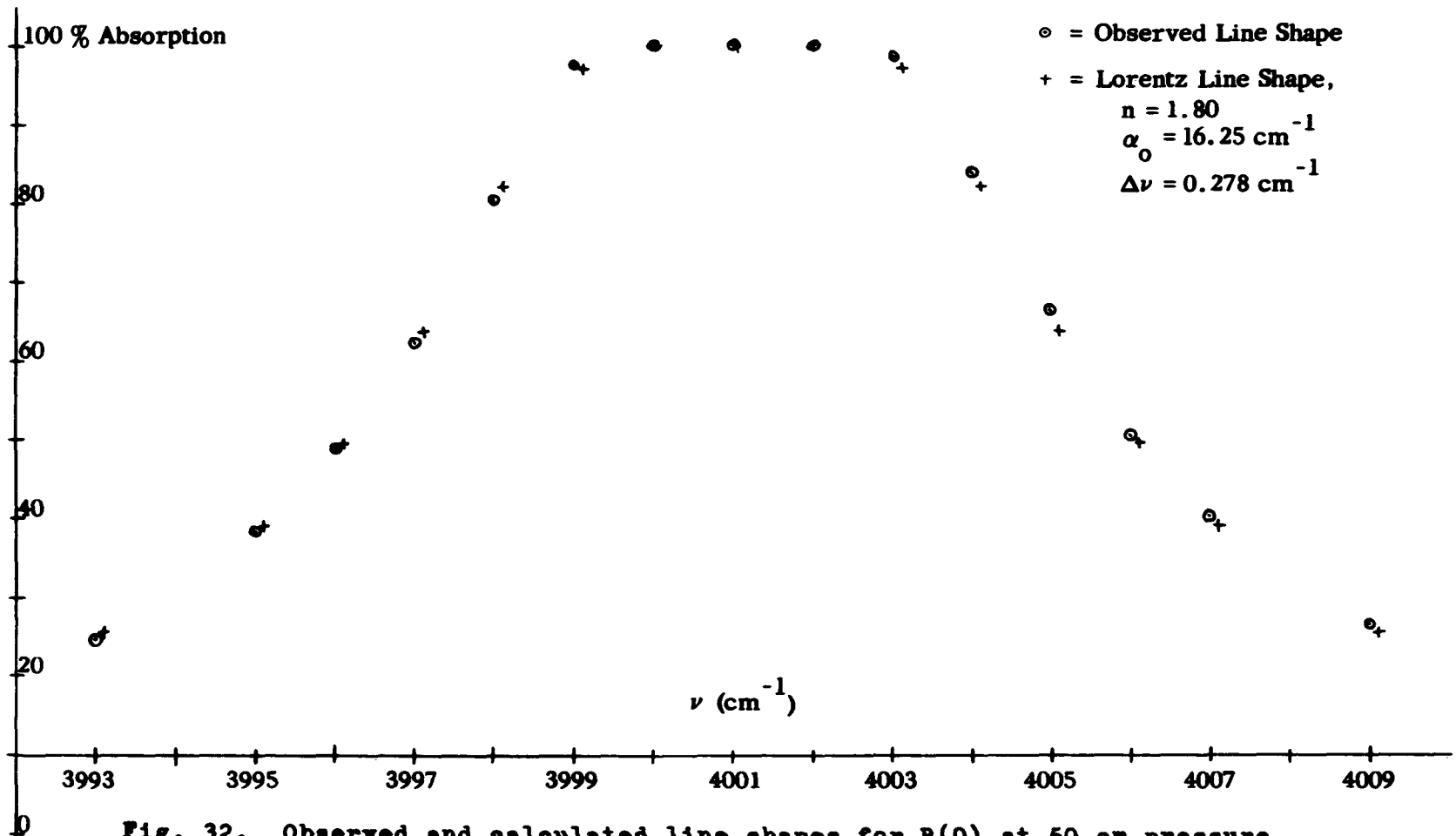

Fig. 32. Observed and calculated line shapes for R(0) at 50 cm pressure.

Line Wings

The wings of the 5 cm and 1 atm pressure lines are fitted rather well by the Lorentz formula with n = 2, as discussed above. This is true even though one may be more than 5 cm^{-1} away from the line center.

Because of the method used to determine per cent absorption in regions where there was line overlap (discussed in the section on data taking and handling), one might have an error of as much as 2 per cent absorption. Therefore, one should probably not place too much importance on the wing measurements for the 50 cm and 5 atm pressure lines. For this reason no graphs will be presented, but the results will be discussed.

After values of α_o and $\Delta\nu$ had been obtained for the 50 cm and 5 atm pressure lines, the absorption in the regions between lines in the R branch was calculated using n = 1.8 for all lines and considering contributions from all possible lines. The calculated absorption was then compared with the observed absorption in the regions between lines. Observed and calculated absorption agreed to within about 1 per cent absorption except for regions next to those lines that had a measured Lorentz exponent of 2 for their central portions. In these regions a better fit to the observed data was obtained if the exponent 2 was used until one was about 15 cm^{-1} away from the line center.

For distances greater than 15 cm^{-1} from the centers of these lines, the absorption became so weak that the difference between an exponent of 2 and one of 1.8 would be negligible.

In the case of the 50 cm pressure data, a slightly better fit to the observed data was obtained if the exponent 1.85 was used for the values of $|\nu - \nu_o|$ less than about 15 cm^{-1} for the lines R(1, 2, 3, and 4).

One thing should certainly be kept in mind, though. The observed absorption was almost always less than the calculated absorption in the regions between lines. Thus it may be that a constant error of about -1 per cent absorption was made in determining the base-line for the 50 cm and 5 atm pressure data. If 1 per cent absorption was added to the observed absorption in the regions between lines, then the calculated absorption, using an exponent of 1.8 would agree very well with the observed absorption in these regions. One would then say that the exponent 1.8 should be used for all lines when one was further than about 5 cm^{-1} from the line center.

Varying the exponents of strong lines from 1.80 to 1.85 would have some effect on the α correction curves that were calculated for each line prior to measuring α_o and $\Delta\nu$. In the case of the 5 atm pressure lines the effect was insignificant. The effect was a little larger

in the case of the 50 cm pressure data, and it was felt that for values of $|\nu - \nu_o|$ greater than about 20 cm^{-1} it was better to use an exponent of 1.80.

Narrow Lines

All 5 cm and 1 atm pressure lines and the high J 50 cm and 5 atm pressure lines were found to be truly Lorentzian in shape. A number of these lines, R(0, 1, and 2) and P(1, 2, and 3) at 1 atm pressure, were wide enough to need no correc ion for instrumental broadening. All lines narrower than these lines should then be Lorentzian unless they were so narrow that Doppler broadening became appreciable. Since there were lines that needed correction for instrumental broadening that turned out to be Lorentzian after correction, one can say that the correction method was a good one, at least for lines that were not too narrow.

A line as narrow as R(7) at 50 cm pressure ($\delta\nu$ = 0.5 cm^{-1}) was corrected properly, as can be seen in Fig. 30. However, when narrower lines such as the high J 5 cm pressure lines and all 1 cm pressure lines were subjected to the correction method, the results were obviously in error. The corrected line center often went well over 100 per cent absorption, and dips were introduced into the wings that sometimes went below zero per cent absorption.

The widest of the 1 cm pressure lines had $\delta\nu = 0.2$ cm^{-1}, approximately.

For the widest of the 1 cm pressure lines Doppler broadening should be completely masked by pressure broadening, and these lines should be Lorentzian. It was decided to estimate the Lorentz half-widths of these lines from the high pressure data and calculate their shapes. The slit function could then be allowed to scan this calculated Lorentz shape, and the result could be compared with the observed data.

Since $\Delta\nu$ is proportional to pressure for pressure broadened lines, $\Delta\nu$ for a particular 1 cm pressure line could be calculated from the 5 cm and 1 atm pressure values of $\Delta\nu$ for that line. Then the value of α_o measured at 1 atm pressure for that line could be used with the Lorentz formula to calculate the line shape. The result of this calculation is shown for R(1) at 1 cm pressure in Fig. 33. The slit function matrix was then multiplied into the column matrix representing the Lorentz line shape. The result of this step is also shown in Fig. 33, along with the observed line shape.

The observed and calculated line shapes differ by about 2 per cent absorption in the regions where absorption changes most rapidly with wave numbers. The difference in values of $\delta\nu$ for the observed and calculated shapes is

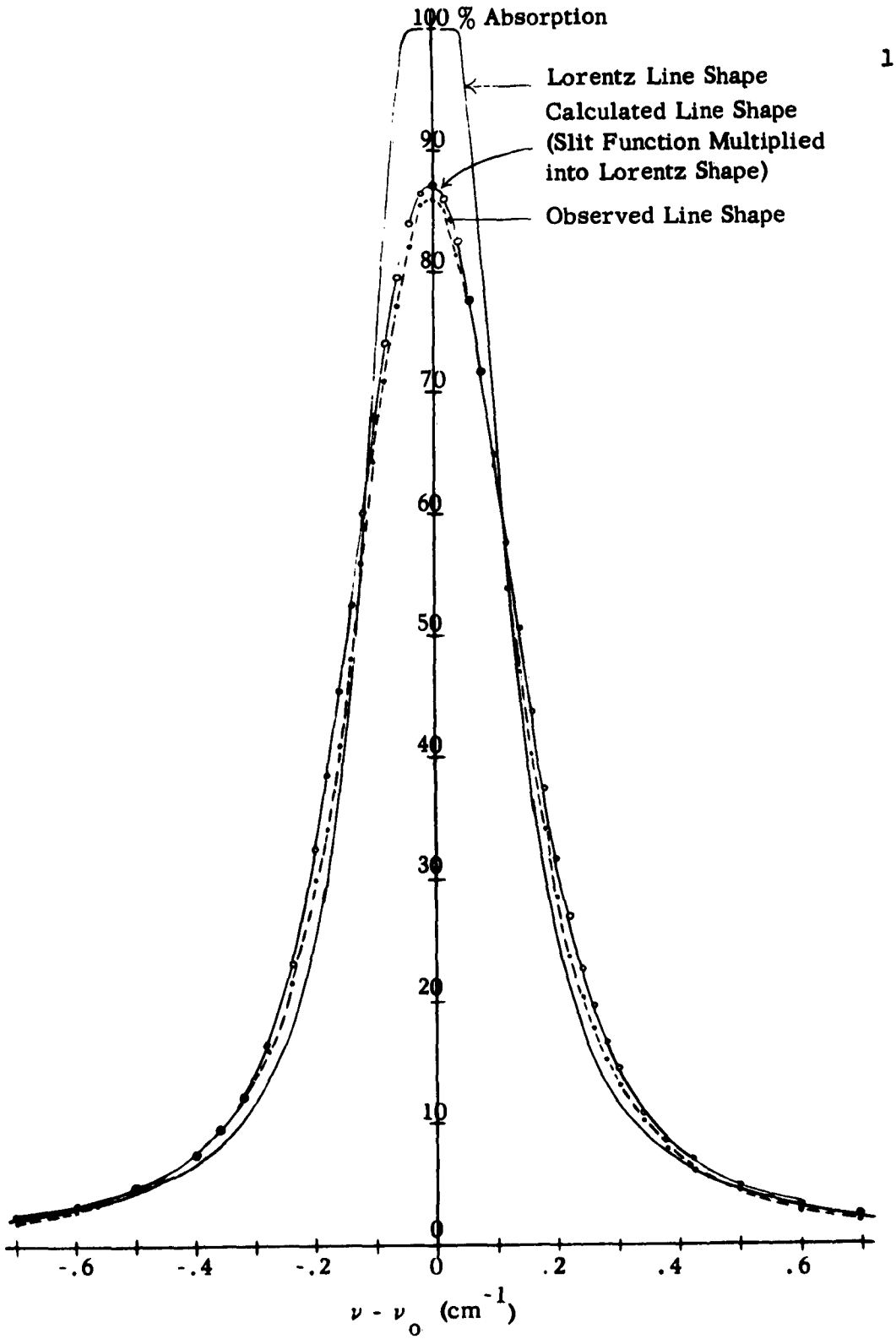

Fig. 33. Lorentz, calculated, and observed line shapes for R(1) at 1 cm pressure.

about 0.01 cm^{-1}. Slight changes in the values of α_o or $\Delta\nu$ affect points within a few hundredths of a wave number of the line center only. The difference in the two curves is therefore thought to occur because the slit function could not be measured precisely enough to correct these very narrow lines.

The above procedure was applied to several of the 1 cm pressure lines, and the results were essentially the same.

Dimer Region

The strongest H_2F_2 absorption lies in the region of P(1, 2, and 3) of the monomer. At 100°C no dimer could be observed at 5 cm pressure in the 10 cm cell or at 1 atm pressure in the 0.047 cm cell. At 100°C and 50 cm pressure in the 10 cm cell and at 120°C and 5 atm pressure in the 0.047 cm cell the dimer absorption became appreciable. On the basis of the 1 and 5 atm pressure data, values of α_o, $\Delta\nu$, and n were estimated, and the monomer absorption was calculated for the region of P(1, 2, and 3). This calculated monomer absorption was subtracted from the observed absorption, which left the dimer absorption. The dimer absorption had the same shape as that reported by Smith (18). Because Smith's experimental conditions were quite different from those of this present work, only a

qualitative comparison could be made. Since one must make assumptions about the monomer spectrum in order to calculate the dimer spectrum, and vice versa, it would take a great deal of experimental work and calculations to separate the two spectra exactly.

As the spectrometer used in this present work was capable of much higher resolution than the one used by Smith, it was considered to be of interest to examine the dimer spectrum under optimum conditions. Smith has found that the ratio of dimer to monomer is greatest at a pressure of 30 cm and a temperature of 29°C. The results of this investigation have already been published by Nielsen and his coworkers (8) and only a brief discussion will be made here.

All of the bands observed by Smith were observed in Nielsen's investigation. In addition, regions of absorption near the monomer band center, between P(1) and P(2), and between P(2) and P(3) were resolved into fine structure. There are evidences of PQR type structure, and a regular spacing of lines can be observed. In the region of the monomer band center the spacing is about 1.5 cm^{-1}. On the low wave number side of P(1) the spacing is about 0.5 cm^{-1}.

CHAPTER IV

SUMMARY AND SUGGESTIONS FOR FUTURE WORK

I. SUMMARY

Experimental Work

No actual research had been performed on the University of Tennessee's vacuum-grating spectrometer prior to this work. Thus several modifications were made on the spectrometer and a few instrumental problems had to be solved before data could be taken on the HF spectrum.

The following changes were made on the spectrometer:

1. The Fabry-Perot interferometer was replaced by a source of neon emission lines in order to provide a more convenient calibration system. Absolute frequency measurements can easily be made to within ±0.02 cm^{-1} in the region of 4000 cm^{-1}.

2. A glower stabilizing circuit was installed so that the glower output could be kept constant. With proper techniques, absorption can be measured to within ±1 per cent absorption.

3. For this present work a band pass filter was substituted for the prism monochromator, which greatly facilitated the taking of data.

The following instrumental problems were solved:

1. The replacement of the prism by a filter partially solved stray light problems. Stray light was further reduced by arranging light baffles in the detector section and by masking off portions of the large flat mirror.

2. Problems arising from the use of glowers in vacuum were solved.

3. Slight motions of some optical parts were detected. Faulty gaskets in the mirror mounts proved to be the main source of this difficulty.

4. A system was developed for removing all remaining traces of water vapor from the spectrometer after evacuation.

5. In order to handle HF safely a gas handling system was constructed almost entirely of monel metal. The pressure and temperature of HF in an absorption cell inside the spectrometer chamber can be measured and controlled from outside the chamber.

Line Positions

The line centers of twenty-one lines of the HF fundamental and seventeen lines of the first overtone were measured. A rotational analysis was carried out, and the results were as follows:

1. Observed and calculated line centers agreed to within ±0.02 cm^{-1}.

2. The band centers obtained for both bands were slightly over 0.1 cm^{-1} lower than the values measured by other workers.

A vibrational analysis was carried out using the fundamental and first overtone band centers of this present work and seven higher overtone band centers measured by other workers. The agreement between observed and calculated band centers was much better (within ±0.025 cm^{-1}) when the fundamental and first overtone band centers of this present work were used with the seven other band centers than when all nine band centers measured by other workers were used. New values of several molecular constants were obtained.

Shifts in line centers that are proportional to pressure were observed and measured. The shifts are strongly J dependent.

Line Shapes

The main goal of this work was to determine experimentally the true shape of the rotational lines of the HF fundamental, and to compare the measured shape with a theoretical line shape. The results are as follows:

1. A technique was developed that permits the correction of measured line shapes for the effects of instrumental broadening. The technique works well on all but the most narrow lines.

2. Observed line shapes can be represented very well by the Lorents expression, except that the exponent of $(\nu - \nu_o)$, n, was found to depend strongly on the half-absorption half-width, $\delta\nu$, for the central portion of the lines.

3. For lines with $\delta\nu$ less than 2.2 cm^{-1}, n = 2.00 gave a good fit between observed and calculated line shapes, regardless of the pressure at which the line was measured. It was found that n = 2 gave a better fit to the wing data, even as far as 10 cm^{-1} from the center of these lines.

4. For lines with $\delta\nu$ greater than 3.0 cm^{-1}, n = 1.85 gave the best fit to all of the data. This value of n gave a better fit to the observed data than n = 2.00 even within a few wave numbers of the center of these lines. For distances greater than 20 cm^{-1} from the line center, n was taken as 1.80 for all lines.

5. R(0) seems to have a slightly lower exponent than other lines. The high pressure lines seem to be slightly asymmetric. Both of these results have been reported by other workers using HCl.

6. The lines P(1, 2, and 3) could not be measured satisfactorily at 50 cm pressure in the 10 cm cell and at 5 atm pressure in the 0.047 cm cell because of H_2F_2 absorption. Fine structure was observed in the H_2F_2 absorption.

7. The Lorentz half-width seems to be proportional to pressure for all lines that have their Lorentz exponent equal to 2. Lines with values of the Lorentz exponent less than 2 have smaller Lorentz half-widths than might be expected.

8. Direct measurements of the Lorentz half-width led to the same results as did the equivalent width method.

The most significant results of this present work have to do with the dependence, or lack of it, of the Lorentz exponent, n, on pressure and on distance from line center. In pressure ranges where pressure broadening is the main contributor to the true line shape, n has no measurable dependence on pressure. The main dependence of n seems to be on the half-absorption half-width, $\delta\nu$. Over the central portion of a line ($|\nu - \nu_o|$ less than 10 cm^{-1}) n was found not to be a function of the distance from the line center, at least within experimental error.

II. SUGGESTIONS FOR FUTURE WORK

1. Measure the center frequencies of high J lines in a cell of several meters path length. Such measurements

would permit a better determination of the smaller rotational constants. Pressure induced line shifts could be measured for these lines.

2. Measure line shapes at pressures from 1 to 5 atm with path lengths from 1 mm to 1 cm, possibly. Such measurements would permit determinations of the Lorentz parameters α_o and $\Delta\nu$ for the high J lines. Per cent absorption could be measured with less per cent error in the region between lines with the above pressures and cell lengths, and thus values of n far from line centers might be determined more accurately than was possible in this work.

3. Measure the temperature dependence of the Lorentz parameters.

4. Measure pressure induced line shifts and broadening caused by a mixture of HF and a noble gas.

5. Measure high pressure absorption of the lines P(1, 2, and 3) at temperatures high enough that H_2F_2 absorption is eliminated, if possible.

6. Measure several lines, say R(2 and 4), in the 0.047 cm cell at pressures ranging from 1 to 5 atm in order to study the Lorentz exponent as it decreases from 2.

BIBLIOGRAPHY

BIBLIOGRAPHY

1. Benedict, W. S., R. Herman, G. E. Moore, and S. Silverman, Can. J. Phys. 34, 830 (1956).

2. Benedict, W. S., R. Herman, G. E. Moore, and S. Silverman, Can. J. Phys. 34, 850 (1956).

3. Ben-Reuven, A., S. Kimel, M. A. Hirshfeld, and J. M. Jaffe, J. Chem. Phys. 35, 955 (1961).

4. Courtoy, Charles P., Ann. de la Soc. de Bruxelles 73, Part I, 5 (1959).

5. Deeds, W. E., N. M. Gailar, W. F. Herget, T. M. Holladay, R. J. Lovell, A. A. Mason, and A. H. Nielsen, "Line Intensity and Pressure Broadening Studies in HF," Air Force Cambridge Research Laboratories Report No. 465 (March 1961).

6. Dunham, J. L., Phys. Rev. 41, 721 (1932).

7. Ebers, E. S., and H. H. Nielsen, Rev. Sci. Inst. 11, 429 (1940).

8. Herget, W. F., N. M. Gailar, R. J. Lovell, and A. H. Nielsen, J. Opt. Soc. Am. 50, 1264 (1960).

9. Herndon, J. A., and A. H. Nielsen, "Design and Construction of a Vacuum-Grating Spectrometer for the Infrared," Technical Report No. 2, Office of Ordinance Research, Department of the Army (December 1957).

10. Herzberg, G., Spectra of Diatomic Molecules (D. Van Nostrand Co., Inc., New York, 1953).

11. Kimel, S., M. A. Hirshfeld, and J. H. Jaffe, J. Chem. Phys. 31, 81 (1959).

12. Kuipers, G. A., "The Spectrum of Monomeric HF: Molecular Constants, Line Shapes, Intensities, and Breadths," Ph.D. Thesis, Department of Physics, University of Tennessee (June 1956).

13. Kirkpatrick, D. E., and E. O. Salant, Phys. Rev. 48, 945 (1935).

14. Mann, D. E., B. A. Thrush, D. R. Lide, Jr., J. J. Ball, and N. Acquista, J. Chem. Phys. 34, 420 (1961).

15. Rank, D. H., A. H. Guenther, G. O. Saksena, J. M. Shearer, and T. A. Wiggins, J. Opt. Soc. Am. 47, 686 (1957).

16. Rao, K. N., L. R. Ryan, and H. H. Nielsen, J. Opt. Soc. Am. 49, 216 (1959).

17. Rao, K. N., T. J. Coburn, J. S. Garing, K. Rossmann, and H. H. Nielsen, J. Opt. Soc. Am. 49, 221 (1959).

18. Smith, D. F., J. Mol. Spectroscopy 3, 473 (1959).

APPENDICES

APPENDIX A

THE SLIT FUNCTION MATRIX

An example of the slit function as measured by the spectrometer was shown in Fig. 14(a). The smooth curve was obtained directly from the recorder chart, with absorption (arbitrary units) plotted against a continuous frequency scale (cm^{-1}). If the continuous frequency scale is replaced by a scale of discrete intervals (0.05 cm^{-1} in this case), the slit function is then represented by the step function (dotted curve). Spectral lines are also plotted as step functions.

The slit function measured with a physical slit width of 100 microns and divided into 0.02 cm^{-1} intervals contained twenty-three steps. The method of construction of the slit function matrix is independent of the number of steps involved, so for simplicity one can assume that the slit function contains, say, five steps. Let the numbers representing the steps be S_1, S_2, . . ., S_5. One can assume that the slit function has already been normalized to unit area, so that $\sum_i S_i = 1$.

The slit function and the line to be corrected for instrumental broadening are divided into steps of equal width in wave numbers. This width is based on the number of steps that are needed to represent satisfactorily the shape of the line in question. Wide lines were divided

into steps of width 0.05 cm^{-1}, and narrow lines were divided into steps of width 0.02 cm^{-1}. Although wide lines were divided into as many as ninety steps, for simplicity one can assume that the portion of a line that required correction required eight steps for proper representation. Let the numbers representing per cent absorption at each step be $A_1, A_2, \ldots, A_8$. The product of the slit function multiplied into the observed line shape, as expressed in Equation (7), would be written as

$$\begin{bmatrix} X_1 \\ X_2 \\ A^{(1)}_1 \\ A^{(1)}_2 \\ A^{(1)}_3 \\ A^{(1)}_4 \\ A^{(1)}_5 \\ A^{(1)}_6 \\ A^{(1)}_7 \\ A^{(1)}_8 \\ X_3 \\ X_4 \end{bmatrix} = \begin{bmatrix} S_3 & S_4 & S_5 & 0 & 0 & 0 & 0 & 0 & 0 & 0 & 0 & 0 \\ S_2 & S_3 & S_4 & S_5 & 0 & 0 & 0 & 0 & 0 & 0 & 0 & 0 \\ S_1 & S_2 & S_3 & S_4 & S_5 & 0 & 0 & 0 & 0 & 0 & 0 & 0 \\ 0 & S_1 & S_2 & S_3 & S_4 & S_5 & 0 & 0 & 0 & 0 & 0 & 0 \\ 0 & 0 & S_1 & S_2 & S_3 & S_4 & S_5 & 0 & 0 & 0 & 0 & 0 \\ 0 & 0 & 0 & S_1 & S_2 & S_3 & S_4 & S_5 & 0 & 0 & 0 & 0 \\ 0 & 0 & 0 & 0 & S_1 & S_2 & S_3 & S_4 & S_5 & 0 & 0 & 0 \\ 0 & 0 & 0 & 0 & 0 & S_1 & S_2 & S_3 & S_4 & S_5 & 0 & 0 \\ 0 & 0 & 0 & 0 & 0 & 0 & S_1 & S_2 & S_3 & S_4 & S_5 & 0 \\ 0 & 0 & 0 & 0 & 0 & 0 & 0 & S_1 & S_2 & S_3 & S_4 & S_5 \\ 0 & 0 & 0 & 0 & 0 & 0 & 0 & 0 & S_1 & S_2 & S_3 & S_4 \\ 0 & 0 & 0 & 0 & 0 & 0 & 0 & 0 & 0 & S_1 & S_2 & S_3 \end{bmatrix} \begin{bmatrix} x_1 \\ x_2 \\ A_1 \\ A_2 \\ A_3 \\ A_4 \\ A_5 \\ A_6 \\ A_7 \\ A_8 \\ x_3 \\ x_4 \end{bmatrix}$$

The slit function is always divided into an odd number of steps. A zero can always be added as an extra step if necessary. The center step, S_3 in the above example, is

always placed along the diagonal of the matrix. The center interval would occur at the frequency at which the spectrometer is actually set. The per cent absorptions x_i are assumed to be far enough into the wings of the line that observed absorption is equal to true absorption, and therefore $x_i = X_i$. The number of elements x_i that are added to each end of matrix (A_n) is equal to one less than the number of non-zero elements in the first and last rows of the slit function matrix, respectively.

Note that X_1 does not equal $S_3x_1 + S_4x_2 + S_5A_1$, since contributions from the two intervals on the line further from the line center than x_1 have not been included. The computer that handles the correction procedure must be programmed to make $X_i = x_i$ for each matrix multiplication. If this "fixing of the end points" is not done, the number of usable elements along a spectral line would diminish with each multiplication by the slit function matrix.

APPENDIX B

VALUES OF THE ABSORPTION COEFFICIENT AT VARIOUS DISTANCES FROM THE CENTER OF THE HF ABSORPTION LINES CORRECTED FOR INSTRUMENTAL BROADENING (IF NECESSARY)

The following tables, Tables X through XIII, list the values of the absorption coefficient α, at various distances from the line center $\nu - \nu_o$, for each spectral line for which a value of the Lorentz exponent n, and the Lorentz half-width $\Delta\nu$, could be determined. Thus all lines are included that were wide enough to be corrected for the effects of instrumental broadening, or were wide enough to need no correction.

All lines measured at the same temperature and pressure and with the same path length are included in the same table.

TABLE X

SPECTRAL LINE SHAPE IN TERMS OF α AND $\nu - \nu_o$ FOR LINES MEASURED AT 5 CM PRESSURE AND 100°C IN THE 10 CM CELL

Spectral Line and Measured Constants	Low Wave Number Side $\nu_o - \nu$ (cm^{-1})	α (cm^{-1})	High Wave Number Side $\nu - \nu_o$ (cm^{-1})	α (cm^{-1})
R(3)	0.30	0.243	0.30	0.239
	.45	.0997	.45	.107
ν_o=4109.95 cm^{-1}	.60	.0593	.60	.0600
	.75	.0376	.75	.0391
α_o=23.142 cm^{-1}	.90	.0268	.90	.0268
	1.05	.0207	1.05	.0200
	1.20	.0159	1.20	.0154
	1.35	.0131	1.35	.0119
	1.50	0.0105	1.50	0.0093
R(2)	0.332	0.277	0.368	0.246
	.432	.165	.518	.122
ν_o=4075.29 cm^{-1}	.582	.0930	.668	.0751
	.732	.0601	.818	.0511
α_o=24.714 cm^{-1}	.882	.0418	.968	.0363
	1.032	.0310	1.118	.0274
	1.182	.0240	1.268	.0216
	1.332	.0199	1.418	.0179
	1.482	.0165	1.568	.0150
	1.632	.0138	1.718	.0125
	1.782	0.0114	1.868	0.0105
R(1)	0.384	0.183	0.316	0.294
	.534	.0955	.466	.128
ν_o=4038.96 cm^{-1}	.684	.0603	.616	.0737
	.834	.0407	.766	.0477
α_o=22.953 cm^{-1}	.984	.0295	.916	.0331
	1.134	.0216	1.066	.0251
	1.284	.0166	1.216	.0191
	1.434	0.0132	1.366	0.0148

TABLE X (continued)

Spectral Line and Measured Constants	Low Wave Number Side $\nu_o - \nu$ (cm^{-1})	α (cm^{-1})	High Wave Number Side $\nu - \nu_o$ (cm^{-1})	α (cm^{-1})
R(0)	0.28	0.185	0.32	0.162
	.38	.102	.42	.0887
ν_o=4001.02 cm^{-1}	.48	.0659	.52	.0613
	.58	.0463	.62	.0428
α_o=16.247 cm^{-1}	.68	.0346	.72	.0321
	.78	.0262	.82	.0242
	.88	.0206	.92	.0191
	.98	.0166	1.02	.0157
	1.08	.0136	1.12	.0131
	1.18	.0119	1.22	.0106
	1.28	.0103	1.32	.00921
	1.38	.00892	1.42	.00840
	1.48	.00774	1.52	0.00714
	1.58	0.00646		
P(1)	0.302	0.135	0.298	0.160
	.402	.0728	.398	.0833
ν_o=3920.33 cm^{-1}	.502	.0517	.498	.0552
	.602	.0384	.598	.0380
α_o=14.494 cm^{-1}	.702	.0287	.698	.0269
	.802	.0223	.798	.0207
	.902	.0167	.898	.0160
	1.002	.0137	.998	.0129
	1.102	.0116	1.098	.0107
	1.202	.00976	1.198	.00913
	1.302	0.00867	1.298	0.00721
P(2)	0.33	0.227	0.32	0.226
	.43	.124	.42	.127
ν_o=3877.72 cm^{-1}	.53	.0809	.52	.0825
	.63	.0575	.62	.0583
α_o=18.458 cm^{-1}	.73	.0435	.72	.0439
	.83	.0339	.82	.0356
	.93	.0265	.92	.0277
	1.03	.0216	1.02	.0216
	1.13	.0179	1.12	.0184
	1.23	0.0147	1.22	.0160
			1.32	.0135
			1.42	.0114
			1.52	.00967
			1.62	0.00839

TABLE X (continued)

Spectral Line and Measured Constants	Low Wave Number Side $\nu_o - \nu$ (cm^{-1})	Low Wave Number Side α (cm^{-1})	High Wave Number Side $\nu - \nu_o$ (cm^{-1})	High Wave Number Side α (cm^{-1})
P(3)	0.327	0.215	0.323	0.208
	.427	.122	.423	.118
ν_o=3833.68 cm^{-1}	.527	.0784	.523	.0763
	.627	.0554	.623	.0571
α_o=17.613 cm^{-1}	.727	.0421	.723	.0433
	.827	.0327	.823	.0323
	.927	.0253	.923	.0264
	1.027	0202	1.023	.0214
	1.127	0.0168	1.123	.0176
			1.223	.0151
			1.323	.0126
			1.423	.0107
			1.523	0.00950
P(4)	0.238	0.271	0.262	0.221
	.338	.132	.362	.118
ν_o=3788.21 cm^{-1}	.438	.0746	.462	.0732
	.538	.0497	.562	.0483
α_o=15.454 cm^{-1}	.638	.0374	.662	.0349
	.738	.0287	.762	.0266
	.838	.0221	.862	.0208
	0.938	0.0179	.962	.0164
			1.062	.0140
			1.162	0.0124

TABLE XI

SPECTRAL LINE SHAPE IN TERMS OF α AND $\nu - \nu_o$ FOR LINES MEASURED AT 50 CM PRESSURE AND 100°C IN THE 10 CM CELL

Spectral Line and Measured Constants	Low Wave Number Side $\nu_o - \nu$ (cm^{-1})	Low Wave Number Side α (cm^{-1})	High Wave Number Side $\nu - \nu_o$ (cm^{-1})	High Wave Number Side α (cm^{-1})
R(8)	0.176	0.167	0.224	0.111
	.276	.0715	.324	.0539
ν_o=4256.33 cm^{-1}	.376	.0400	.424	.0324
	.476	.0262	.524	.0208
α_o=1.26 cm^{-1}	.576	.0183	.624	.0146
	.676	.0129	0.724	0.0109
	0.776	0.00971		
R(7)	0.43	0.113	0.47	0.114
	.58	.0647	.62	.0646
ν_o=4230.78 cm^{-1}	.73	.0435	.77	.0441
	.88	.0313	.92	.0302
α_o=3.022 cm^{-1}	1.03	.0232	1.07	.0230
	1.18	.0175	1.22	.0170
	1.33	.0139	1.37	.0136
	1.48	.0109	1.52	.0113
	1.63	0.00926	1.67	0.00945
R(6)	0.68	0.194	0.72	0.187
	.88	.119	.92	.118
ν_o=4203.31 cm^{-1}	1.08	.0794	1.12	.0761
	1.28	.0573	1.32	.0541
α_o=8.278 cm^{-1}	1.48	.0422	1.52	.0398
	1.68	.0322	1.72	.0305
	1.88	.0253	1.92	.0242
	2.08	.0202	2.12	.0189
	2.48	0.0127	2.52	0.0132
R(5)	1.2	0.217	1.2	0.236
	1.6	.127	1.6	.132
ν_o=4173.99 cm^{-1}	2.0	.0825	2.0	.0837
	2.4	.0584	2.4	.0576
α_o=13.463 cm^{-1}	3.1	.0343	2.7	.0468
	3.9	0.0210	3.5	.0269
			4.3	.0177
			5.1	.0128
			5.9	0.00948

TABLE XI (continued)

Spectral Line and Measured Constants	Low Wave Number Side $\nu_o - \nu$ (cm^{-1})	α (cm^{-1})	High Wave Number Side $\nu - \nu_o$ (cm^{-1})	α (cm^{-1})
R(4)	1.76	0.236	1.74	0.336
	2.26	.158	2.24	.188
ν_o=4142.85 cm^{-1}	2.76	.112	2.74	.126
	3.26	.0833	3.24	.0905
α_o=18.712 cm^{-1}	3.76	.0647	3.74	.0675
	4.26	.0519	4.24	.0523
	4.76	.0430	4.74	.0424
	5.26	.0358	5.24	.0353
	5.76	.0304	5.74	.0302
	6.76	.0224	6.24	.0261
	7.76	0.0171	7.24	.0200
			8.24	.0161
			9.24	.0134
			10.24	0.0112
R(3)	2.34	0.327	2.16	0.381
	2.84	.225	2.66	.271
ν_o=4109.95 cm^{-1}	3.34	.169	3.16	.196
	3.84	.132	3.66	.149
α_o=23.142 cm^{-1}	4.34	.105	4.16	.113
	4.84	.0862	4.66	.0932
	5.34	.0726	5.16	.0768
	5.84	.0619	5.66	.0652
	6.34	.0536	6.16	.0563
	6.84	.0463	7.16	.0420
	7.84	.0357	8.16	.0322
	8.84	0.0283	9.16	0.0246
R(2)	3.3	0.258	2.7	0.394
	4.3	.161	3.7	.221
ν_o=4075.29 cm^{-1}	5.3	.112	4.7	.148
	6.3	.0815	5.7	.103
α_o=24.707 cm^{-1}	7.3	.0624	6.7	.0759
	8.3	.0493	7.7	.0574
	9.3	.0397	8.7	.0445
	10.3	0.0325	9.7	0.0356

TABLE XI (continued)

Spectral Line and Measured Constants	Low Wave Number Side $\nu_o - \nu$ (cm^{-1})	Low Wave Number Side α (cm^{-1})	High Wave Number Side $\nu - \nu_o$ (cm^{-1})	High Wave Number Side α (cm^{-1})
R(1)	4.1	0.183	3.9	0.194
	6.1	.0891	5.9	.0932
ν_o=4038.96 cm^{-1}	8.1	.0517	7.9	.0559
	10.1	.0337	9.9	.0367
α_o=22.947 cm^{-1}	12.1	.0245	11.9	.0259
	14.1	.0186	13.9	.0192
	16.1	.0150	15.9	.0146
	18.1	0.0126	17.9	0.0121
R(0)	3.1	0.165	2.9	0.182
	5.1	.0675	4.9	.0709
ν_o=4001.02 cm^{-1}	7.1	.0361	6.9	.0395
	9.1	.0236	8.9	.0249
α_o=16.242 cm^{-1}	11.1	.0168	10.9	.0171
	13.1	0.0123	12.9	.0127
			14.9	0.00971
P(5)	2.09	0.170	1.80	0.178
	2.57	.117	2.41	.113
ν_o=3741.48 cm^{-1}	2.90	.0837	2.82	.0872
	3.31	.0593	3.23	.0685
α_o=13.109 cm^{-1}	3.72	.0497	4.06	.0440
	4.53	.0339	5.71	0.0257
	6.58	0.0170		

TABLE XII

SPECTRAL LINE SHAPE IN TERMS OF α AND $\nu - \nu_o$ FOR LINES MEASURED AT 1 ATM PRESSURE AND 100°C IN THE 0.047 CM CELL

Spectral Line and Measured Constants	Low Wave Number Side $\nu_o - \nu$ (cm^{-1})	α (cm^{-1})	High Wave Number Side $\nu - \nu_o$ (cm^{-1})	α (cm^{-1})
R(6)	0.068	7.240	0.082	6.359
	.118	5.790	.132	4.817
ν_o=4203.29 cm^{-1}	.168	4.080	.182	3.425
	.218	2.823	.232	2.454
α_o=8.278 cm^{-1}	.268	2.178	.332	1.539
	.368	1.316	.432	.998
	.468	.784	0.532	0.599
	.568	.579		
	0.668	0.500		
R(5)	0.267	5.884	0.283	5.737
	.367	4.058	.383	3.809
ν_o=4173.97 cm^{-1}	.467	2.760	.483	2.615
	.567	1.958	.583	1.911
α_o=13.467 cm^{-1}	.667	1.561	.683	1.457
	.767	1.292	.783	1.134
	.867	.959	.883	.899
	0.967	0.771	0.983	0.694
R(4)	0.18	14.666	0.22	13.479
	.23	12.960	.32	10.474
ν_o=4142.83 cm^{-1}	.33	9.918	.42	7.737
	.43	7.322	.52	5.786
α_o=18.712 cm^{-1}	.53	5.758	.62	4.460
	.63	4.523	.72	3.502
	.73	3.573	.82	2.884
	.83	2.787	.92	2.412
	.93	2.337	1.17	1.544
	1.03	2.135	1.67	0.824
	1.53	0.980		

TABLE XII (continued)

Spectral Line and Measured Constants	Low Wave Number Side $\nu_o - \nu$ (cm^{-1})	Low Wave Number Side α (cm^{-1})	High Wave Number Side $\nu - \nu_o$ (cm^{-1})	High Wave Number Side α (cm^{-1})
R(3)	0.177	20.013	0.173	20.102
	.277	16.290	.273	16.874
ν_o=4109.91 cm^{-1}	.377	13.395	.373	13.664
	.477	10.796	.473	10.794
α_o=23.142 cm^{-1}	.577	8.664	.573	8.613
	.677	7.196	.673	6.948
	.777	5.848	.773	5.676
	.877	4.636	.873	4.785
	1.407	2.242	.973	3.960
	1.907	1.226	1.073	3.539
			1.593	1.659
			2.093	0.980
R(2)	0.08	24.177	0.12	23.589
	.28	19.495	.32	18.359
ν_o=4075.28 cm^{-1}	.48	13.669	.52	12.681
	.68	9.529	.72	8.744
α_o=24.714 cm^{-1}	.88	6.901	.92	6.263
	1.08	5.125	1.12	4.668
	1.28	3.851	1.32	3.558
	1.48	2.914	1.52	2.817
	1.68	2.336	1.72	2.242
	1.88	1.890	2.22	1.407
	2.08	1.751	2.72	0.913
	2.28	1.271		
R(1)	0.100	21.910	0.209	16.568
	.205	19.442	.404	13.548
ν_o=4039.00 cm^{-1}	.314	16.064	.504	11.154
	.417	13.189	.607	9.166
α_o=22.953 cm^{-1}	.516	10.869	.705	7.589
	.625	8.841	.806	6.349
	.725	7.317	.910	5.286
	.824	6.064	1.02	4.457
	.926	5.015	1.54	2.242
	1.04	4.171	2.04	1.316
	1.53	2.077	2.49	0.869
	2.05	1.226		
	2.57	0.780		

TABLE XII (continued)

Spectral Line and Measured Constants	Low Wave Number Side $\nu_o - \nu$ (cm^{-1})	α (cm^{-1})	High Wave Number Side $\nu - \nu_o$ (cm^{-1})	α (cm^{-1})
R(0)	0.04	16.110	0.16	14.326
	.24	12.720	.36	9.932
ν_o=4001.05 cm^{-1}	.44	8.489	.56	6.435
	.64	5.451	.76	4.274
α_o=16.246 cm^{-1}	.84	3.609	.96	2.963
	1.04	2.527	1.16	2.194
	1.24	1.890	1.36	1.659
	1.44	1.407	1.56	1.294
	1.64	1.069	1.76	.935
	1.84	.824	1.96	.692
	2.04	.648	2.46	0.430
	2.54	0.408		
P(1)	0.313	9.890	0.287	10.904
	.513	6.696	.487	7.407
ν_o=3920.30 cm^{-1}	.713	4.431	.687	4.748
	.913	2.963	.887	3.135
α_o=14.494 cm^{-1}	1.113	2.171	1.087	2.218
	1.313	1.613	1.287	1.567
	1.513	1.242	1.487	1.159
	1.713	0.935	1.687	0.869
P(2)	0.214	16.201	0.286	14.709
	.314	14.078	.386	12.643
ν_o=3877.76 cm^{-1}	.414	11.923	.486	10.587
	.514	10.034	.586	8.905
α_o=18.458 cm^{-1}	.614	8.489	.686	7.498
	.714	7.108	.786	6.149
	.814	5.980	.886	5.178
	.914	5.042	.986	4.431
	1.314	2.963	1.086	3.888
	1.814	1.728	1.186	3.209
	2.314	1.091	1.686	1.774
	2.814	.692	2.186	1.204
	3.314	0.473	2.686	.824
			3.186	0.582

TABLE XII (continued)

Spectral Line and Measured Constants	Low Wave Number Side $\nu_o - \nu$ (cm^{-1})	α (cm^{-1})	High Wave Number Side $\nu - \nu_o$ (cm^{-1})	α (cm^{-1})
P(3)	0.28	14.410	0.22	14.962
	.38	12.223	.32	13.110
ν_o=3833.72 cm^{-1}	.48	10.205	.42	11.226
	.58	8.521	.52	9.495
α_o=17.613 cm^{-1}	.68	7.049	.62	7.985
	.78	5.839	.72	6.638
	.88	4.962	.82	5.616
	.98	4.196	.92	4.748
	1.08	3.710	1.02	3.990
	1.38	2.479	1.12	3.458
	1.88	1.339	1.62	1.844
	2.38	.824	2.12	1.091
	2.88	0.582	2.62	0.692
P(4)	0.245	12.267	0.205	12.512
	.345	9.989	.305	10.541
ν_o=3788.22 cm^{-1}	.445	7.931	.405	8.657
	.545	6.302	.505	6.864
α_o=15.454 cm^{-1}	.645	5.205	.605	5.620
	.745	4.015	.705	4.635
	.845	3.199	.805	3.750
	.945	2.982	.905	3.144
	1.245	1.774	1.005	2.547
	1.745	.980	1.255	1.774
	2.245	0.604		
P(5)	0.276	6.774	0.224	8.358
	.376	5.053	.324	5.753
ν_o=3741.48 cm^{-1}	.476	3.668	.425	4.255
	.576	2.711	.524	3.144
α_o=13.110 cm^{-1}	.676	2.041	.624	2.323
	.776	1.625	0.724	1.702
	.876	1.337		
	0.976	1.221		

TABLE XIII

SPECTRAL LINE SHAPE IN TERMS OF α AND $\nu - \nu_o$ FOR LINES MEASURED AT 5 ATM PRESSURE AND 120°C IN THE 0.047 CM CELL

Spectral Line and Measured Constants	Low Wave Number Side $\nu_o - \nu$ (cm^{-1})	α (cm^{-1})	High Wave Number Side $\nu - \nu_o$ (cm^{-1})	α (cm^{-1})
R(6)	0.34	7.081	0.26	7.950
	.54	5.639	.46	6.563
ν_o=4203.14 cm^{-1}	.74	4.418	.66	5.139
	.94	3.419	.86	3.886
α_o=8.744 cm^{-1}	1.14	2.687	1.06	2.921
	1.34	2.162	1.26	2.286
	1.54	1.789	1.46	1.797
	1.74	1.507	1.66	1.454
	1.94	1.349	1.86	1.148
	2.14	1.091	2.06	1.041
	2.64	.714	2.36	.736
	3.14	0.517	2.86	0.473
R(5)	0.47	11.614	0.33	12.678
	.67	10.077	.53	11.210
ν_o=4173.88 cm^{-1}	.87	8.515	.73	9.532
	1.07	7.150	.93	8.071
α_o=13.642 cm^{-1}	1.27	6.095	1.13	6.075
	1.47	5.171	1.33	5.503
	1.67	4.392	1.53	4.577
	1.87	3.716	1.73	3.896
	2.37	2.693	1.93	3.261
			2.13	2.840
			2.63	2.092
R(4)	0.50	16.474	0.50	16.621
	.70	15.158	.70	15.123
ν_o=4142.70 cm^{-1}	1.10	12.281	1.10	12.066
	1.50	9.476	1.50	9.360
α_o=18.412 cm^{-1}	1.90	7.389	1.90	7.201
	2.20	6.113	2.30	5.574
	2.70	4.503	2.80	4.063
	3.20	3.407	3.30	3.047
	3.70	2.705	3.80	2.339
	4.70	1.875	4.30	1.795
	5.70	1.350	5.30	1.061
			6.30	0.661

TABLE XIII (continued)

Spectral Line and Measured Constants	Low Wave Number Side $\nu_o - \nu$ (cm^{-1})	α (cm^{-1})	High Wave Number Side $\nu - \nu_o$ (cm^{-1})	α (cm^{-1})
R(3)	1.49	14.050	1.39	15.217
	2.05	10.934	1.95	11.456
ν_o=4109.82 cm^{-1}	2.61	8.247	2.51	8.486
	3.17	6.321	3.07	6.546
α_o=22.473 cm^{-1}	3.73	5.096	3.63	5.177
	4.85	3.462	4.19	4.206
	5.97	2.593	5.31	2.827
	7.09	1.851	6.43	2.027
	8.21	1.455	7.55	1.462
	9.33	1.181	8.67	1.072
R(2)	2.16	12.437	2.20	12.751
	2.70	10.111	2.75	9.800
ν_o=4075.29 cm^{-1}	3.25	7.951	3.29	8.048
	3.79	6.573	3.84	6.634
α_o=25.393 cm^{-1}	4.34	5.446	4.38	5.448
	5.43	3.999	5.47	4.002
	6.52	2.989	6.56	2.968
	7.61	2.651	7.65	2.265
	8.70	1.857	8.74	1.816
	9.79	1.531		
R(1)	1.97	13.932	1.74	13.849
	2.50	10.557	2.80	9.245
ν_o=4039.01 cm^{-1}	3.56	7.121	3.86	6.197
	4.62	4.776	4.92	4.361
α_o=23.605 cm^{-1}	5.68	3.512	5.98	3.365
	6.73	2.632	7.04	2.653
	7.79	2.142	8.10	2.082
	8.85	1.709	9.15	1.802
R(0)	1.01	13.139	1.04	12.531
	1.53	9.995	1.55	10.038
ν_o=4001.17 cm^{-1}	2.04	7.995	2.07	7.775
	2.55	6.254	2.58	6.213
α_o=16.497 cm^{-1}	3.07	4.943	3.09	4.865
	3.58	3.963	4.13	3.465
	4.09	3.303	5.19	2.633
	5.11	2.399	6.19	1.924
	6.13	1.928		

TABLE XIII (continued)

Spectral Line and Measured Constants	Low Wave Number Side $\nu_o - \nu$ (cm^{-1})	Low Wave Number Side α (cm^{-1})	High Wave Number Side $\nu - \nu_o$ (cm^{-1})	High Wave Number Side α (cm^{-1})
P(4)	1.08	11.517	1.04	11.627
	1.50	9.529	1.47	9.495
ν_o=3788.21 cm^{-1}	1.93	7.407	1.89	7.468
	2.78	4.962	2.32	6.235
α_o=15.704 cm^{-1}	3.63	3.333	3.17	4.016
	4.48	2.242	4.02	2.768
P(5)	0.76	10.552	0.86	9.729
	1.17	8.050	1.27	7.589
ν_o=3741.49 cm^{-1}	1.57	6.178	1.67	5.783
	2.38	3.609	2.49	3.811
α_o=13.174 cm^{-1}	3.19	2.289	3.30	2.623
	4.00	1.521	4.11	1.751

List G-A

Code	Organization	No. Copies
1-1	Science Advisor Department of State Washington 25, D.C. (U)	1
1-6	Office of Secretary of Defense (DDR&E, Tech. Library Washington 25, D.C. (U)	1
2-2	Institute of Technology Library MCLI-LIB, Bldg. 125, Area B Wright-Patterson Air Force Base, Ohio	1
2-4	Hq USAF (AFCSA, Secretary) Washington 25, D.C.	1
2-6	Hq USAF (AFRDR) Washington 25, D.C.	1
2-8	AFCRL, OAR (CRIPA) Stop 39 L.G. Hanscom Field Bedford, Massachusetts	20
2-10	ESD (ESRDG) L.G. Hanscom Field Bedford, Massachusetts	1
2-14	ASD (ASAPRD-Dist) Wright-Patterson AFB, Ohio	1
2-16	ACIC (ACDEL-7) 2d & Arsenal, St. Louis 18, Mo. (U)	1
2-19	NAFEC LIBRARY BRANCH, Bld.3 Atlantic City, New Jersey Attn: RD-702	1
2-31	AFCRL, OAR (CRT, Dr. A.M.Gerlach) L.G. Hanscom Field, Bedford, Mass.	1
2-51	AFOSR (SRGL) Washington 25, D.C.	1
2-107	AWS (AWSSS/TIPD), Scott AFB, Ill.	1
2-119	A.U. (Library) Maxwell AFB, Alabama	1
3-8	Dept. of the Army (SIGRD-8-B-5) Washington 25, D.C.	1
3-9	Technical Documents Center Evans Signal Labs Belmar, New Jersey	1
4-20	Technical Reports Librarian U.S. Naval Postgraduate School Monterey, California (U)	1

Code	Organization	No. of Copies
4-25	Director, U.S.Naval Research Lab. Code 2027 Washington 25, D.C.	1
4-41	ONR (Geophysics Code N-416) Office of Naval Research Washington 25, D.C.	1
5-9	Documents Expediting Project (UNIT X) Library of Congress Washington 25, D.C. (U)	1
5-14	Superintendent of Documents Government Printing Office Washington 25, D.C. (U)	1
5-65	ASTIA (TIPAA) Arlington Hall Station Arlington 12, Virginia	10
5-18	National Research Council 2101 Constitution Avenue Washington 25, D.C. (U)	1
5-23	NASA; Attn: Library, Code AFET-LA Stop 85 Washington 25, D.C.	1
5-26	Librarian, Boulder Laboratories National Bureau of Standards Boulder, Colorado (U)	1
5-28	Library, Natl. Bureau of Standards Washington 25, D.C. (U)	1
5-46	Director of Meteorological Research U.S. Weather Bureau Washington 25, D.C. (U)	1
5-53	Library, U.S.Weather Bureau Suitland, Md. (U)	1
6-87	Director, USAF Project RAND The Rand Corporation 1700 Main St., Santa Monica, Calif. Thru: A. F. Liaison Office	1
6-90	Dr. William W. Kellogg Rand Corporation, 1700 Main St. Santa Monica, California (U)	1
7-8	Mr. Malcolm Rigby American Meteorological Society P. O. Box 1736, Washington 13, D.C. (U)	1
7-35	Institute of Aerospace Sciences, Inc. 2 East 64th St., New York 21, N.Y. (U)	1

Code	Organization	No. of Copies
8-5	Library, Geophysical Institute University of Alaska P.O.Box 938, College, Alaska (U)	1
8-41	Dr. Joseph Kaplan Dept of Physics University of California Los Angeles, California (U)	1
8-47	Prof. Fred L. Whipple Harvard College Observatory 60 Garden St., Cambridge 38, Mass. (U)	1
8-48	Dr. David Fultz Dept of Meteorology University of Chicago Chicago, Illinois (U)	1
8-365	Dr. A. M. Peterson Stanford University Stanford, California (U)	1
8-366	Professor Clarence Palmer Inst. of Geophysics, Univ. of California Los Angeles 24, California (U)	1
9-6	Technical Information Office European Office, Aerospace Research Shell Building, 47 Cantersteen Brussels, Belgium (U)	1
	HQ AFCRL, OAR (CRZC) John S. Garing L. G. Hanscom Field Bedford, Massachusetts	
	BAMIRAC - Library Attn: B. R George Univ. of Michigan Willow Run Laboratories P. O. Box 2008 Ann Arbor, Michigan	1